Defence Research and Development Canada
Recherche et développement pour la défense Canada

DEFENCE R&D DÉFENSE

Advanced Beamformers

Stergios Stergiopoulos

Defence R&D Canada
Technical Report
DRDC Toronto TR 2008-101
September 2008

Canada

Advanced beamformers

Stergios Stergiopoulos

Defence R&D Canada – Toronto

Technical Report
DRDC Toronto TR 2008-101
September 2008

Principal Author

Original signed by Stergios Stergiopoulos, PhD

Stergios Stergiopoulos, PhD

Diagnosis and Prevention Group, Individual Readiness Section

Approved by

Original signed by Bob Cheung, PhD

Bob Cheung, PhD

Acting Head, Individual Readiness Section

Approved for release by

Original signed by K.C. Wulterkens

K.C. Wulterkens

for Chair, Document Review and Library Committee

Abstract

The aim with this report is to bring together some of the recent theoretical developments on beamformers; and provide suggestions of how modern technology can be applied to the development of current and next generation ultrasound systems and integrated active and passive sonars. It will focus on the development of an advanced beamforming structure that allows the implementation of adaptive and synthetic aperture signal processing techniques in ultrasound systems and integrated active-passive sonars deploying multi-dimensional arrays of sensors.

Résumé

Le but du présent rapport est de faire le point sur les avancées théoriques récentes en matière de conformateurs de faisceaux et de formuler des propositions sur la façon dont la technologie moderne peut être appliquée au perfectionnement des systèmes à ultrasons en place et de prochaine génération et des sonars actifs et passifs intégrés. Le présent rapport porte principalement sur la mise au point d'une structure évoluée de mise en forme de faisceaux qui permet la mise en place de techniques de traitement de signaux de radar à ouverture synthétique et de radar adaptatif dans des systèmes à ultrasons et des sonars actifs-passifs intégrés déployant des réseaux de capteurs à plusieurs dimensions.

This page intentionally left blank.

Executive summary

Advanced beamformers

Stergios Stergiopoulos; DRDC Toronto TR 2008-101; Defence R&D Canada – Toronto; September 2008.

Introduction or background: The concept of implementing successfully adaptive schemes in 2-dimensional (2-D) and 3-dimensional (3-D) arrays of sensors, such as planar, circular, cylindrical and spherical arrays, is similar to that of line arrays. In particular, the basic step is to minimize the number of degrees of freedom associated with the adaptation process. The material of this report is focused on the definition of a generic beamforming structure that decomposes the beamforming process of 2-D and 3-D sensor arrays into sub-sets of coherent processes. The approach is to fractionate the computationally intensive multi-dimensional beamformer into two simple modules, which are line and circular array beamformers.

Results: As a result of the decomposition process, application of spatial shading to reduce the side-lobe structures can now be easily incorporated in 2-D & 3-D beamformers of real-time ultrasound, sonar and radar systems that include arrays with hundreds of sensors. Then the next step is to define a generic sub-aperture scheme for 2-D and 3-D sensor arrays. The multi-dimensional generic sub-aperture structure leads to minimization of the associated convergence period and makes the implementation of adaptive schemes with near instantaneous convergence practically feasible.

Significance: The reported real data results show that the adaptive processing schemes provide improvements in array gain for signals embedded in a partially correlated noise field. For ultrasound medical imaging systems, practically realizable angular resolution improvements have been quantitatively assessed to be equivalent with those provided by the conventional beamformer of a two times longer physical aperture and for broadband FM and CW type of active pulses. The same set of results demonstrate also that the combined implementation of a synthetic aperture and the sub-aperture adaptive scheme suppresses significantly the side lobe structure of CW pulses for medical imaging applications. In summary, the reported development of the generic multi-dimensional beamforming structure has the capability to include several algorithms (adaptive, synthetic aperture, conventional beamfomers, matched filters and spectral analyzers) working in synergism.

Future plans: The development of this multi-dimensional advanced beamforming structure is part of a major development project that aims to provide robust medical diagnostic imaging and monitoring vital signs technologies that have capabilities to provide valuable diagnostic assessment of injured personnel in far-forward operations of interest to the CFs.

Sommaire

Advanced beamformers

Stergios Stergiopoulos; DRDC Toronto TR 2008-101; R & D pour la défense Canada – Toronto; Septembre 2008.

Introduction : Le principe de la mise en place réussie de configurations adaptatives dans des réseaux de capteurs à deux dimensions (2D) et à trois dimensions (3D), comme des réseaux planaires, circulaires, cylindriques et sphériques, est semblable au concept des réseaux en ligne. En particulier, l'opération fondamentale consiste à réduire au minimum le nombre de degrés de liberté associés au processus d'adaptation. Le présent rapport porte principalement sur la définition d'une structure générique de mise en forme de faisceaux qui décompose le processus de mise en forme de faisceaux des réseaux de capteurs 2D et 3D en sous-ensembles de processus cohérents. L'approche consiste à fractionner le conformateur de faisceaux comportant de nombreux calculs en deux modules simples, soit des conformateurs de faisceaux circulaires et des conformateurs de faisceaux en ligne.

Résultats : Résultat du processus de décomposition, l'application de l'effet d'ombrage spatial en vue d'une réduction des structures des lobes secondaires peut maintenant être facilement intégrée aux conformateurs de faisceaux 2D et 3D de systèmes radar, sonar et à ultrasons en temps réel qui comportent des réseaux composés de centaines de capteurs. La prochaine étape consiste en la définition d'une configuration générique d'ouverture secondaire pour les réseaux de capteurs 2D et 3D. La structure générique d'ouverture secondaire à plusieurs dimensions mène à la réduction au minimum de la période de convergence connexe et rend pratiquement possible la mise en œuvre de configurations adaptatives ayant une convergence quasi instantanée.

Portée : Les résultats signalés au moyen de données réelles montrent que les configurations de traitement adaptatif comportent des améliorations sur le plan du gain dans le cas des signaux intégrés dans un champ de bruit en corrélation partielle. Dans le cas des systèmes d'imagerie médicale par échographie, des améliorations pratiquement réalisables du pouvoir séparateur angulaire ont été jugées quantitativement équivalentes aux améliorations que permet le conformateur classique de faisceaux dans le cas d'une ouverture matérielle deux fois plus longue et d'impulsions actives de types à ondes entretenues et FM à large bande. Les mêmes résultats montrent aussi que la mise en œuvre combinée d'une ouverture synthétique et de la configuration adaptative d'une ouverture secondaire permet de supprimer significativement la structure des lobes secondaires des impulsions à ondes entretenues pour les applications en imagerie médicale. En résumé, le perfectionnement signalé de la structure générique de mise en forme de faisceaux à plusieurs dimensions a la capacité de comprendre plusieurs algorithmes fonctionnant en synergie (configuration adaptative, ouverture synthétique, conformateurs classiques de faisceaux, filtres adaptés et analyseurs de spectre).

Recherches futures : Le perfectionnement de cette structure évoluée de mise en forme de faisceaux à plusieurs dimensions s'inscrit dans le cadre d'un important projet de perfectionnement visant la prestation de solides techniques d'imagerie de diagnostic médical et de surveillance des signes vitaux qui offrent la capacité de fournir une évaluation diagnostique utile de blessés dans des opérations avancées comportant un intérêt pour les FC.

Table of contents

List of figures

List of tables

1 Background

In general, the mainstream conventional signal processing of current sonar and ultrasound systems consists of a selection of temporal and spatial processing algorithms [2,3,4,5,6]. These algorithms are designed to increase the signal-to-noise ratio for improved signal delectability while simultaneously providing parameter estimates such as frequency, time-delay, Doppler and bearing for incorporation into localization, classification and signal tracking algorithms. Their implementation in real time systems had been directed at providing high-quality, artifact-free conventional beamformers, currently used in operational ultrasound and sonar systems. However, aberration effects associated with ultrasound system operations and the drastic changes in the threat acoustic signatures associated with sonars suggest that fundamentally new concepts need to be introduced into the signal processing structure of next-generation ultrasound and sonar systems.

To provide a context for the material contained in this report, it would seem appropriate to review briefly the basic requirements of high-performance sonar systems deploying multi-dimensional arrays of sensors. Figure 1 shows one possible high-level view of a generic warfare sonar system. The upper part of the figure presents typical sonar mine-hunting operations carried out by naval platforms (i.e., surface vessels). The lower left hand side part of the figure provides a schematic representation of the coordinate system for a hull mounted cylindrical array of an active sonar [7,8]. The lower right hand side part of Figure 3.1 provides a schematic representation of the coordinate system for a variable depth active sonar deploying a spherical array of sensors for mine warfare operations [9]. In particular, it is assumed that the sensors form a cylindrical or spherical array that allows for beam steering across 0 - 360^{o} in azimuth and a 180^{o} angular searching sector in elevation along the vertical axis of the coordinate system.

Thus, for effective sonar operations, the beam-width and the side-lobe structure of the beam steering patterns, (shown in the lower part of Figure 1 for a given azimuth θs and elevation Φs beam steering), should be very small to allow for high image and spatial resolution of detected mines that are in close proximity with other objects. More specifically, the beam steering pattern characteristics of a mine hunting sonar define its performance in terms of image and spatial resolution characteristics. For a given angular resolution in azimuth and elevation, a mine hunting sonar would not be able to distinguish detected objects and mines that are closer than the angular resolution performance limits. Moreover, the beam steering side-lobe structure would affect the image resolution performance of the system. Thus, for a high performance sonar it is desirable that the system should provide the highest possible angular resolution in azimuth and elevation as well as the lowest possible levels of side lobe structures, properties that are defined by the aperture size of the receiving array. The above arguments are equally valid for ultrasound system operations since the beamforming process for ultrasound imaging assumes plane wave arrivals.

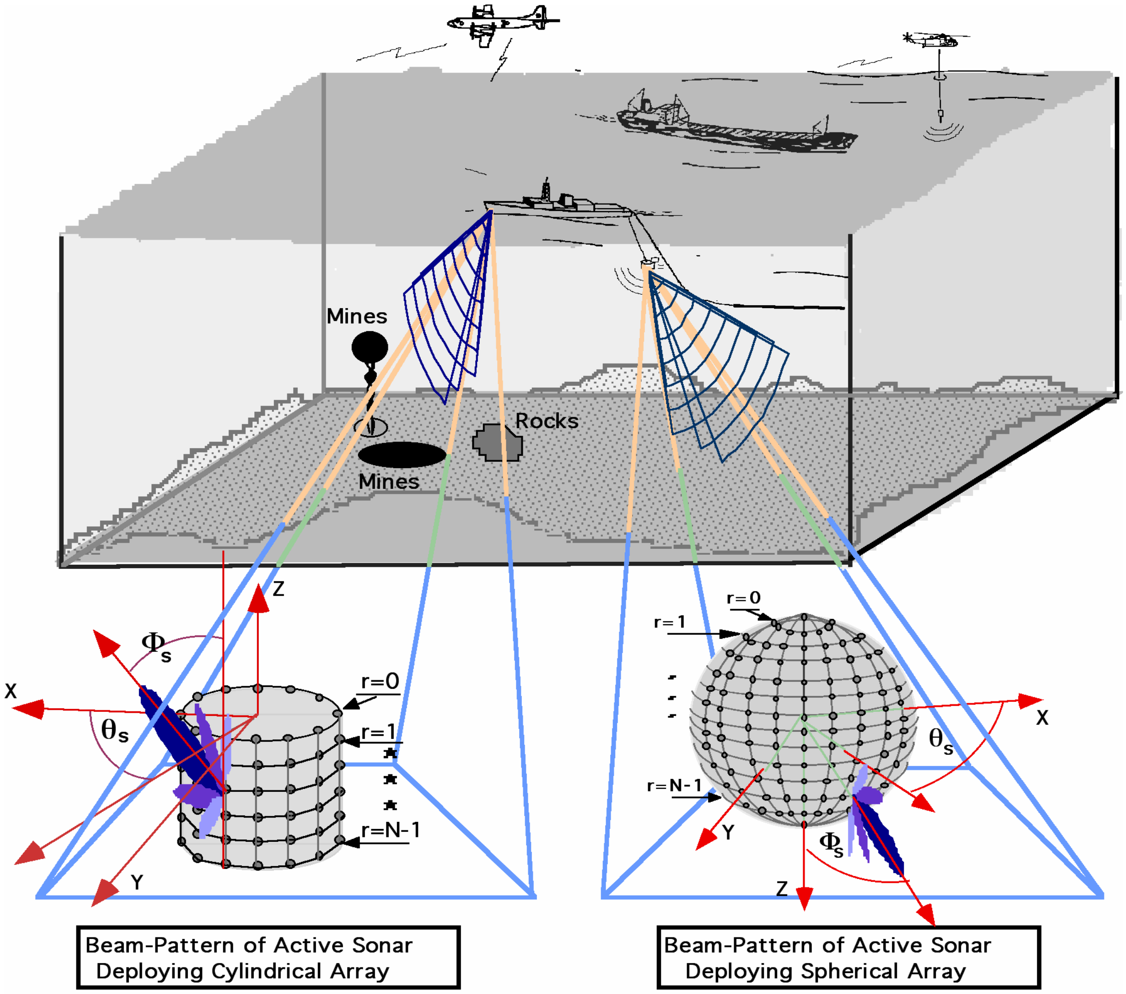

Figure 1: Upper part: Mine warefare sonar operations. Lower part (left): Schematic representation of the coordinate system for a hull mounted cylindrical array of an active sonar. Lower part (Right): Schematic representation of the coordinate system for a variable depth spherical array of an active sonar.

Because the increased angular resolution means longer sensor arrays with consequent technical and operational implications, many attempts have been made to increase the effective array length by synthesizing additional sensors (i.e. synthetic aperture processing) [1,6,11-16] or using adaptive beam processing techniques[1-5,17-24].

In previous studies, the impact and merits of these techniques have been assessed for towed array [1,4,5,10-20] and cylindrical array hull mounted [2,4,7,25,26] sonars and contrasted with those obtained using the conventional beamformer. The present material extends previous investigations and further assesses the performance characteristics of ultrasound and sonars systems that are assumed to include adaptive processing schemes integrated with a plane wave conventional beamforming structure.

2 Theoretical Remarks

Sonar operations can be carried out by a wide variety of naval platforms, as shown in Figure 1. This includes surface vessels, submarines and airborne systems such as airplanes and helicopters. Shown also in Figure 1 is a schematic representation of active and passive sonar operations in an underwater sea environment. Active sonar and ultrasound operations involve the transmission of well defined acoustic signals, called replicas, which illuminate targets in an underwater or human body medium, respectively. The reflected acoustic energy from a target or body organ provides the array receiver with a basis for detection and estimation. Passive sonar operations base their detection and estimation on acoustic sounds, which emanate from submarines and ships. Thus, in passive systems only the receiving sensor array is under the control of the sonar operators. In this case, major limitations in detection and classification result from imprecise knowledge of the characteristics of the target radiated acoustic sounds.

The passive sonar concept can be made clearer by comparing sonar systems with radars, which are always active. Another major difference between the two systems arises from the fact that sonar system performance is more affected than that of radar systems by the underwater medium propagation characteristics. All the above issues have been discussed in several review articles [1-6] that form a good basis for interested readers to become familiar with “main stream” sonar signal processing developments. Therefore, discussions of issues of conventional sonar signal processing, detection, estimation and influence of medium on sonar system performance are beyond the scope of this report. Only a very brief overview of the above issues will be highlighted in this section in order to define the basic terminology required for the presentation of the main theme of the present article. Let us start with a basic system model that reflects the interrelationships between the target, the underwater sea environment or the human body (medium) and the receiving sensor array of a sonar or an ultrasound system.

A schematic diagram of this basic system is shown in 3.2, where array signal processing is shown to be two-dimensional [1,5,10,12,18] in the sense that it involves both temporal and spatial spectral analysis. The temporal processing provides spectral characteristics that are used for target classification and the spatial processing provides estimates of the directional characteristics, (i.e., bearing and possibly range), of a detected signal. Thus, *Space-Time Processing* is the fundamental processing concept in sonar and ultrasound systems and it will be the subject of our discussion in the next section.

2.1 Space-Time Processing

For geometrical simplicity and without any loss of generality, we consider here a combination of N equally spaced acoustic transducers in a linear array, which may form a towed or hull mounted array system that can be used to estimate the directional properties of echoes and acoustic signals. As shown in Figure 2, a direct analogy between sampling in space and sampling in time is a natural extension of the sampling theory in space-time signal representation and this type of space-time sampling is the basis in array design that provides a description of an array system response. When the sensors are arbitrarily distributed, each element will have an added degree of freedom, which is its position along the axis of the array. This is analogous to non-uniform temporal sampling of a signal. In this report we extend our discussion to multi-dimensional array systems.

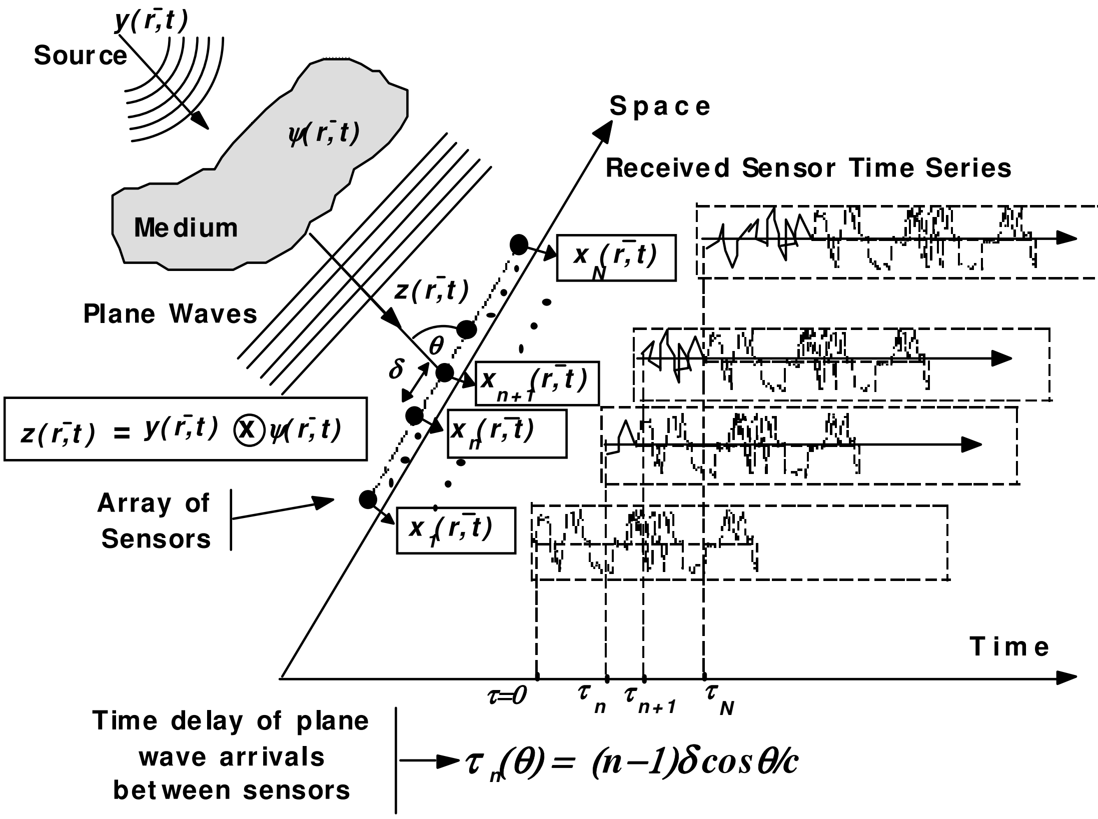

Figure 2: A model of space-time signal processing. It shows that ultrasound and sonar signal processing is two dimensional in the sense that it involves both temporal and spatial spectral analysis. The temporal processing provides characteristics for target classification and the spatial processing provides estimates of the directional characteristics (bearing, range-depth) of detected echoes (active case) or signals of interest (passive case).

Sources of sound that are of interest in sonar and ultrasound system applications are harmonic narrowband, broadband and satisfy the wave equation [2,10]. Furthermore, their solutions have the property that their associated temporal-spatial characteristics are separable [10]. Therefore, measurements of the pressure field $z(\bar{r},t)$ which is excited by acoustic source signals, provide the spatial-temporal output response, designated by $x(\bar{r},t)$ of the measurement system. The vector $\bar{r}$ refers to the source-sensor relative position and t is the time. The output response $x(\bar{r},t)$ is the convolution of $z(\bar{r},t)$ with the line array system response $h(\bar{r},t)$ [10,30]

$$x(\bar{r},t) = z(\bar{r},t) \otimes h(\bar{r},t) \tag{1}$$

where $\otimes$ refers to convolution. Since $z(\bar{r},t)$ is defined at the input of the receiver, it is the convolution of the source's characteristics $y(\bar{r},t)$ with the underwater medium's response $\psi(\bar{r},t)$,

$$z(\bar{r},t) = y(\bar{r},t) \otimes \psi(\bar{r},t) \tag{2}$$

Fourier transformation of Equation (1) provides:

$$X(\omega,\bar{k}) = \left\{ Y(\omega,\bar{k}) \cdot \Psi(\omega,\bar{k}) \right\} \cdot H(\omega,\bar{k}) \tag{3}$$

where, $\omega, \bar{k}$ are the frequency and wavenumber parameters of the temporal and spatial spectrums of the transform functions in Equations (1) & (2). Signal processing, in terms of beamforming operations, of the receiver's output $x(\bar{r},t)$, provides estimates of the source bearing and possibly of the source range. This is a well-understood concept of the forward problem, which is concerned with determining the parameters of the received signal $x(\bar{r},t)$ given that we have information about the other two functions $z(\bar{r},t)$ and $h(\bar{r},t)$ [5]. The inverse problem is concerned with determining the parameters of the impulse response of the medium $\psi(\bar{r},t)$ by extracting information from the received signal $x(\bar{r},t)$ assuming that the function $h(\bar{r},t)$ is known [5]. The ultrasound and sonar problems, however, are quite complex and include both forward and inverse problem operations. In particular, detection, estimation and tracking-localization processes of sonar and ultrasound systems are typical examples of the forward problem, while target classification for passive-active sonars and diagnostic ultrasound imaging are typical examples of the inverse problem. In general, the inverse problem is a computationally very costly operation and typical examples in acoustic signal processing are seismic deconvolution and acoustic tomography.

2.2 Definition of Basic Parameters

This section outlines the context in which the sonar or the ultrasound problem can be viewed in terms of simple models of acoustic signals and noise fields. The signal processing concepts that are discussed in this report have been included in sonar and radar investigations with sensor arrays having circular, planar, cylindrical and spherical geometric configurations [7,25,26,28]. Thus, we consider a multi-dimensional array of equally spaced sensors with spacing δ. The output of the nth sensor is a time series denoted by $x_n(t_i)$, where $(i=1,..., M_s)$ are the time samples for each sensor time series. * denotes complex conjugate transposition so that $\bar{x}^*$ is the row vector of the received $\aleph$ - sensor time series $\{x_n(t_i), n=1,2,..., \aleph\}$.

Then $x_n(t_i) = s_n(t_i) + \varepsilon_n(t_i)$, where $s_n(t_i)$, $\varepsilon_n(t_i)$ are the signal and noise components in the received sensor time series. $\bar{S}$, $\bar{\varepsilon}$ denote the column vectors of the signal and noise components of the vector $\bar{x}$ of the sensor outputs (i.e. $\bar{x} = \bar{s} + \bar{\varepsilon}$). $X_n(f) = \sum_{i=1}^{M_s} x_n(t_i) \exp(-j2\pi f t_i)$ is the Fourier transform of $x_n(t_i)$ at the signal with frequency f, $c = f\lambda$ is the speed of sound in the underwater, or human-body medium and λ is the wavelength of the frequency *f*. $S = E\{\bar{S}\ \ \bar{S}^*\}$ is the spatial correlation matrix of the signal vector $\bar{S}$, whose *n*th element is expressed by,

$$s_n(t_i) = s_n[t_i + \tau_n(\theta, \phi)] \tag{4}$$

E{...} denotes expectation and $\tau_n(\theta, \phi)$ is the time delay between the (n-1)st and the nth sensor of the array for an incoming plane wave with direction of propagation of azimuth angle θ and an elevation angle ϕ, as depicted in Figure 2. In frequency domain, the spatial correlation matrix **S** for the plane wave signal $s_n(t_i)$ is defined by:

$$S(f_i, \theta, \phi) = A_s(f_i)\bar{D}(f_i, \theta, \phi)\bar{D}^*(f_i, \theta, \phi) \tag{5}$$

where $A_s(f_i)$ is the power spectral density of $s(t_i)$ for the ith frequency bin; and $\bar{D}(f, \theta, \phi)$ is the steering vector with the nth term being denoted by $d_n(f, \theta, \phi)$. Then matrix $\boldsymbol{S}(f_i \theta, \phi)$ has as its *n*th row and *m*th column defined by, $S_{nm}(f_i, \theta, \phi) = A_s(f_i) d_n(f_i \theta, \phi) d^*_m(f_i \theta, \phi)$. Moreover, $R(f_i)$ is the spatial correlation matrix of received sensor time series with elements, $R_{nm}(f, d_{nm})$. $R_\varepsilon(f_i) = \sigma_n^2(f_i) R_\varepsilon(f_i)$ is the spatial correlation matrix of the noise for the ith frequency bin with $\sigma_n^2(f_i)$ being the power spectral density of the noise, $\varepsilon_n(t_i)$. In what is considered as an estimation procedure in this report, the associated problem of detection is defined in the classical sense as a hypothesis test that provides a detection probability and a probability of false alarm [31-33]. This choice of definition is based on the standard CFAR (constant false alarm rate) processor, which is based on the Neyman-Pearson criterion [31]. The CFAR processor provides an estimate of the ambient noise or clutter level so that the threshold can be varied dynamically to stabilize the false alarm rate. Ambient noise estimates for the CFAR processor are provided mainly by noise normalization techniques [34] that account for the slowly varying changes in the background noise or clutter. The above estimates of the ambient noise are based upon the average value of the received signal, the desired probability of detection and probability of false alarms.

At this point, a brief discussion on the fundamentals of detection and estimation process is required in order to address implementation issues of signal processing schemes in sonar and ultrasound systems.

2.3 Detection and Estimation

In passive systems, in general, we do not have the *a priori* probabilities associated with the hypothesis H_1 that the signal is assumed present and the null hypothes is H_0 that the received time series consists only of noise. As a result, costs can not be assigned to the possible outcomes of the experiment. In this case, the Neyman-Pearson (N-P) Criterion [31] is applied because it requires only a knowledge of the signal's and noise's probability density functions (*pdf*).

Let $x_{n=1}(t_i)$, $(i=1,...,M)$ denote the received vector signal by a single sensor. Then for hypothesis H_1, which assumes that the signal is present, we have:

$$H_1: \qquad x_{n=1}(t_i) = s_{n=1}(t_i) + \varepsilon_{n=1}(t_i),$$

where $s_{n=1}(t_i)$ and $\varepsilon_{n=1}(t_i)$ are the signal and noise vector components in the received signal and $p_1(x)$ is the pdf of the received signal $x_{n=1}(t_i)$ given that H_1 is true. Similarly, for hypothesis H_0:

$$H_0: \qquad x_{n=1}(t_i) = \varepsilon_{n=1}(t_i)$$

and $p_0(x)$ is the pdf of the received signal given that H_0 is true. The N-P criterion requires maximization of probability of detection for a given probability of false alarm. So, there exists a non-negative number η such that if hypothesis H_1 is chosen then

$$\lambda(x) = \frac{p_1(x)}{p_o(x)} \geq \eta \tag{6}$$

which is the likelihood ratio. By using the analytic expressions for $p_0(x)$ (the pdf for H_0) and $p_1(x)$ (the pdf for H_1) in Eq. (6) and by taking the $\ln[\lambda(x)]$, we have [31],

$$\lambda_\tau = \ln[\lambda(x)] = \overline{s^*} R_\varepsilon^{'} \overline{x} \tag{7}$$

where, λ_τ is the log likelihood ratio and $R_\varepsilon^{'}$ is the covariance matrix of the noise vector, as defined in the previous section 3.2.2. For the case of white noise with $R_\varepsilon^{'} = \sigma_n^2 I$ and I the unit matrix, the test statistic in expression (7) is simplified into a simple correlation receiver (or replica correlator)

$$\lambda_\tau = \overline{s^*} \otimes \overline{x} \tag{8}$$

For the case of anisotropic noise, however, an optimum detector should include the correlation properties of the noise in the correlation receiver as this is defined in Eq. (7).

For plane wave arrivals that are observed by a N –sensor array receiver the test statistics are [31]:

$$\lambda_\tau = \sum_{i=1}^{\frac{M_s}{2}-1} \overline{X^*}(f_i) \cdot R_\varepsilon^{/}(f_i) \cdot S(f_i,\phi,\theta) \cdot \left[S(f_i,\phi,\theta) + R_\varepsilon^{/}(f_i)\right]^{-1} \cdot \overline{X}(f_i) \tag{9}$$

where, the above statistics are for the frequency domain with parameters defined in Eqs. (4) & (5) in the previous Section 3.2.2. Then, for the case of an array of sensors receiving plane wave signals, the log likelihood ratio λ_τ in Eq. (9) is expressed by the following equation, which is the result of simple matrix manipulations based on the frequency domain expressions (4.4), (3.5) and their parameter definitions presented in Section 2.2. Thus,

$$\lambda_\tau = \sum_{i=1}^{\frac{M}{2}-1} \left| \varphi(f_i) \overline{D^*}(f_i, \phi, \theta) R_\varepsilon^{'}(f_i)^{-1} \overline{X}(f_i) \right|^2 \tag{10}$$

where [31],

$$\varphi^2(f_i) = \frac{A_s(f_i) / \sigma_n^2(f_i)}{1 + A_s(f_i) \overline{D^*}(f_i, \phi, \theta) R_\varepsilon^{'-1}(f_i) \overline{D}(f_i) / \sigma_n^2(f_i)} \tag{11}$$

Eq. (10) can be written also as follows,

$$\lambda_\tau = \sum_{i=1}^{\frac{M}{2}-1} \left[\sum_{n=1}^{N} \zeta_n^*(f_i, \phi, \theta) X_n(f_i) \right]^2 \tag{12}$$

This last expression (3.12) of the log likelihood ratio indicates that an optimum detector in this case requires the filtering of each one of the N -sensor received time series X_n (f_i) with a set of filters being the elements of the vector,

$$\overline{\zeta}(f_i, \phi, \theta) = \varphi(f_i) \overline{D^*}(f_i, \phi, \theta) R_\varepsilon^{'}(f_i)^{-1} \tag{13}$$

Then, the summation of the filtered sensor outputs in frequency domain according to Eq. (13) provides the test statistics for optimum detection. For the simple case of white noise $R_\varepsilon^{'} = \sigma_n^2 I$ and for a line array receiver, the filtering operation in (3.13) indicates plane wave conventional beamforming in frequency domain,

$$\lambda_\tau = \sum_{i=1}^{\frac{M}{2}-1} \left[\psi \sum_{n=1}^{N} d_n^*(f_i, \theta) X_n(f_i) \right]^2 \tag{14}$$

where, $\psi = \varsigma / (1 + N\varsigma)$, is a scalar, which is a function of the signal-to-noise ratio, $\varsigma = A_s^2 / \sigma_n^2$.

For the case of narrowband signals embedded in spatially and or temporarily correlated noise or interferes, it has been shown [13] that the deployment of very long arrays or application of acoustic synthetic aperture will provide sufficient array gain and will achieve optimum detection and estimation for the parameters of interest.

For the general case of broadband and narrowband signals embedded in a spatially anisotropic and temporally correlated noise field, expression (14) indicates that the filtering operation for optimum detection and estimation requires adaptation of the sonar and ultrasound signal processing according to the ambient noise's and human body's noise characteristics, respectively. The family of algorithms for optimum beamforming that use the characteristics of the noise, are called *Adaptive Beamformers* [3,17-20,22,23]; and <u>a detailed definition of an adaptation process requires knowledge of the correlated noise's covariance matrix</u> $R'_{\varepsilon}(f_i)$. However, if the required knowledge of the noise's characteristics is inaccurate, the performance of the optimum beamformer will degrade dramatically [18,23]. As an example, the case of cancellation of the desired signal is often typical and significant in adaptive beamforming applications [18,24]. This suggests that the implementation of useful adaptive beamformers in real time operational systems is not a trivial task. The existence of numerous articles on adaptive beamforming suggests the dimensions of the difficulties associated with this kind of implementation. In order to minimize the generic nature of the problems associated with adaptive beamforming the concept of partially adaptive beamformer design was introduced. This concept reduces the degrees of freedom, which results in lowering the computational requirements and often improving the adaptive response time [17,18]. However, the penalty associated with the reduction of the degrees of freedom in partially adaptive beamformers is that they cannot converge to the same optimum solution as the fully adaptive beamformer.

Although a review of the various adaptive beamformers would seem relevant at this point, we believe that this is not necessary since there are excellent review articles [3,17,18,21] that summarize the points that have been considered for the material of this report. There are two main families of adaptive beamformers, the Generalized Side-lobe Cancellers (GSC) [44,45] and the Linearly Constrained Minimum Variance Beamformers (LCMV) [18]. A special case of the LCMV is Capon's Maximum Likelihood Method [22], which is called Minimum Variance Distortionless Response (MVDR) [17,18,22,23,38,39]. This algorithm has proven to be one of the more robust of the adaptive array beamformers and it has been used by numerous researchers as a basis to derive other variants of MVDR [18]. In this report we will address implementation issues for various partially adaptive variants of the MVDR and a GSC adaptive beamformer [1], which are discussed in Section 4.2.

In summary, the classical estimation problem assumes that the *a priori* probability of the signal's presence $p\ (H_1)$ is unity [31-33]. However, if the signal's parameters are not known *a priori* and $p\ (H_1)$ is known to be less than unity, then a series of detection decisions over an exhaustive set of source parameters constitutes a detection procedure, where the results incidentally provide an estimation of source's parameters. As an example, we consider the case of a matched filter, which is used in a sequential manner by applying a series of matched filter detection statistics to estimate the range and speed of the target, which are not known *a priori* . This kind of estimation procedure is not optimal since it does not constitute an appropriate form of Bayesian minimum variance or minimum mean square error procedure.

Thus, the problem of detection [31-33] is much simpler than the problem of estimating one or more parameters of a detected signal. Classical decision theory [31-33,] treats signal detection and signal estimation as separate and distinct operations. A detection decision as to the presence or absence of the signal is regarded as taking place independently of any signal parameter or waveform estimation that may be indicated as the result of detection decision. However, interest in joint or simultaneous detection and estimation of signals arises frequently. Middleton and Esposito [46] have formulated the problem of simultaneous optimum detection and estimation of signals in noise by viewing *estimation* as a generalized detection process. Practical considerations, however, require different cost functions for each process [46]. As a result, it is more effective to retain the usual distinction between detection and estimation.

Estimation, in passive sonar and ultrasound systems, includes both the temporal and spatial structure of an observed signal field. For active systems, correlation processing and Doppler (for moving target indications) are major concerns that define the critical distinction between these two approaches (i.e., *passive, active*) to sonar and ultrasound processing. In this report, we restrict our discussion only to topics related to spatial signal processing for estimating signal parameters. However, spatial signal processing has a direct representation that is analogous to the frequency-domain representation of temporal signals. Therefore, the spatial signal processing concepts discussed here have direct applications to temporal spectral analysis.

2.4 Cramer-Rao Lower Bound (CRLB) Analysis

Typically, the performance of an estimator is represented as the variance in the estimated parameters. Theoretical bounds associated with this performance analysis are specified by the Cramer-Rao bound [31-33] and that has led to major research efforts by the sonar signal processing community in order to define the idea of an optimum processor for discrete sensor arrays [12,16, 56-59]. If the *a priori* probability of detection is close to unity then the minimum variance achievable by any unbiased estimator is provided by the *Cramer-Rao Lower Bound* (CRLB) [31,32,46].

More specifically, let us consider that the received signal by the nth sensor of a receiving array is expressed by,

$$x_n(t_i) = s_n(t_i) + \varepsilon_n(t_i) \tag{15}$$

where, $s_n(t_i, \overline{\Theta}) = s_n[t_i + \tau_n(\theta, \phi)]$, defines the received signal model with $\tau_n(\theta, \phi)$ being the time delay between the (n-1)st and the nth sensor of the array for an incoming plane wave with direction of propagation of azimuth angle θ and an elevation angle ϕ, as depicted in Figure 2. The vector $\overline{\Theta}$, includes all the unknown parameters considered in relation (3.15). Let $\sigma^2_{\theta_i}$ denote the variance of an unbiased estimate of an unknown parameter θ_i in the vector $\overline{\Theta}$. The Cramer-Rao [31-33] bound states that the best unbiased estimate $\tilde{\Theta}$ of the parameter vector $\overline{\Theta}$ has the covariance matrix

$$\operatorname{cov}\tilde{\Theta} \geq J\left(\overline{\Theta}\right)^{-1} \tag{16}$$

where J is the Fisher information matrix whose elements are:

$$J_{ij} = -E\left(\frac{\vartheta^2 \ln P\langle \overline{X} | \overline{\Theta} \rangle}{\vartheta\theta_i \vartheta\theta_j}\right) \tag{17}$$

In Eq. (3.17), $P\langle \overline{X} | \overline{\Theta} \rangle$, is the probability density function (pdf) governing the observations:

$\overline{X} = [x_1(t_i), x_2(t_i), x_3(t_i), \ldots x_N(t_i)]^*$, for each of the N and M_S independent spatial and temporal samples respectively that are described by the model in Eq. (15). The variance of the unbiased estimates $\tilde{\Theta}$ has a lower bound (called the CRLB), which is given by the diagonal elements of expression (16). This CRLB is used as standard of performance and provides a good measure for the performance of a signal-processing algorithm which gives unbiased estimates $\tilde{\Theta}$ for the parameter vector $\overline{\Theta}$. In this case, if there exists a signal processor to achieve the CRLB, it will be the maximum-likelihood estimation (MLE) technique. The above requirement associated with the *a priori* probability of detection is very essential because if it is less than one, then the estimation is biased and the theoretical CRLBs do not apply. This general framework of optimality is very essential in order to account for Middleton's [32] warning that a system optimized for the one function (detection or estimation) may not be necessarily optimized for the other.

For a given model describing the received signal by a sonar or ultrasound system, the CRLB analysis can be used as a tool to define the information inherent in a sonar system. This is an important step related to the development of the signal processing concept for a sonar system as well as in defining the optimum sensor configuration arrangement under which we can achieve, in terms of system performance, the optimum estimation of signal parameters of our interest. This approach has been applied successfully to various studies related to the present development [12,15,56-59].

As an example, let us consider the simplest problem of one source with the bearing θ_1 being the unknown parameter. Following relation (17), the results of the variance $\sigma_{\theta_1}^2$ in the bearing estimates are,

$$\sigma_{\theta_i}^2 = \frac{3}{2\psi N}\left(\frac{B_w}{\pi \sin \theta_1}\right)^2 \tag{18}$$

where, $\psi = M_s A_1^2 / \sigma_N^2$, the parameter $B_w = \lambda / (N-1)\delta$ gives the beamwidth of the physical aperture that defines the angular resolution associated with the estimates of θ_1. The signal to noise ratio (SNR) at the sensor level is $SNR = 10 \times \log_{10}(\psi)$ or

$$SNR = 20 \times \log_{10}(A_1 / \sigma_1) + 10 \times \log_{10}(M_s) \qquad (19)$$

It is obvious from the above relations (3.18) and (3.19) that the variance of the bearing $\sigma_{\theta_1}^2$ can get smaller when the observation period $T = M_s / f_s$ becomes long and the receiving array size, $L = (N-1)\lambda$ gets very long .

The next question needed to be addressed is about the unbiased estimator that can exploit this available information and provide results asymptotically reaching the CRLBs. For each estimator it is well known that there is a range of *Signal-to-Noise Ratio* (SNR) in which the variance of the estimates rises very rapidly as SNR decreases. This effect, which is called the *threshold effect of the estimator*, determines the range of SNR of the received signals for which the parameter estimates can be accepted. In passive sonar systems the SNR of signals of interest are often quite low and probably below the threshold value of an estimator. In this case, high frequency resolution in both time and spatial domains for the parameter estimation of narrowband signals is required. In other words, the threshold effect of an estimator determines the frequency resolution for processing and the size of the array receivers required in order to detect and estimate signals of interest that have very low SNR [12,14,53,61,62]. The CRLB analysis has been used in many studies to evaluate and compare the performance of the various non-conventional processing schemes [17,18,55] that have been considered for implementation in the generic beamforming structure to be discussed in Section 3.4.1. In general, array signal processing includes a large number of algorithms for a variety of systems that are quite diverse in concept. There is a basic point that is common in all of them, however, and this is the beamforming process, which we are going to examine in the next section 3.

3 Optimum Estimators For Array Signal Processing

Sonar signal processing includes mainly estimation (after detection) of the source's bearing, which is the main concern in sonar array systems because in most of the sonar applications the acoustic signal's wavefronts tend to be planar, which assumes distant sources. Passive ranging by measurement of wavefront curvature is not appropriate for the far-field problem. The range estimate of a distant source, in this case, must be determined by various target-motion analysis methods discussed in Reference [1], which address the localization-tracking performance of non-conventional beamformers with real data.

More specifically, a one dimensional (1-D) device such as a line sensor array satisfies the basic requirements of a spatial filter. It provides direction discrimination, at least in a limited sense, and a signal-to-noise ratio improvement relative to an omni-directional sensor. Because of the simplified mathematics and reduced number of the involved sensors, relative to multi-dimensional arrays, most of the researchers have focused on the investigation of the line sensor arrays in system applications [1-6]. Furthermore, implementation issues of synthetic aperture and adaptive techniques in real time systems have been extensively investigated for line arrays as well [1,5,6,12,17,19,20]. However, the configuration of the array depends on the purpose for which it is to be designed. For example, if a wide range of horizontal angles is to be observed, a circular configuration may be used, given rise to beam characteristic that are independent of the direction of steering. Vertical direction may be added by moving into cylindrical configuration [8]. In more general case, where both vertical and horizontal steering is to be required and where a large range of angles is to be covered, a spherically symmetric array would be desirable [9]. In modern ultrasound imaging systems planar arrays are required to reconstruct real-time 3-D images. However, the huge computational load required for multi-dimensional conventional and adaptive beamformers makes the applications of these 2-D & 3-D arrays in real-time systems non feasible.

Furthermore, for modern sonar & radar systems, it has become a necessity these days that all possible active and passive modes of operation should be exploited under an integrated processing structure that reduces redundancy and provides cost effective real time system solutions [6]. Similarly, the implementation of computationally intensive data adaptive techniques in real time systems is also an issue of equal practical importance. However, when theses systems include multi-dimensional (2-D, 3-D) arrays with hundreds of sensors, then the associated beamforming process requires very large memory and very intensive throughput characteristics, something that makes its implementation in real time systems a very expensive and difficult task.

To counter this implementation problem, the present report introduces a generic approach of implementing conventional beamforming processing schemes with integrated passive and active modes of operations in systems that may include, planar, cylindrical or spherical arrays [25-28]. This approach decomposes the 2-D and 3-D beamforming process into sets of line and/or circular array beamformers. Because of the decomposition process, the fully multi-dimensional beamformer can now be divided into sub-sets of coherent processes that can be implemented in small size CPU's that can be integrated under the parallel configuration of existing computing architectures. Furthermore, application of spatial shading for multidimensional beamformers to control side-lobe structures can now be easily incorporated. This is because the problem of spatial shading for line arrays has been investigated thoroughly [36] and the associated results can be integrated into a circular and a multi-dimensional beamformer, which can be decomposed now into coherent sub-sets of line and or circular beamformers of the proposed generic processing structure.

As a result of the decomposition process, provided by the generic processing structure, the implementation effort for adaptive schemes is reduced to implementing adaptive processes in line and circular arrays. Thus, a multi-dimensional adaptive beamformer can now be divided into two coherent modular steps which lead to efficient system oriented implementations. In summary, the proposed approach demonstrates that the incorporation of adaptive schemes with near-instantaneous convergence in multi-dimensional arrays is feasible [7,25-28].

At this point it is important to note that the proposed decomposition process of 2-D and 3-D conventional beamformers into sets of line and/or circular array beamformers is an old concept that has been exploited over the years by sonar system designers. Thus, references on this subject may exist in Navy-Labs' and Industrial-Institutes' Technical Reports that are not always readily available and the author of this report is not aware of any kind of reports in this area. Previous efforts attempted to address practical implementation issues and had been focused on cylindrical arrays. As an example, a cylindrical array beamformer is decomposed into time-delay line array beamformers providing beams along elevation angles of the cylindrical array. These are called staves. Then, the beam time series associated with a particular elevation steering of interest are provided at the input of a circular array beamformer.

In this report the attempt is to provide a higher degree of development than the one discussed above for cylindrical arrays. The task is to develop a generic processing structure that integrates the decomposition process of multi-dimensional planar, cylindrical and spherical array beamformers into line and or circular array beamformers. Furthermore, the proposed generic processing structure integrates passive and active modes of operation into a single signal processing scheme.

3.1 Generic Multi-Dimensional Conventional Beamforming Structure

3.1.1 Line-Array Conventional Beamformer

Consider an *N*-sensor line array receiver with uniform sensor spacing δ, shown in Figure 3, receiving plane-wave arrivals with direction of propagation θ. Then, as a follow up of the parameter definition in Section 2,

$$\tau_n(\theta) = (n-1)\delta\cos\theta / c \tag{20}$$

is the time delay between the 1st and the nth sensor of the line array for an incoming plane wave with direction θ, as this is illustrated in Figure 3.

$$d_n(f_i, \theta) = \exp\left[j2\pi \frac{(i-1)f_s}{M} \tau_n(\theta) \right] \tag{21}$$

is the n[th] term of the steering vector $\overline{D}(f,\theta)$. Moreover, because of relations (13) and (14) the plane wave response of the *N*-sensor line array steered at a direction θ_S can be expressed by,

$$B(f,\theta_s) = \overline{D}^*(f,\theta_s)\overline{X}(f) \tag{22}$$

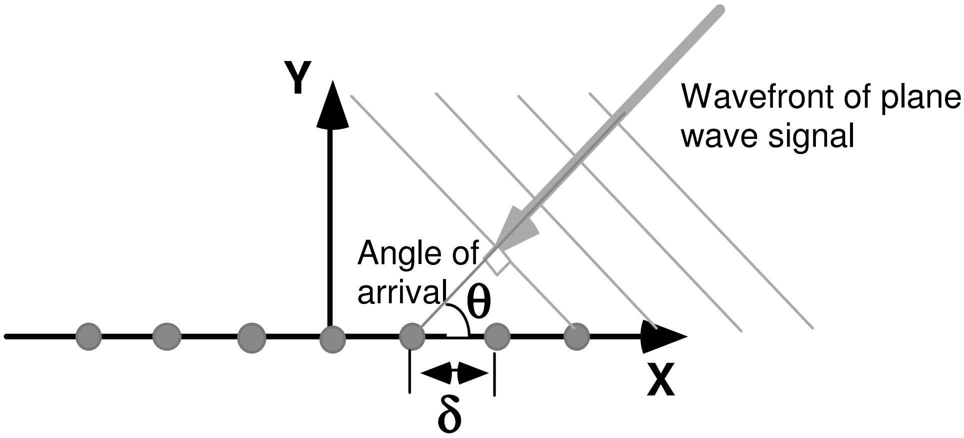

Figure 3: Geometric configuration and coordinate system for a line array of sensors.

Previous studies [1] have shown that for a single source this conventional beamformer without shading is an optimum processing scheme for bearing estimation. The side lobe structure can be suppressed at the expense of a beam width increase by applying different weights (i.e., spatial shading window) [36]. The angular response of a line-array is ambiguous with respect to the angle θ_s, responding equally to targets at angle θ_s and $-\theta_s$ where θ_s varies over $[0,\pi]$.

Eq. (22) is basically a mathematical interpretation of Figure 3 and shows that a line array is basically a spatial filter because by steering a beam in a particular direction we spatially filter the signal coming from that direction, as this is illustrated in Figure 3. On the other hand, Eq. (22) is fundamentally a discrete Fourier transform relationship between the hydrophone weightings and the beam pattern of the line array and as such it is computationally a very efficient operation. However, Eq. (22) can be generalized for non-linear 2-dimensional and 3-dimensional arrays and this is discussed in the next section.

As an example, let us consider a distant monochromatic source. Then the plane wave signal arrival from the direction θ received by a N-hydrophone line array is expressed by Eq. (21). The beam power pattern $P(f,\theta_S)$ is given by $P(f,\theta_s) = B(f,\theta_s)\times B^*(f,\theta_s)$ that takes the form

$$P(f,\theta_s) = \sum_{n=1}^{N}\sum_{m=1}^{N} X_n(f)X_m^*(f)\exp\left[\frac{j2\pi f\delta_{nm}\cos\theta_s}{c}\right] \tag{23}$$

where δ_{nm} is the spacing $\delta(n\text{-}m)$ between the n^{th} and m^{th} sensors. As a result of Eq. (23), the expression for the power beam pattern $P(f, \theta_s)$, is reduced to:

$$P(f,\theta_s) = \left\{ \frac{\sin\left[N \dfrac{\pi\delta}{\lambda} (\sin\theta_s - \sin\theta) \right]}{\sin\left[\dfrac{\pi\delta}{\lambda} (\sin\theta_s - \sin\theta) \right]} \right\}^2 \tag{24}$$

Let us consider for simplicity the source bearing θ to be at array broadside, $\delta=\lambda/2$ and $L = (N-1)\delta$ is the array size. Then Equation (24) is modified as [4,10]:

$$P(f,\theta_s) = \frac{N^2 \sin^2\left[\dfrac{\pi L \sin\theta_s}{\lambda} \right]}{\left(\dfrac{\pi L \sin\theta_s}{\lambda} \right)^2} \tag{25}$$

which is the farfield radiation or directivity pattern of the line array as opposed to near field regions. The results in Equations (24) and (25) are for a perfectly coherent incident acoustic signal and an increase in array size L results in additional power output and a reduction in beamwidth, which are similar arguments with those associated with the CRLB analysis expressed by Eq. (18). The side-lobe structure of the directivity pattern of a line array, which is expressed by Eq. (24), can be suppressed at the expense of a beamwidth increase by applying different weights. The selection of these weights will act as spatial filter coefficients with optimum performance [5,17,18]. There are two different approaches to select the above weights: **pattern optimization and gain optimization**. For pattern optimization the desired array response pattern $P(f, \theta_S)$ is selected first. A desired pattern is usually one with a narrow main lobe and low sidelobes. The weighting or shading coefficients in this case are real numbers from well known window functions that modify the array response pattern. Harris' review [36] on the use of windows in discrete Fourier transforms and temporal spectral analysis is directly applicable in this case to spatial spectral analysis for towed line array applications.

Using the approximation $\sin\theta \cong \theta$ for small θ at array broadside, the first null in Eq. (22) occurs at $\pi L \sin\theta/\lambda = \pi$ or $\Delta\theta \times L/\lambda \cong 1$. The major conclusion drawn here for line array applications is that [4,10]:

$$\Delta\theta \approx \lambda / L \text{ and } \Delta f \times T = 1 \tag{26}$$

where $T=M_S/F_S$ is the sensor time series length. Both the above relations in Eq. (26) express the well known temporal and spatial resolution limitations in line array applications that form the driving force and motivation for adaptive and synthetic aperture signal processing that we will discuss later.

An additional constraint for sonar and ultrasound applications requires that the frequency resolution Δf of the hydrophone time series for spatial spectral analysis that is based on FFT beamforming processing must be such that

$$\Delta f \times \frac{L}{c} \langle\langle 1 \tag{27}$$

in order to satisfy *frequency quantization* effects associated with discrete frequency domain beamforming following the FFT of sensor data [17,42]. This is because, in conventional beamforming **F**inite-duration **I**mpulse **R**esponse (FIR) filters are used to provide realizations in designing digital phase shifters for beam steering. Since fast-convolution signal processing operations are part of the processing flow of a sonar signal processor, the effective beamforming filter length needs to be considered as the overlap size between successive snapshots. In this way, the overlap process will account for the wraparound errors that arise in the fast-convolution processing [1,40-42]. It has been shown [42] that an approximate estimate of the effective beamforming filter length is provided by Eqs. (25) and (27).

Because of the linearity of the conventional beamforming process, an exact equivalence of the frequency domain narrowband beamformer with that of the time-domain beamformer for broadband signals can be derived [42,43]. Based on the model of Figure 2, the time-domain beamformer is simply a time delaying [43] and summing process across the hydrophones of the line array, which is expressed by,

$$b(\theta_s, t_i) = \sum_{n=1}^{N} x_n(t_i - \tau_s) \tag{28}$$

Since,

$$b(\theta_S, t_i) = \mathrm{IFFT}\{B(f, \theta_S)\} \tag{29}$$

by using FFTs and fast convolution procedures, continuous beam-time sequences can be obtained at the output of the frequency domain beamformer [42]. This is a very useful operation when the implementation of beamforming processors in sonar systems is considered.

The beamforming operation in Eq. (28) is not restricted only for plane wave signals. More specifically, consider an acoustic source at the near field of a line array with r_s the source range and θ its bearing. Then the time delay for steering at θ is

$$\tau_s = \left(r_s^2 + d_{nm}^2 - 2 r_s d_{nm} \cos\theta\right)^{1/2} / c \tag{30}$$

As a result of Eq. (3.30), the steering vector $d_n(f, \theta_S) = exp[j2\pi f \tau_S]$ will include two parameters of interest, the bearing θ and range r_s of the source. In this case the beamformer is called *focussed beamformer*, which is used mainly in ultrasound system applications. There are, however, practical considerations restricting the application of the focused beamformer in passive sonar line array systems and these have to do with the fact that effective range focussing by a beamformer requires extremely long arrays.

3.1.2 Circular Array Conventional Beamformer

Consider *M*-sensors distributed uniformly on a ring of radius R receiving plane-wave arrivals at an azimuth angle θ and an elevation angle ϕ as shown in Figure 4. The plane-wave response of this circular array for azimuth steering θ_s and an elevation steering ϕ_s can be written as follows:

$$B(f,\theta_s,\phi_s) = \overline{D}^*(f,\theta_s,\phi_s)W(\theta_s)\overline{X}(f) \tag{31}$$

where $\overline{D}(f,\theta_s,\phi_s)$ is the steering vector with the m[th] term being expressed by $d_m(f,\theta_s,\phi_s) = \exp(j2\pi fR\sin\phi_s\cos(\theta_s-\theta_m)/c)$ and $\theta_m = 2\pi m/M$ is the angular location of the m[th] sensor with $m = 0,1,...M-1$. $W(\theta_s)$ is a diagonal matrix with the off diagonal terms being zero and the diagonal terms being the weights of a spatial window to reduce the side-lobe structure [36]. This spatial window, in general, is not uniform and depends on the sensor location (θ_m) and the beam steering direction (θ_s). The beam power pattern $P(f,\theta_s,\phi_s)$ is given by $P(f,\theta_s,\phi_s) = B(f,\theta_s,\phi_s)\times B^*(f,\theta_s,\phi_s)$. The azimuth angular response of the circular array covers the range $[0\ ,\ 2\pi]$ and therefore there is no ambiguity with respect to the azimuth angle θ.

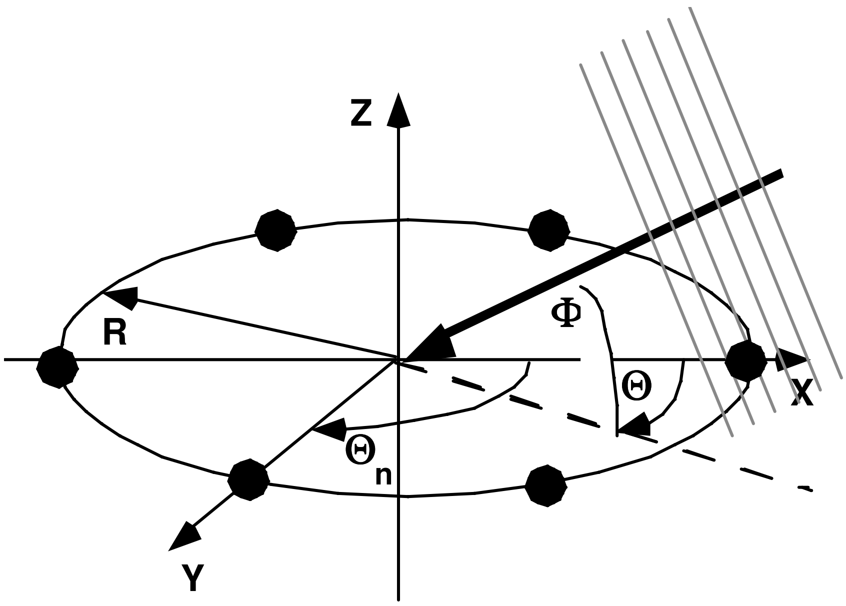

Figure 4: Geometric configuration and coordinate system for a circular array of sensors.

3.2 Multidimensional (3-D) Array Conventional Beamformer

Presented in this section is a generic approach to decompose the planar, cylindrical and spherical array beamformers into coherent sub-sets of line and/or circular array beamformers. In this report, we will restrict the discussion on 3D arrays with cylindrical and planar geometric configuration. The details of the decomposition process for spherical arrays are similar and can be found in [7,25-28].

3.2.1 Decomposition Process for 2-D & 3-D Sensor Array Beamformers

3.2.1.1 Cylindrical Array Beamformer

Consider the cylindrical array shown in Figure 5 with $\aleph$ sensors and $\aleph = NM$, where N is the number of circular rings and M is the number of sensors on each ring. The angular response of this cylindrical array to a steered direction at (θ_s, ϕ_s) can be expressed as

$$B(f,\theta_s,\phi_s) = \sum_{r=0}^{N-1}\sum_{m=0}^{M-1} w_{r,m} X_{r,m}(f) d^*_{r,m}(f,\theta_s,\phi_s) \tag{32}$$

where $w_{r,m}$ is the (r,m)$^{\text{th}}$ term of a 3-D spatial window, $X_{r,m}(f)$ is the (r,m)$^{\text{th}}$ term of the matrix $\underline{X}(f)$, or $X_{r,m}(f)$ is the Fourier transform of the signal received by the m$^{\text{th}}$ sensor on the r$^{\text{th}}$ ring and $d_{r,m}(f,\theta_s,\phi_s) = \exp\{j2\pi f[(r\delta_z \cos\phi_s + R\sin\phi_s \cos(\theta_s - \theta_m)/c)]\}$ is the (r,m)$^{\text{th}}$ steering term of $\overline{D}(f,\theta_s,\phi_s)$. R is the radius of the ring, δ_z is the distance between each ring along z-axis, r is the index for the r$^{\text{th}}$ ring and $\theta_m = 2\pi m/M$, $m = 0,1,\ldots,M-1$. Assuming $w_{r,m} = w_r \times w_m$, Eq. (32) can be re-arranged as follows:

$$B(f,\theta_s,\phi_s) = \sum_{r=0}^{N-1} w_r d^*_r(f,\theta_s,\phi_s) \left[\sum_{m=0}^{M-1} X_{r,m}(f) w_m d^*_m(f,\theta_s,\phi_s) \right] \tag{33}$$

where $d_r(f,\theta_s,\phi_s) = \exp\{j2\pi f(r\delta_z \cos\phi_s / c)\}$ is the r$^{\text{th}}$ term of the steering vector for line-array beamforming, w_r is the r$^{\text{th}}$ term of a spatial window for line array spatial shading, $d_m(f,\theta_s,\phi_s) = \exp\{j2\pi f(R\sin\phi_s \cos(\theta_s - \theta_m)/c)\}$ is the m$^{\text{th}}$ term of the steering vector for a circular beamformer, discussed in Section 1, and w_m is the m$^{\text{th}}$ term of a spatial window for circular array shading.

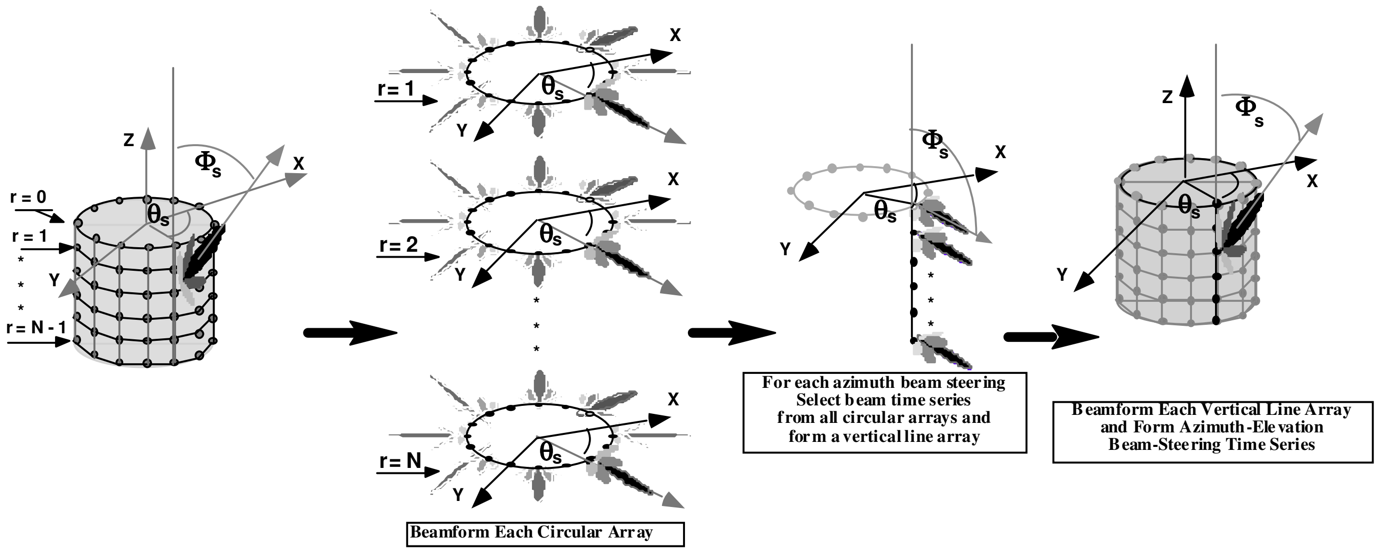

Figure 5: Coordinate system and geometric representation of the concept of decomposing a cylindrical array beamformer. The $\aleph = NM$ sensor cylindrical array beamformer consists of N circular arrays with M being the number of sensors in each circular array. Then, the beamforming structure for cylindrical arrays is reduced into coherent sub-sets of circular (for 0^o - 360^o azimuth bearing estimates) and line array (for 0^o - 180^o angular elevation bearing estimates) beamformers.

Thus, Eq. (33) suggests the decomposition of the cylindrical array beamformer into two steps, which is a well-known process in array theory. The first step is to perform circular array beamforming for each of the *N* rings with *M* sensors on each ring. The second step is to perform line array beamforming along z-axis on the *N*-beam time series outputs of the first step. This kind of implementations, which is based on the decomposition of the cylindrical beamformer into line and circular array beamformers is shown in Figure 5. The coordinate system is identical to that shown in Figure 4. The decomposition process of Eq. (33) makes also the design and incorporation of 3-D spatial windows much simpler. Non-uniform shading windows can be applied to each circular beamformer to improve the angular response with respect to the azimuth angle, θ. A uniform shading window can then be applied to the line array beamformer to improve the angular response with respect to the elevation angle, ϕ. Moreover, the decomposition process, shown in Figure 5, leads to an efficient implementation in computing architectures based on the following two factors:

- The number of sensors for each of these circular and line array beamformers is much less than the total number of sensors, $\aleph$, of the cylindrical array. This kind of decomposition process for the 3-D beamformer eliminates the need for very large memory and CPU's with very high throughput requirements in one board for real time system applications.
- All the circular and line array beamformers can be executed in parallel, which allows their implementations in much simpler parallel architectures with simpler CPU's, which is a practical requirement for real time system applications.

Thus, under the restriction $w_{r,m} = w_r$ x w_m for 3-D spatial shading, the decomposition process provides equivalent beam time series with those that would have been provided by a 3-D cylindrical beamformer, as this is shown by Eqs. (32) & (33).

3.2.1.2 Planar Array Beamformer

Consider the discrete planar array shown in Figure 6 with $\aleph$ sensors where $\aleph = NM$ and M, N are the number of sensors along x-axis and y-axis, respectively. The angular response of this planar array to a steered direction (θ_s, ϕ_s) can be expressed as

$$B(f,\theta_s,\phi_s) = \sum_{r=0}^{N-1}\sum_{m=0}^{M-1} w_{r,m} X_{r,m}(f) d^*_{r,m}(f,\theta_s,\phi_s) \tag{34a}$$

where $w_{r,m}$ is the (r,m)th term of matrix $W(\theta,\phi)$ including the weights of a 2-D spatial window, $X_{r,m}(f)$ is the (r,m)th term of the matrix $\underline{X}(f)$ including the Fourier transform of the received signal by the (m,r)th sensor along x-axis and y-axis, respectively. $\underline{D}(f,\theta_s,\phi_s)$ is the steering matrix having its (r,m)th term defined by

$$d_{r,m}(f,\theta_s,\phi_s) = \exp(j2\pi f(m\delta_x \sin\theta_s + r\delta_y \cos\theta_s \cos\phi_s)/c) \tag{34b}$$

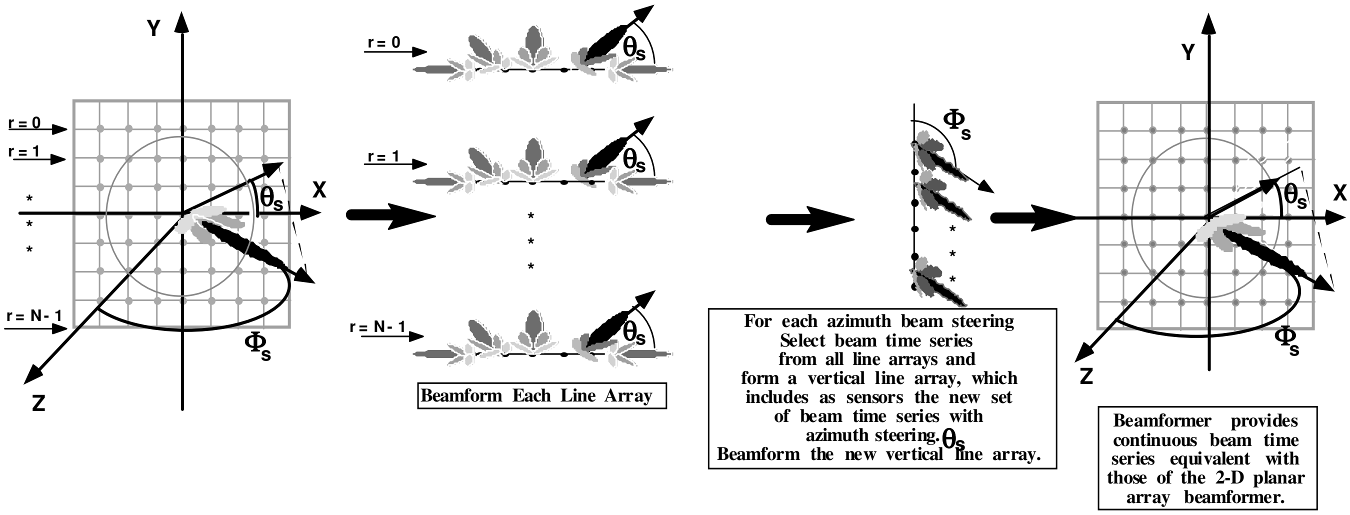

Figure 6: Coordinate system and geometric representation of the concept of decomposing a planar array beamformer. The $\aleph = NM$ sensor planar array beamformer consists of N line arrays with M being the number of sensors in each line array. Then, the beamforming structure for planar arrays is reduced into coherent sub-sets of line (for 0^o - 180^o azimuth bearing estimates) and line array (for 0^o - 180^o elevation bearing estimates) beamformers.

Assuming that the matrix of spatial shading (weighting) $W(\theta,\phi)$ is separable (i.e., $\underline{W}(\theta,\phi) = \underline{W}_1(\theta)\underline{W}_2(\phi)$), Eq. (34) can be simplified as follows:

$$B(f,\theta_s,\phi_s) = \sum_{r=0}^{N-1} w_{1,r} d_r^*(f,\theta_s,\phi_s) \left[\sum_{m=0}^{M-1} w_{2,m} X_{r,m}(f) d_m^*(f,\theta_s,\phi_s) \right] \tag{35a}$$

where, $d_r(f,\theta_s,\phi_s) = \exp(j2\pi fr\delta_y \cos\theta_s \cos\phi_s / c)$, is the rth term of the steering vector, $\overline{D}_y(f,\theta_s,\phi_s)$ and $d_m(f,\theta_s,\phi_s) = \exp(j2\pi fm\delta_x \sin\theta_s / c)$ is the mth term of the steering vector, $\overline{D}_x(f,\theta_s,\phi_s)$. The summation term enclosed by parenthesis in Eq. (35a) is equivalent to the response of a line array beamformer along x-axis. Then all the steered beams from this summation term form a vector denoted by $\overline{B}_y(f,\theta_s)$. This vector defines a line array with directional sensors, which are the beams defined by the second summation process of Eq. (35a). Therefore Eq. (35a) can be expressed as:

$$B(f,\theta_s,\phi_s) = \overline{D}_y^*(f,\theta_s,\phi_s)\underline{W}_1(\theta)\overline{B}_y(f,\theta_s) \tag{35b}$$

Eq. (35b) suggests that the 2-D planar array beamformer can be decomposed into two line array beamforming steps. The first step includes a line-array beamforming along x-axis and will be repeated N- times to get the vector $\overline{B}_y(f,\theta_s)$ that includes the beam times series $b_r(f,\theta_s)$, where the index $r = 0,1,..., N-1$ is along the axis y. The second step includes line array beamforming along y-axis and will be done only once by treating the vector $\overline{B}_y(f,\theta_s)$ as the input signal for the line array beamformer to get the output $B(f,\theta_s,\phi_s)$. The separable spatial windows can now be applied separately on each line-array beamformer to suppress side-lobe structures. Figure 6 shows the involved steps of decomposing the 2-D planar array beamformer into two steps of line-array beamformers. The coordinate system is identical with that shown in Figure 3. The decomposition of the planar array beamformer into these two line-array beamforming steps leads to an efficient implementation based on the following two factors. First, the number of the involved sensors for each of these line array beamformers is much less than the total number of sensors, $\aleph$ of the planar array. This kind of decomposition process for the 2-D beamformer eliminates the need for very large memory and CPU's with very high throughput requirements in one board for real time system applications. Secondly, all these line array beamformers can be executed in parallel, which allows their implementation in much simpler parallel architectures with simpler CPU's, which is a practical requirement for real time system application. Besides the advantage of the efficient implementation, the proposed decomposition approach makes the application of the spatial window much simpler to be incorporated.

3.3 Influence of the Medium's Propagation Characteristics on the Performance of a Receiving Array

In ocean acoustics and medical ultrasound imaging the wave propagation problem is highly complex due to the spatial properties of the non-homogeneous underwater and human body mediums. For stationary source and receiving arrays, the space time properties of the acoustic pressure fields include a limiting resolution imposed by these mediums. This limitation is due either to the angular spread of the incident energy about a single arrival as a result of the scattering phenomena, or to the multipaths and their variation over the aperture of the receiving array.

More specifically, an acoustic signal that propagates through anisotropic mediums will interact with the transmitting medium microstructure and the rough boundaries, resulting in a net field that is characterized by irregular spatial and temporal variations. As a consequence of these interactions, a point source detected by a high-angular resolution receiver is perceived as a source of finite extent. It has been suggested [47] that due to the above spatial variations the sound field consists not of parallel, but of superimposed wavefronts of different directions of propagation. As a result, coherence measurements of this field by a receiving array give an estimate for the spatial coherence function. In the model for the spatial uncertainty of the above study [47], the width of the coherence function is defined as the coherence length of the medium and its reciprocal value is a measure of the angular uncertainty caused by the scattered field of the underwater environment.

By the *coherence* of acoustic signals in the sea or the human body, we mean the degree to which the acoustic pressures are the same at two points in the medium of interest located a given distance and direction apart. Pressure sensors placed at these two points will have phase coherent outputs if the received acoustic signals are perfectly coherent; if the two sensor outputs, as a function of space or time, are totally dissimilar, the signals are said to be incoherent. Thus, the loss of spatial coherence results in an upper limit on the useful aperture of a receiving array of sensors [10]. Consequently, knowledge of the angular uncertainty of the signal caused by the medium is considered essential in order to determine quantitatively the influence of the medium on the array gain, which is also influenced significantly by a partially directive anisotropic noise background. Therefore, for a given non-isotropic medium, it is desirable to estimate the optimum array size and achievable array gain for sonar and ultrasound array applications.

For geometrical simplicity and without any loss of generality we consider the case of a receiving line array. Quantitative estimates of the spatial coherence for a receiving line array are provided by the cross spectral density matrix in frequency domain between any set of two sensor time series of the line array. An estimate of the cross spectral density matrix *R(f)* with its nm[th] term defined by

$$R_{nm}(f,\delta_{nm}) = E\left[X_n(f)X_m^*(f)\right] \tag{36}$$

The above space-frequency correlation function can be related to the angular power directivity pattern of the source, $\Psi_S(f,\theta)$, via a Fourier transformation by using a generalization of Bello's concept [48] of time-frequency correlation function $\left[t \Leftrightarrow 2\pi f\right]$ into space $\left[\delta_{nm} \Leftrightarrow 2\pi f \sin\theta / c\right]$, which gives

$$R_{nm}(f,\delta_{nm}) = \int_{-\pi/2}^{\pi/2} \Psi_s(f,\theta)\exp\left[\frac{-j2\pi f\delta_{nm}\theta}{c}\right]d\theta \tag{37}$$

or

$$\Psi_s(f,\theta) = \int_{-N\delta/2}^{N\delta/2} R_{nm}(f,\delta_{nm})\exp\left[\frac{j2\pi f\delta_{nm}\theta}{c}\right]d\left(\delta_{nm}\right) \tag{38}$$

The above transformation can be converted into the following summation:

$$R_{nm}(f_o,\delta_{nm}) = \Delta\theta \sum_{g=-G/2}^{G/2} \Psi_s(f_o,\theta_g)\exp\left[\frac{-j2\pi f_o\delta_{nm}\sin(g\Delta\theta)}{c}\right]\cos(g\Delta\theta) \tag{39}$$

where $\Delta\theta$ is the angle increment for sampling the angular power directivity pattern, $\theta_g = g\Delta\theta$, g is the index for the samples and G is the total number of samples.

For line array applications, the power directivity pattern (calculated for a homogeneous free space) due to a distant source, which is treated as a point source, should be a delta function. Estimates, however, of the source's directivity from a line array operating in an anisotropic ocean are distorted by the underwater medium. In other words, the directivity pattern of the received signal is the convolution of the original pattern and the angular directivity of the medium (i.e., the angular scattering function of the underwater environment). As a result of the above, the angular pattern of the received signal, by a receiving line array system, is the scattering function of the medium.

In this report, the concept of spatial coherence is used to determine the statistical response of a line array to the acoustic field. This response is the result of the multipath and scattering phenomena discussed before, and there are models [10,47] to relate the spatial coherence with the physical parameters of an anisotropic medium for measurement interpretation. In these models, the interaction of the acoustic signal with the transmitting medium is considered to result in superimposed wavefronts of different directions of propagation. Then Eqs. (21), (22), which define a received sensor signal from a distant source, are expressed by

$$x_n(t_i) = \sum_{l=1}^{J} A_l \exp\left[-j2\pi f_l \left(t_i - \frac{\delta(n-1)}{c}\, \theta_l\right) \right] + \varepsilon_{n,i}(0, \sigma_e) \tag{40}$$

where $l = 1, 2, \ldots, J$, and J is the number of superimposed waves. As a result, a generalized form of the crosscorrelation function between two sensors, which has been discussed by Carey and Moseley [10], is

$$R_{nm}(f, \delta_{nm}) = \bar{X}^2(f) \exp\left[-\left(\frac{\delta_{nm}}{L_c} \right)^k \right], \quad k = 1, \quad or \quad 1.5 \quad or \quad 2, \tag{41}$$

(3.41)

where L_c is the correlation length and $\bar{X}^2(f)$ is the mean acoustic intensity of a received sensor time sequence at the frequency bin f. A more explicit expression for the Gaussian form of Eq. (41) is given in [47],

$$R_{nm}(f, \delta_{nm}) \approx \bar{X}^2(f) \exp\left[-\left(\frac{2\pi f \delta_{nm} \sigma_\theta}{c} \right)^2 / 2 \right] \tag{42}$$

and the crosscorrelation coefficients are given from

$$\rho_{nm}(f, \delta_{nm}) = R_{nm}(f, \delta_{nm}) / \bar{X}^2(f). \tag{43}$$

At the distance $L_c = c / (2\pi f \sigma_\theta)$, called "*the coherence length* ", the correlation function in Eq. (3.43) will be 0.6. This critical length is determined from experimental coherence measurements plotted as a function of δ_{nm}. Then a connection between the medium's angular uncertainty and the measured coherence length is derived as

$$\sigma_\theta = 1 / L_c, \qquad and \qquad L_c = 2\pi\delta_{1m} f / c \tag{44}$$

here δ_{1m} is the critical distance between the first and the m th sensors at which the coherence measurements get smaller than 0.6. Using the above parameter definition, the effective aperture size and array gain of a deployed towed line array can be determined [10,47] for a specific underwater ocean environment.

Since the correlation function for a Gaussian acoustic field is given by Eq. (42), the angular scattering function $\Phi(f,\theta)$ of the medium can be derived. Using Eq. (38) and following a rather simple analytical integral evaluation, we have

$$\Phi(f,\theta) = \frac{1}{\sigma_\theta \sqrt{2\pi}} \exp\left[-\frac{\theta^2}{2\sigma_\theta^2} \right], \tag{45}$$

where $\sigma_\theta = c/(2\pi f \delta_{nm})$. This is an expression for the angular scattering function of a Gaussian underwater ocean acoustic field [10,47].

It is apparent from the above discussion that the estimates of the cross-correlation coefficients $\rho_{nm}(f_i, \delta_{nm})$ are necessary in order to define experimentally the coherence length of an underwater or human body medium. For details on experimental studies on coherence estimation for underwater sonar applications the reader may review the references [10, 30].

3.4 Array Gain

The performance of a line array to an acoustic signal embodied in a noise field is characterized by the "*array gain* " parameter, **AG**. The mathematical relation of this parameter is defined by

$$AG = 10 \log \frac{\sum_{n=1}^{N} \sum_{m=1}^{N} \bar{\rho}_{nm}(f, \delta_{nm})}{\sum_{n=1}^{N} \sum_{m=1}^{N} \bar{\rho}_{\varepsilon,nm}(f, \delta_{nm})} \tag{46}$$

Where $\rho_{nm}(f_i, \delta_{nm})$ and $\rho_{\varepsilon,nm}(f, \delta_{nm})$ denote the normalized cross-correlation coefficients of the signal and noise field, respectively. Estimates of the correlation coefficients are given from Eq. (43).

If the noise field is isotropic that it is not partially directive, then the denominator in Eq. (49) is equal to N, (i.e. $\sum_{n=1}^{N}\sum_{m=1}^{N}\rho_{\varepsilon,nm}(f,\delta_{nm}) = N$), because the non diagonal terms of the cross-correlation matrix for the noise field are negligible. Then Equation (46) simplifies to,

$$AG = 10\log\frac{\sum_{n=1}^{N}\sum_{m=1}^{N}\rho_{nm}(f,\delta_{nm})}{N} \tag{47}$$

For perfect spatial coherence across the line array the normalized crosscorrelation coefficients are $\rho_{nm}(f,\delta_{nm}) \cong 1$ and the expected values of the array gain estimates are, $AG = 10\times\log N$. For the general case of isotropic noise and for frequencies smaller than the towed array's design frequency the array gain term **AG** is reduced to the quantity called Directivity Index,

$$DI = 10\times\log\left[(N-1)\delta/(\lambda/2)\right] \tag{48}$$

When $\delta << \lambda$ and the conventional beamforming processing is employed, Eq. (26) indicates that the deployment of very long line arrays is required in order to achieve sufficient array gain and angular resolution for precise bearing estimates. Practical deployment considerations, however, usually limit the overall dimensions of a hull mounted line or towed array. In addition, the medium's spatial coherence [10, 30] sets an upper limit on the effective towed array length. In general, the medium's spatial coherence length is of the order of $O(10^2)\lambda$ [10,30]. In addition to the above, for sonar systems very long towed arrays suffer degradation in the array gain due to array shape deformation and increased levels of self noise [49-53]. Although, towed line array shape estimation techniques [53] have solved the array deformation problem during course alterations of the vessels towing these arrays, the deployment issues of long towed arrays in littoral waters remains a prohibited factor for their effective use in sonar surveillance operations.

Alternatives to large aperture sonar arrays are signal processing schemes discussed in [1]. Theoretical and experimental investigations have shown that bearing resolution and detectability of weak signals in the presence of strong interferences can be improved by applying non-conventional beamformers such as adaptive beamforming [1-5,17-24], or acoustic synthetic aperture processing [1,11-16] to the sensor time series of deployed short sonar and ultrasound arrays, which are discussed in the next section.

4 Advanced Beamformers

4.1 Synthetic Aperture Processing

Various synthetic aperture techniques have been investigated to increase signal gain and improve angular resolution for line array systems. While these techniques have been successfully applied to aircraft and satellite-active radar systems, they have not been successful with sonar and ultrasound systems. In this section we will review synthetic aperture techniques that have been tested successfully with real data [11-16]. They are summarized in terms of their experimental implementation and the basic approach involved.

Let us start with the a few theoretical remarks. The plane wave response of a line array to a distant monochromatic signal, received by the n[th] element of the array, is expressed by Eqs. (20), (21) and (22). In the above expressions, the frequency f includes the Doppler shift due to a combined movement of the receiving array and the source (or object reflecting the incoming acoustic wavefront) radiating signal. Let υ, denote the relative speed; it is assumed here that the component of the source's velocity along its bearing is negligible. If f_o is the frequency of the stationary field, then the frequency of the received signal is expressed by

$$f = f_o(1 \pm \upsilon \sin\theta / c) \tag{49}$$

and an approximate expression for the received sensor time series (15) and (40) is given by

$$x_n(t_i) = A\exp\left[j2\pi f_o\left(t_i - \frac{\upsilon t_i + (n-1)\delta}{c}\sin\theta \right)\right] + \varepsilon_{n,i} \tag{50}$$

τ seconds later, the relative movement between the receiving array and the radiated source is $\upsilon\tau$. By proper choice of the parameters υ and τ, we have $\upsilon\tau = q\delta$, where q represents the number of sensor positions that the array has moved, and the received signal, $x_n(t_i+\tau)$ is expressed by,

$$x_n(t_i+\tau) = \exp(j2\pi f_o\tau) A\exp\left[j2\pi f_o\left(t_i - \frac{\upsilon t_i + (q+n-1)\delta}{c}\sin\theta \right)\right] + \varepsilon^{\tau}_{n,i} \tag{51}$$

As a result, we have the Fourier transform of $x_n(t_i+\tau)$, as

$$\tilde{X}_n(f)_\tau = \exp(j2\pi f_o\tau)\tilde{X}_n(f) \tag{52}$$

where $\tilde{X}_n(f)_\tau$ and $\tilde{X}_n(f)$ are the DFTs of $x_n(t_i+\tau)$, and $x_n(t_i)$, respectively. If the phase term $\exp(-j2\pi f_o\tau)$ is used to correct the line array measurements shown in (52), then the spatial information included in the successive measurements at $t=t_i$ and $t=t_i+\tau$ is equivalent to that derived from a line array of (q+N) sensors. When idealized conditions are assumed, the phase correction factor for (49) in order to form a synthetic aperture, is $\exp(-j2\pi f_o\tau)$. However, this phase correction estimate requires *a priori* knowledge of the source receiver relative speed, υ and accurate estimates for the frequency f of the received signal. An additional restriction is that the synthetic aperture processing techniques have to compensate for the disturbed paths of the receiving array during the integration period that the synthetic aperture is formed. Moreover, the temporal coherence of the source signal should be greater or at least equal to the integration time of the synthetic aperture.

At this point it is important to review a few fundamental physical arguments associated with passive synthetic aperture processing. In the past [13] there was a conventional wisdom regarding synthetic aperture techniques, which held that practical limitations prevent them from being applicable to real-world systems. The issues were threshold.

1. Since passive synthetic aperture can be viewed as a scheme that converts temporal gain to spatial gain, most signals of interest do not have sufficient temporal coherence to allow a long spatially coherent aperture to be synthesized.

2. Since past algorithms required *a priori* knowledge of the source frequency in order to compute the phase correction factor, as shown by (3.49)-(3.52), the method was essentially useless in any bearing estimation problem since Doppler would introduce an unknown bias on the frequency observed at the receiver.

3. Since synthetic aperture processing essentially converts temporal gain to spatial gain, there was no "new" gain to be achieved, and therefore, no point to the method.

Recent work [12-16] has shown that there can be realistic conditions under which all of these objections are either not relevant or do not constitute serious impediments to practical applications of synthetic aperture processing in operational systems [1]. Theoretical discussions have shown [13] that the above three arguments are valid for cases that include the formation of synthetic aperture in mediums with isotropic noise characteristic. However, when the noise characteristics of the received signal are non-isotropic and the receiving array includes more than one sensor, then there is spatial gain available from passive synthetic aperture processing and this has been discussed analytically in [13]. Recently, there have been only two passive synthetic aperture techniques [11-16,54] and an MLE estimator [12] published in the open literature that deal successfully with the above restrictions. In this section, they are summarized in terms of their experimental implementation for sonar and ultrasound applications. For more details about these techniques the reader may review the references [11-16, 54, 55].

4.1.1 FFT Based Synthetic Aperture Processing (FFTSA Method)

Shown in the upper part of Figure 7, under the title *Physical Aperture*, are the basic processing steps of Eqs. (3.20-3.23) for conventional beamforming applications including line arrays. This processing includes the generation of the aperture function of the line array via FFT transformation (i.e., Eq. (22)), with the beamforming done in the frequency domain. The output (i.e., Eq. (23)) provides the directionality power pattern of the acoustic signal/noise field received by the N sensors of the line array. As an example, the theoretical response of the power pattern for a 64-sensor line array is given in Figure 8. In the lower part of Figure 7, under the title *Synthetic Aperture*, the concept of an FFT based synthetic aperture technique called FFTSA [55], is presented. The experimental realization of this method includes:

1. the time series acquisition, using the N sensor line array, of a number M of snapshots of the acoustic field under surveillance taken every τ seconds,

2. the generation of the aperture function for each of the M snapshots,

3. the beamforming in the frequency domain of each generated aperture function.

This beamforming processor provides M beam patterns with N beams each. For each beam of the beamforming output, there are M time-dependent samples with a τ seconds sampling interval.

The FFT transformation in the time domain of the M time-dependent samples of each beam provides the synthetic aperture output, which is expressed analytically by Eq. (53). For more details please refer to [55].

$$P(f,\theta_s)_M = \left\{ \frac{\sin\left[N \frac{\pi\delta}{\lambda} (\sin\theta_s) \right]}{\sin\left[\frac{\pi\delta}{\lambda} (\sin\theta_s) \right]} \cdot \frac{\sin\left[M \frac{N}{2} \frac{\pi\delta}{\lambda} (\sin\theta_s) \right]}{\sin\left[\frac{N}{2} \frac{\pi\delta}{\lambda} (\sin\theta_s) \right]} \right\}^2 \tag{53}$$

The above expression assumes that $\upsilon\tau = (N\delta)/2$, which indicates that there is a 50% spatial overlap between two successive set of the M measurements and that the source bearing of θ is approximately at the boresight. The azimuthal power pattern of Eq. (53) for the beamforming output of the FFTSA method is shown in Figure 9.

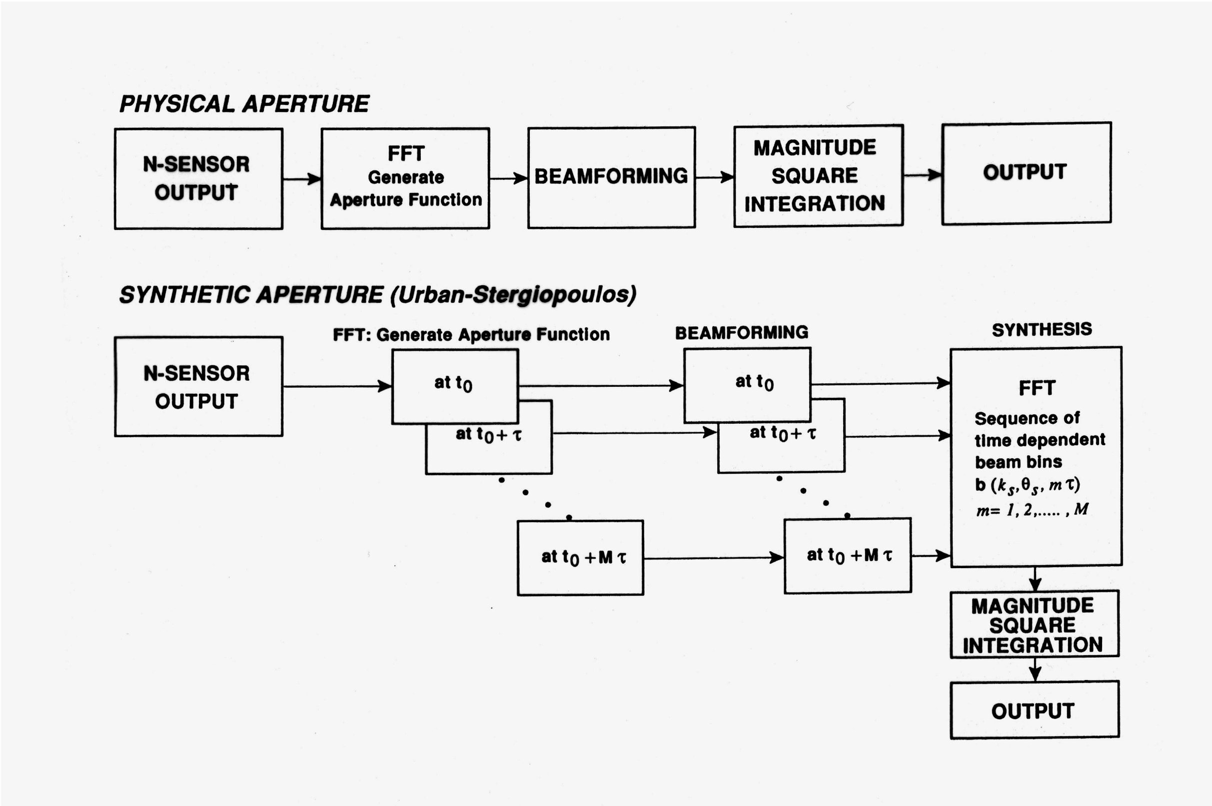

Figure 7: Shown in the upper part under the title Physical Aperture is conventional beamforming processing in the frequency domain for a physical line array. Presented in the lower part under the title Synthetic Aperture is the signal processing concept of the FFTSA method.

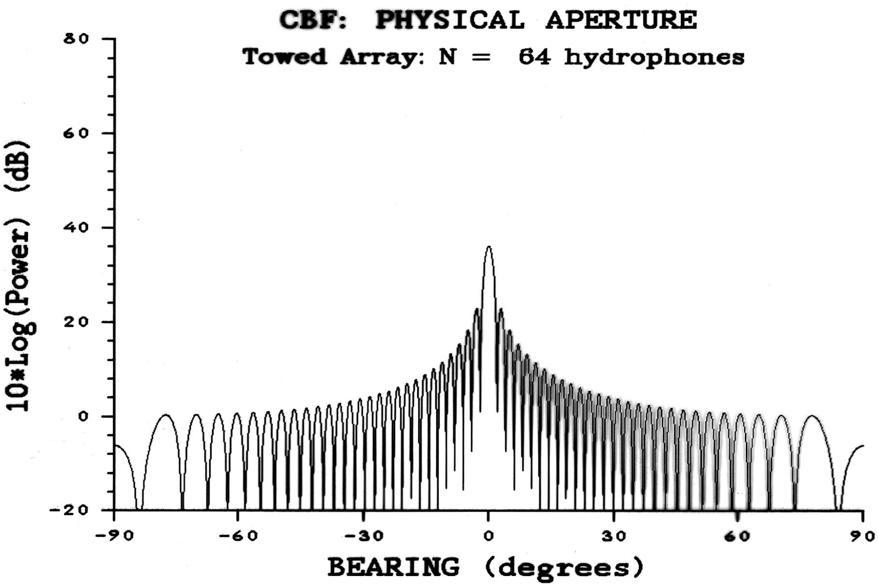

Figure 8: The azimuth power pattern from the beamforming output of the 64-sensor line array considered for the synthetic aperture processing in Figure 9.

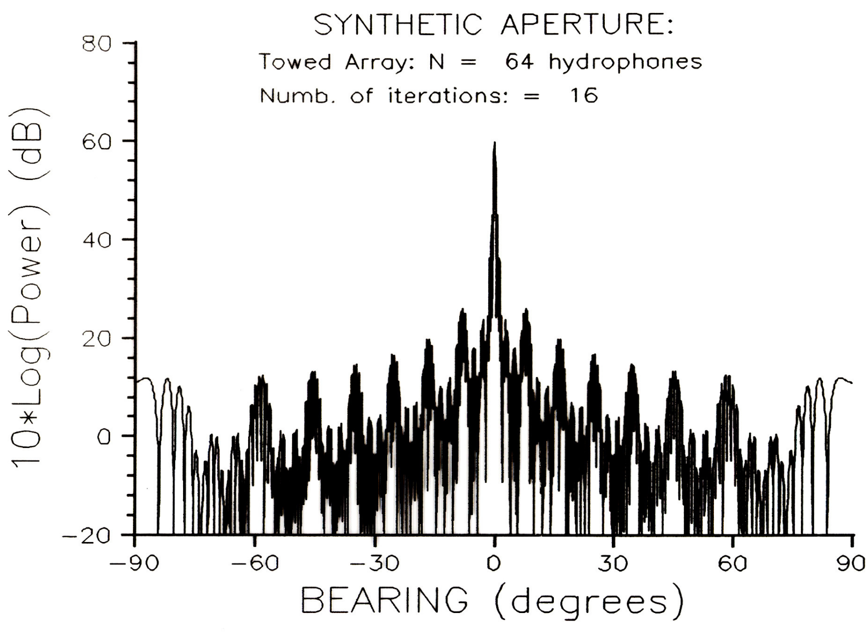

Figure 9: The azimuth power pattern from the beamforming output of the FFTSA method.

4.1.2 Yen & Carey's Synthetic Aperture Method

The concept of the experimental implementation of Yen and Carey's synthetic aperture method [54] is shown in Figure 10, which is also expressed by the following relation,

$$B(f_o, \theta_s)_M = \sum_{m=1}^{M} b(f_o, \theta_s)_{m\tau} \exp(-j\phi_m) \tag{54}$$

which assumes that estimates of the phase corrector ϕ_m require knowledge of the relative source receiver speed, υ or the velocity filter concept, introduced by Yen and Carey [54]. The basic difference of this method [54] with the FFTSA [55] technique is the need to estimate a phase correction factor ϕ_m in order to synthesize the M time-dependent beam patterns. Estimates of ϕ_m are given by

$$\phi_m = 2\pi f_o (1 \pm \upsilon \sin\theta_s / c) m\tau \tag{55}$$

and the application of a velocity filter concept for estimating the relative source receiver speed, υ. This method has been successfully applied to experimental sonar data including CW signals and the related application results have been reported [10,54].

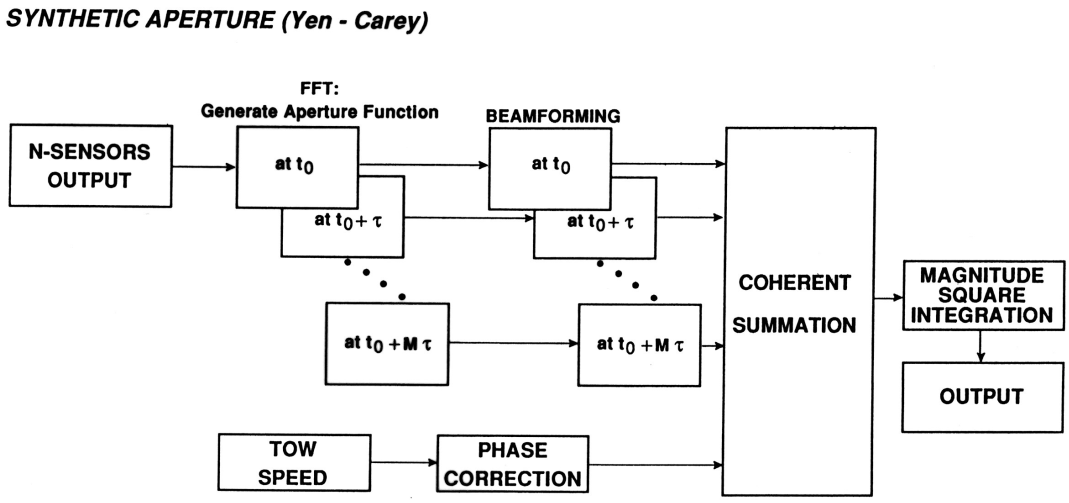

Figure 10: The concept of the experimental implementation of Yen-Carey's synthetic aperture method is shown under the same arrangement as the FFTSA method for comparison.

4.1.3 Nuttall's MLE Method for Synthetic Aperture Processing

It is also important to mention here the development by Nuttall [12] of an MLE estimator for synthetic aperture processing. This MLE estimator requires the acquisition of very long sensor time series over an interval T, which corresponds to the desired length υT of the synthetic aperture. This estimator includes searching for the values of ϕ and ω that maximize the term,

$$MLE(\omega,\phi) = \left| \Delta t \sum_{n=0}^{N-1} \exp(-jn\phi) \left[\sum_{m=1}^{M} x_n(m\Delta t) \exp(-jm\Delta t\omega) \right] \right| \tag{56}$$

where,

$$\omega = 2\pi f_o \left(1 - \frac{\upsilon \sin\theta}{c} \right), \qquad \phi = \frac{\delta}{c} 2\pi f_o \sin\theta \tag{57}$$

The above relations indicate that the N complex vectors $X_n(\omega) = \sum_{m=1}^{M} x_n(t_m)\exp(-j\omega\Delta t)$, which give the spectra for the very long sensor time series $x_n(t)$ at ω, are phased together by searching ϕ over *(-p, p)*, until the largest vector length occurs in (56). Estimates of (θ, f), are determined from (57) using the values of ϕ and ω, that maximize (56). The MLE estimator has been applied on real sonar data sets and the related application results have been reported [12].

A physical interpretation of the above synthetic aperture methods is that the realistic conditions for effective acoustic synthetic aperture processing can be viewed as schemes that convert temporal gain to spatial gain. Thus a synthetic aperture method requires that successive snapshots of the received acoustic signal have good cross-correlation properties in order to synthesize an extended aperture and the speed fluctuations are successfully compensated by means of processing. It has been also suggested [11-16] that the prospects for successfully extending the physical aperture of a line array require algorithms which are not based on the synthetic aperture concept used in active radars. The reported results in [10-16,54,55] have shown that the problem of creating an acoustic synthetic aperture is centered on the estimation of a phase correction factor, which is used to compensate for the phase differences between sequential line-array measurements in order to coherently synthesize the spatial information into a synthetic aperture. When the estimates of this phase correction factor are correct, then the information inherent in the synthetic aperture is the same as that of an array with an equivalent physical aperture [11-16].

4.1.4 Spatial Overlap Correlator for Synthetic Aperture Processing (ETAM Method)

Recent theoretical and experimental studies have addressed the above concerns and indicated that the space and time coherence of the acoustic signal in the sea [10-16] appears to be sufficient to extend the physical aperture of a moving line array. In the above studies the fundamental question related to the angular resolution capabilities of a moving line array and the amount of information inherent in a received signal have been addressed. These investigations included the use of the CRLB analysis and showed that for long observation intervals of the order of 100 seconds the additional information provided by a moving line array over a stationary array is expressed as a large increase in angular resolution, which is due to the Doppler caused by the movement of the array (see Figure 3 in [12]). A summary of these research efforts has been reported in a special issue in the IEEE J. Oceanic Eng. [13]. The synthetic aperture processing scheme that has been used in broadband sonar applications [1] is based on the Extended Towed Array Measurements (ETAM) algorithm, which was invented by Stergiopoulos and Sullivan [11]. The basic concept of this algorithm is a phase-correction factor that is used to combine coherently successive measurements of the towed array to extend the effective towed array length.

Shown in Figure 11 is the experimental implementation of the ETAM algorithm in terms of the line array speed and sensor positions as a function of time and space. Between two successive positions of the N-sensor line array with sensor spacing δ, there are $(N-q)$ pairs of space samples of the acoustic field that have the same spatial information, their difference being a phase factor [11-12,55] related to the time delay these measurements were taken. By cross-correlating the (N-q) pairs of the sensor time series that overlap, the desired phase correction factor is derived, which compensates for the time delay between these measurements and the phase fluctuations caused by irregularities of the tow path of the physical array or relative speed between source and receiver; this is called the *overlap correlator*. Following the above, the key parameters in the ETAM algorithm are the time increment $\tau = q\delta/\upsilon$ between two successive sets of measurements, where υ is the tow speed and q represents the number of sensor positions that the towed array has moved during the τ seconds, or the number of sensors to which the physical aperture of the array is extended at each successive set of measurements. The optimum overlap size, $(N\text{-}q)$, which is related to the variance of the phase correction estimates, has been shown [13] to be $N/2$. The total number of sets of measurements required to achieve a desired extended aperture size is then defined by $J = (2/N)(T\upsilon/\delta)$, where T is the period taken by the towed array to travel a distance equivalent to the desired length of the synthetic aperture.

Then, for the frequency bin f_i and between two successive j[th] and (j+1)[th] snapshots, the phase-correction factor estimate is given by,

$$\hat{\Psi}_j(f_i) = \arg\left\{ \frac{\sum_{n=1}^{N/2} X_{j,(\frac{n}{2}+n)}(f_i) \times X^*_{(j+1),n}(f_i) \times \rho_{j,n}(f_i)}{\sum_{n=1}^{N/2} \rho_{j,n}(f_i)} \right\} \tag{58}$$

where, for a frequency band with central frequency f_i and observation bandwidth Δf or $f_i - \Delta f/2 < f_i < f_i + \Delta f/2$, the coefficients

$$\rho_{j,n}(f_i) = \frac{\left| \sum_{i=-Q/2}^{Q/2} X_{j,(\frac{n}{2}+n)}(f_i) \times X^*_{(j+1),n}(f_i) \right|}{\sqrt{\sum_{i=-Q/2}^{Q/2} \left| X_{j,(\frac{n}{2}+n)}(f_i) \right|^2 \times \sum_{i=-Q/2}^{Q/2} \left| X^*_{(j+1),n}(f_i) \right|^2}} \tag{59}$$

are the normalized cross-correlation coefficients or the coherence estimates between the $N/2$ pairs of sensors that overlap in space. The above coefficients are used as weighting factors in Eq. (58) in order to optimally weight the good against the bad pairs of sensors during the estimation process of the phase-correction factor.

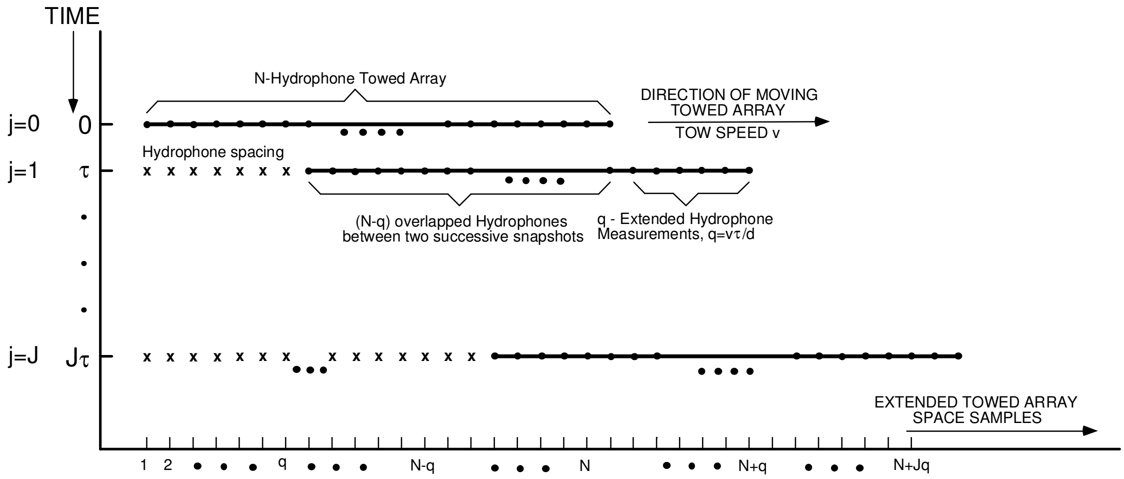

Figure 11: Concept of the experimental implementation of ETAM algorithm in terms of towed array positions and speed as a function of time and space.

The performance characteristics and expectations from the ETAM algorithm have been evaluated experimentally and the related results have been reported [1,12,55]. The main conclusion drawn from these experimental results is that for narrowband signals or for FM type of pulses from active sonar systems the overlap correlator in ETAM compensates successfully the speed fluctuations and effectively extends the physical aperture of a line array more than eight times. On the other hand, the threshold value of ETAM is -8 dB re 1-Hz band at the sensor. For values of SNR higher than this threshold, it has been shown that ETAM achieves the theoretical CRLB bounds and it has comparable performance to the maximum-likelihood estimator [12].

4.2 Adaptive Beamformers

Despite the geometric differences between the line and circular arrays, the underline beamforming processes for these arrays, as expressed by Eqs. (8) & (9) respectively, are time delay beamforming estimators, which are basically spatial filters. However, optimum beamforming requires the beamforming filter coefficients to be chosen based on the covariance matrix of the received data by the N -sensor array in order to optimize the array response [15,16], as discussed in Section 2. The family of algorithms for optimum beamforming that use the characteristics of the noise, are called *Adaptive Beamformers* [3,17,18,19,20,22,23]. In this section we will address implementation issues for various partially adaptive variants of the MVDR method and a GSC adaptive beamformer [1,37].

Furthermore, the implementation of adaptive schemes in real time systems is not restricted into one method, such as the MVDR technique that is discussed next. In fact, the generic concept of the sup-aperture multi-dimensional array introduced in the report allows for the implementation of a wide variety of adaptive schemes in operational systems [7,25-28]. As for the implementation of adaptive processing schemes in active systems, the following issues need to be addressed.

For active applications that include matched filter processing, the outputs of the adaptive algorithms are required to provide coherent beam time series to facilitate the post-processing. This means that these algorithms should exhibit near-instantaneous convergence and provide continuous beam time series that have sufficient temporal coherence to correlate with the reference signal in matched filter processing [1].

In a previous study [1], possible improvement in convergence periods of two algorithms in the sub-aperture configuration was investigated. The Griffiths-Jim Generalized Side-lobe Canceller (GSC) [18,44] coupled with the Normalized Least Mean Square (NLMS) adaptive filter [45] has been shown to provide near-instantaneous convergence under certain conditions [1,37]. The GSC/NLMS in the sub-aperture configuration was tested under a variety of conditions to determine if it could yield performance advantages, and if its convergence properties could be exploited over a wider range of conditions [1,37]. The Steered Minimum Variance Beamformer (STMV) is a variant of the Minimum Variance Distortionless Response (MVDR) beamformer [38]. By applying narrowband adaptive processing on bands of frequencies, extra degrees of freedom are introduced. The number of degrees of freedom is equal to the number of frequency bins in the processed band. In other words, increasing the number of frequency bins processed decreases the convergence time by a corresponding factor. This is due to the fact that convergence now depends on the observation time bandwidth product, as opposed to observation time in the MVDR algorithm [38,39].

The STMV beamformer in its original form was a broadband processor. In order to satisfy the requirements for matched filter processing, it was modified to produce coherent beam time series [1]. The ability of the STMV narrowband beamformer to produce coherent beam time series has been investigated in another study [37]. Also, the STMV narrowband processor was implemented in the sub-aperture configuration to produce near-instantaneous convergence and to reduce the computational complexity required. The convergence properties of both the full aperture and sub-aperture implementations have been investigated for line arrays of sensors [1,37].

4.2.1 Minimum Variance Distortionless Response (MVDR)

The goal is to optimize the beamformer response so that the output contains minimal contributions due to noise and signals arriving from directions other than the desired signal direction. For this optimization procedure it is desired to find a linear filter vector $\overline{W}(f_i,\theta)$ which is a solution to the constrained minimization problem that allows signals from the look direction to pass with a specified gain [17,18],

Minimize: $$\sigma_{MV}^2 = \overline{W}^*(f_i,\theta)R(f_i)\overline{W}(f_i,\theta) \quad \text{, subject to} \quad \overline{W}^*(f_i,\theta)\overline{D}(f_i,\theta) = 1 \tag{60}$$

where $\overline{D}(f_i,\theta)$ is the conventional steering vector based on Eq. (3.21). The solution is given by,

$$\overline{W}(f_i,\theta) = \frac{R^{-1}(f_i)\overline{D}(f_i,\theta)}{\overline{D}^*(f_i,\theta)R^{-1}(f_i)\overline{D}(f_i,\theta)} \tag{61}$$

The above solution provides the adaptive steering vectors for beamforming the received signals by the N –hydrophone line array. Then in frequency domain, an adaptive beam at a steering θ_S is defined by

$$B(f_i,\theta_s)=\overline{W}^*(f_i,\theta_s)\overline{X}(f_i) \tag{62}$$

and the corresponding conventional beams are provided by Equation (22).

4.2.2 Generalized Sidelobe Canceller (GSC)

The Generalized Sidelobe Canceller (GSC) [44] is an alternative approach to the MVDR method. It reduces the adaptive problem to an unconstrained minimization process. The GSC formulation produces a much less computationally intensive implementation. In general GSC implementations have complexity O(N^2), as compared to O(N^3) for MVDR implementations, where N is the number of sensors used in the processing. The basis of the reformulation of the problem is the decomposition of the adaptive filter vector $\overline{W}(f_i,\theta)$ into two orthogonal components, $\overline{w}$ and $-\overline{v}$, where $\overline{w}$ and $\overline{v}$ lie in the range and the null space of the constraint of Eq. (3.60), such that $\overline{W}(f_i,\theta)=\overline{w}(f_i,\theta)-\overline{v}(f_i,\theta)$. A matrix $\boldsymbol{C}$ which is called signal blocking matrix, may be computed from $\boldsymbol{C}\ \overline{I}=0$ where $\overline{I}$ is a vector of ones. This matrix $\boldsymbol{C}$ whose columns form a basis for the null space of the constraint of Eq. (3.60) will satisfy $\overline{v}=C\overline{u}$, where $\overline{u}$ is defined below by Eq. (3.64). The adaptive filter vector may now be defined as $\overline{W}=\overline{w}-C\overline{u}$ and yields the realization shown in Figure 12. Then the problem is reduced to:

$$\text{Minimize: } \sigma_u^2=\{[\overline{w}-C\overline{u}]^* R\,[\overline{w}-C\overline{u}]\} \tag{63}$$

which is satisfied by:

$$\overline{u}_{opt}=\left(C^*RC\right)^{-1}C^*R\overline{w} \tag{64}$$

$\boldsymbol{u_{opt}}$ being the value of the weights at convergence.

The Griffiths-Jim Generalized Sidelobe Canceller (GSC) in combination with the Normalized Least Mean Square (NLMS) adaptive algorithm has been shown to yield near instantaneous convergence [44,45]. Figure 12 shows the basic structure of the so called Memoryless Generalized Sidelobe Canceller. The time delayed by $\tau_n(\theta_s)$ sensor time series defined by Equations (4), (20) and Figure 2 form the presteered sensor time series, which are denoted by $x_n\left(t_i,\tau_n(\theta_s)\right)$. In frequency domain these presteered sensor data are denoted by $X_n\left(f_i,\theta_s\right)$ and form the input data vector for the adaptive scheme in Figure 12. On the left hand side branch of this figure the intermediate vector $\overline{Z}\left(f_i,\theta_s\right)$ is the result of the signal blocking matrix $\boldsymbol{C}$ being applied to the input $\overline{X}\left(f_i,\theta_s\right)$. Next, the vector $\overline{Z}\left(f_i,\theta_s\right)$ is an input to the NLMS adaptive filter. The output of the right hand branch is simply the shaded conventional output. Then, the output of this processing scheme is the difference between the adaptive filter output, and the "conventional" output:

$$e(f_i,\theta_s)=b(f_i,\theta_s)-\overline{u}^*(f_i,\theta_s)\overline{Z}(f_i,\theta_s) \tag{65}$$

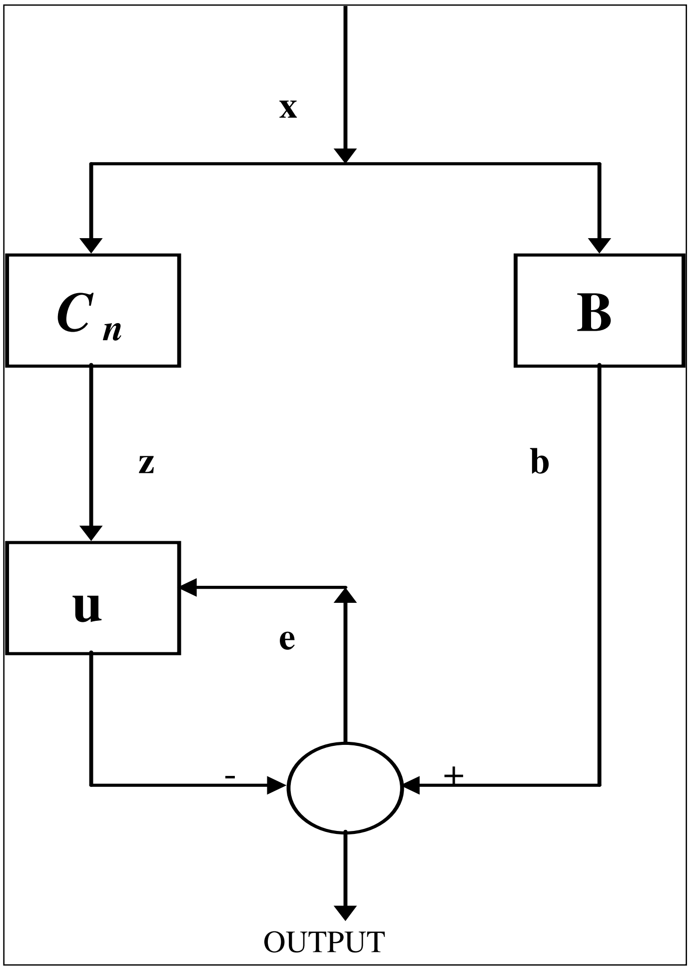

Figure 12: Basic processing structure for the memoryless GSC. The right hand side branch is simply the shaded conventional beamformer. The left hand side branch of this figure is the result of the signal blocking matrix (constraints) applied to presteered sensor time series. The output of the signal blocking matrix is the input to the NLMS adaptive filter. Then, the output of this processing scheme is the difference between the adaptive filter and the "conventional" output.

The adaptive filter, at convergence, reflects the sidelobe structure of any interferers present, and it is removed from the conventional beamformer output. In the case of the Normalized LMS (NLMS) this adaptation process can be represented by:

$$\overline{u}_{k+1}(f_i,\theta_s)=\overline{u}_k(f_i,\theta_s)+\frac{\mu\times e_k^*(f_i,\theta_s)}{\alpha+\overline{X}^*(f_i,\theta_s)\overline{X}(f_i,\theta_s)}\overline{Z}(f_i,\theta_s) \tag{66}$$

where, k is the iteration number, α is a small positive number designed to maintain stability. The parameter μ is the convergence controlling parameter or “step size” for the NLMS algorithm.

4.2.3 Steered Minimum Variance Broadband Adaptive (STMV)

Krolik and Swingler [38] have shown that the convergence time for broad-band source location can be reduced by using the space-time statistic called the steered covariance matrix (STCM). This method achieves significantly shorter convergence times than adaptive algorithms that are based on the narrowband cross spectral density matrix (CSDM) [17,18] without sacrificing spatial resolution. In fact, the number of statistical degrees of freedom available to estimate the STCM is approximately the time-bandwidth product (Tx BW) as opposed to the observation time, ($T=M/F_s$, F_s being the sampling frequency) in CSDM methods. This provides an improvement of approximately BW, the size of the broad-band source bandwidth, in convergence time. The conventional beamformer's output in frequency domain is shown by Eq. (22). The corresponding time domain conventional beamformer output $b(t_i, \theta_s)$ is the weighted sum of the steered sensor outputs, as expressed by Eq. (29). Then, the expected broadband beam power , $B(\theta)$ is given by:

$$B(\theta_s) = E\{|b(\theta_s, t_i)|\} = \overline{h}^* E\{\overline{x}^*(t_i, \tau_n(\theta))\overline{x}(t_i, \tau_m(\theta))\}\overline{h} \tag{67}$$

where the vector $\overline{h}$ includes the weights for spatial shading [36].

The term
$$\Phi(t_i, \theta_s) = E\{\overline{x}(t_i, \tau_n(\theta_s))\overline{x}^*(t_i, \tau_m(\theta_s))\} \tag{68}$$

is defined as the steered covariance matrix (STCM) in time domain and is assumed to be independent of t_i in stationary conditions. The name STCM is derived from the fact that the matrix is computed by taking the covariance of the pre-steered time domain sensor outputs. Suppose $X_n(f_i)$ is the fourier transform of the sensor outputs $x_n(t_i)$ and assuming that the sensor outputs are approximately band limited. Under these conditions the vector of steered (or time delayed) sensor outputs $x_n(t_i, \tau_n(\theta_s))$ can be expressed by

$$\overline{x}(t_i, \tau_n(\theta_s)) = \sum_{k=l}^{l+H} T_k(f_k, \theta_s)\overline{X}(f_k)\exp(j2\pi f_k t_i) \tag{69}$$

where $T(f_k, \theta)$ is the diagonal steering matrix in Eq. (70) below with elements identical to the elements of the conventional steering vector, $\overline{D}(f_i, \theta)$

$$T(f_k,\theta)=\begin{bmatrix} 1 & & . & . & . & 0 \\ 0 & d_1(f_k,\theta) & & & & \\ . & & . & & & . \\ . & & & . & & . \\ . & & & & . & . \\ 0 & & . & . & . & d_N(f_k,\theta) \end{bmatrix} \tag{70}$$

Then it follows directly from the above equations that

$$\Phi(\Delta f,\theta_s)=\sum_{k=l}^{l+H} T(f_k,\theta_s)R(f_k)T^*(\theta_s) \tag{71}$$

where the index $k = l, l+1, \ldots, l+H$ refers to the frequency bins in a band of interest Δf, and $R(f_k)$ is the Cross Spectral Density Matrix for the frequency bin f_k. This suggests that $\Phi(\Delta f, \theta_s)$ in Eq. (68) can be estimated from the CSDM, $R(f_k)$ and $T(f_k,\theta)$ expressed by Eq. (70). In the steered minimum variance method (STMV), the broadband spatial power spectral estimate $B(\theta_s)$ is given by [38]:

$$B(\theta_s)=\left[\bar{I}^*\Phi(\Delta f,\theta_s)^{-1}\bar{I}\right]^{-1} \tag{72}$$

The Steered Minimum Variance Algorithm differs from the basic MVDR algorithm in that the STMV algorithm yields a STCM that is composed from a band of frequencies and the MVDR algorithm uses a CSDM that is derived from a single frequency bin. Thus, the additional degrees of freedom of STMV compared to those of CSDM provide a more robust adaptive process.

However, estimates of $B(\theta)$ according to Eq. (72) do not provide coherent beam time series, since they represent the broadband beam power output of an adaptive process. In this investigation [1] we have modified the estimation process of the STMV matrix in order to get the complex coefficients of $\Phi(\Delta f, \theta_s)$ for all the frequency bins in the band of interest.

The STMV algorithm may be used in its original form to generate an estimate of $\Phi(\Delta f, \theta)$ for all the frequency bands Δf, across the band of the received signal. Assuming stationarity across the frequency bins of a band Δf, then the estimate of the STMV may be considered to be approximately the same with the narrowband estimate $\Phi(f_o, \theta)$ for the center frequency f_o of the band Δf. In this case, the narrowband adaptive coefficients may be derived from

$$\overline{w}(f_o,\theta)=\frac{\Phi(f_o,\Delta f,\theta)^{-1}\overline{D}(f_o,\theta)}{\overline{D}^*(f_o,\theta)\Phi(f_o,\Delta f,\theta)^{-1}\overline{D}(f_o,\theta)} \tag{73}$$

The phase variations of $\overline{w}(f_o, \theta)$ across the frequency bins $i=l,,l+1,...,l+H$ (where H is the number of bins in the band Δf), are modeled by,

$$w_n(f_i, \theta)=exp[2\pi f_i \Psi(\Delta f, \theta)], \quad i=l,l+1,...,l+H \tag{74}$$

where, $\Psi_n(\Delta f, \theta)$ is a time delay term derived from,

$$\Psi_n(\Delta f, \theta) = F[w_n(\Delta f, \theta), 2\pi f_o] \tag{75}$$

Then by using the adaptive steering weights $w_n(\Delta f, \theta)$, that are provided by Eq. (74), the adaptive beams are formed as shown by Eq. (62). Figure 13 shows the realization of the STMV beamformer and provides a schematic representation of the basic processing steps that include:

1. Time series segmentation, overlap and FFT, shown by the group of blocks at the top-left part of the schematic diagram.

2. Formation of steered covariance matrix, [Eqs. (68), (71)] shown by the two blocks at the bottom left hand side of Figure 13.

3. Inversion of covariance matrix using Cholesky factorization, estimation of adaptive steering vectors and formation of adaptive beams in frequency domain, presented by the middle and bottom blocks at the right hand side of Figure 13; and finally

4. Formation of adaptive beams in time domain through IFFT, discardation of overlap and concatenation of segments to form continuous beam time series, which is shown by the top right hand side block.

The various indexes in Figure 13 provide details for the implementation of the STMV processing flow in a generic computing architecture. The same figure indicates that estimates of the Steered Covariance Matrix (STCM) is based on an exponentially weighted time average of the current and previous STCM, which is discussed in the next section.

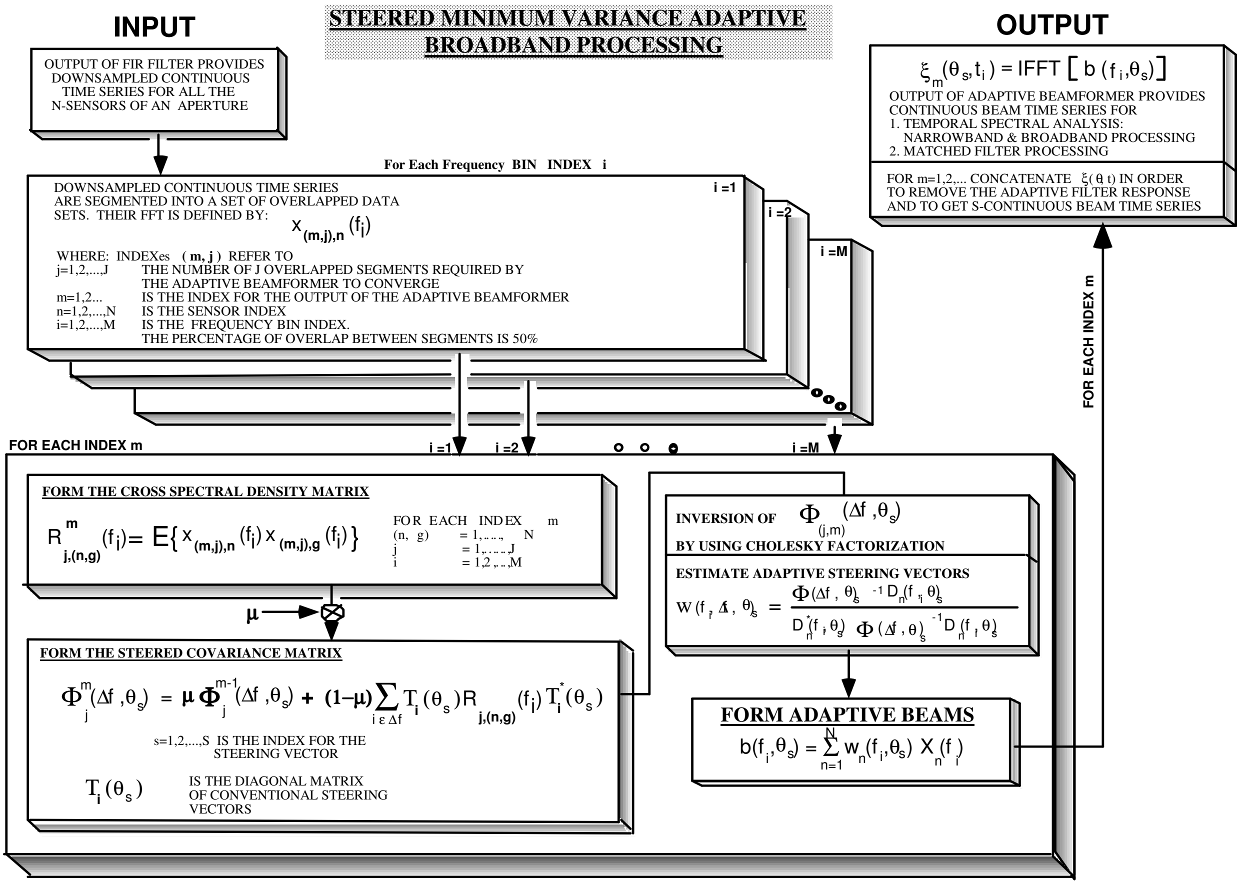

Figure 13: Realization of the steered covariance adaptive beamformer. The basic processing steps include: (1) time series segmentation, overlap and FFT, shown by the group of blocks at the top-left part of the schematic diagram, (2) formation of steered covariance matrix, shown by the two blocks at the bottom left hand side, (3) inversion of covariance matrix using Cholesky factorization, estimation of adaptive steering vectors and formation of adaptive beams in frequency domain (middle and bottom blocks at the right hand side), and finally (4) formation of adaptive beams in time domain through IFFT, discardation of overlap and concatenation of segments to form continuous beam time series (top right hand side block). The various indexes provide details for the implementation of the STMV processing flow in a generic computing architecture.

5 Implementation Considerations

The conventional and adaptive steering vectors for steering angles θ_s , ϕ_s discussed in Sections 3 and 4 are integrated in a frequency domain beamforming scheme, which is expressed by Eqs. (22),(25), (31) and (62). The beam time series are formed by (29). Thus, the frequency domain adaptive and conventional outputs are made equivalent to the fast Fourier transform (FFT) of the time domain beamforming outputs with proper selection of beamforming weights and careful data partitioning. This equivalence corresponds to implementing FIR filters via circular convolution [40-42].

Matrix inversion is another major implementation issue for the adaptive schemes discussed in this report. Standard numerical methods for solving systems of linear equations can be applied to solve for the adaptive weights. The range of possible algorithms includes:

- Cholesky factorization of the covariance matrix $R(f_i)$, [17,29]. This allows the linear system to be solved by backsubstitution in terms of the received data vector. Note that there is no requirement to estimate the sample covariance matrix and that there is a continuous updating of an existing Cholesky factorization.
- QR decomposition of the received vector $\overline{X}(f_i)$, that includes the conversion of a matrix to upper triangular form via rotations. The QR decomposition method has better stability than the Cholesky factorization algorithm, but it requires twice as much computational efforts than the Cholesky approach.
- SVD (Singular Value Decomposition) method. This is the most stable factorization technique. It requires, however, three times more computational requirements than the QR decomposition method.

In this implementation study we have applied the Cholesky factorization and the QR decomposition techniques in order to get solutions for the adaptive weights. Our experience suggests that there are no noticeable differences in performance between the above two methods [1].

The main consideration, however, for implementing adaptive schemes in real time systems are associated with the requirements derived from Eqs. (61), (62), which require knowledge of second order statistics for the noise field. Although these statistics are usually not known, they can be estimated from the received data [17,18,23] by averaging a large number of independent samples of the covariance matrixes $R(f_i)$ or by allowing the iteration process of the adaptive GSC schemes to converge [1,37]. Thus, if K is the effective number of statistically independent samples of $R(f_i)$, then the variance on the adaptive beam output power estimator detection statistic is inversely proportional to $(K-N+1)$, [17,18,22], where N is the number of sensors. Theoretical suggestions [23] and our empirical observations suggest that K needs to be three to four times the size of N in order to get coherent beam time series at the output of the above adaptive schemes. In other words, for arrays with a large number of sensors, the implementation of adaptive schemes as statistically optimum beamformers would require the averaging of a very large number of independent samples of $R(f_i)$ in order to derive an unbiased estimate of the adaptive weights [23]. In practice this is the most serious problem associated with the implementation of adaptive beamformers in real time systems.

Owsley [17,29] has addressed this problem with two important contributions. His first contribution is associated with the estimation procedure of $R(f_i)$. His argument is that in practice, the covariance matrix cannot be estimated exactly by time averaging because the received signal vector $\overline{X}(f_i)$ is never truly stationary and/or ergodic. As a result, the available averaging time is limited. Accordingly, one approach to the time-varying adaptive estimation of $R(f_i)$ at time t_k is to compute the exponentially time averaged estimator (geometric forgetting algorithm) at time t_k:

$$R^{t_k}(f_i) = \mu R^{t_{k-1}}(f_i) + (1-\mu)\overline{X}(f_i)\overline{X}^*(f_i) \tag{76}$$

where μ is a smoothing factor $(0<\mu<1)$ that implements the exponentially weighted time averaging operation. The same principle has also been applied in the GSC scheme [1,37]. Use of this kind of exponential window to update the covariance matrix is a very important factor in the implementation of adaptive algorithms in real time systems.

Owsley's [29] second contribution deals with the dynamics of the data statistics during the convergence period of the adaptation process. As mentioned above, the implementation of an adaptive beamformer with a large number of adaptive weights in a large array sonar system, requires very long convergence periods that will eliminate the dynamical characteristics of the adaptive beamformer to detect the time varying characteristics of a received signal of interest. A natural way to avoid this kind of temporal stationarity limitation is to reduce the number of adaptive weights requirements. Owsley's [29] sub-aperture configuration for line array adaptive beamforming reduces significantly the number of degrees of freedom of an adaptation process. His concept has been applied to line arrays, as discussed in References [1,37]. However, extension of the sub-aperture line array concept for multi-dimensional arrays is not a trivial task. In the following sections, the sup-aperture concept is generalized for circular, cylindrical, planar and spherical arrays.

5.1 Evaluation of Convergence Properties of Adaptive Schemes

To test the convergence properties of the various adaptive beamformers of this study, synthetic data were used that included one CW signal. The frequency of the monochromatic signal was selected to be 330-Hz, and the angle of arrival at 68.9 degrees to directly coincide with the steering direction of a beam. The signal to noise ratio (SNR) of the received synthetic signal was very high, 10dB at the sensor. By definition the adaptive beamformers allow signals in the look direction to pass undistorted, while minimizing the total output power of the beamformer. Therefore in the ideal case the main beam output of the adaptive beamformer should resemble the main beam output of the conventional beamformer, while the side beams outputs will be minimized to the noise level. To evaluate the convergence of the beamformers two measurements were made. From Eq. (65), the mean square error (MSE) between the normalized main beam outputs of the adaptive beamformer and the conventional beamformer was measured, and the mean of the normalized output level of the side beam, which is the MSE when compared with zero, was measured. The averaging of the errors were done with a sliding window of four snapshots to provide a time varying average, and the outputs were normalized so that the maximum output of the conventional beamformer was unity.

5.1.1 Convergence Characteristics of GSC and GSC-SA Beamformers

The GSC/NLMS adaptive algorithm, which has been discussed in Section 4.2, and its sub-aperture configuration denoted by GSC-SA/NLMS were compared against each other to determine if the use of the sub-aperture configuration produced any improvement in the time required for convergence. The graph in the upper part of Figure 14 shows the comparison of the MSE of the main beams of both algorithms for the same step size μ, which is defined in Eq. (65). The graphs show that the convergence rates of the main beams are approximately the same for both algorithms, reaching a steady state value of MSE within a few snapshots. The value of MSE that is achieved is dictated by the miss-adjustment, which depends on μ. The higher MSE produced by the GSC-SA algorithm indicates that the algorithm exhibits a higher miss-adjustment.

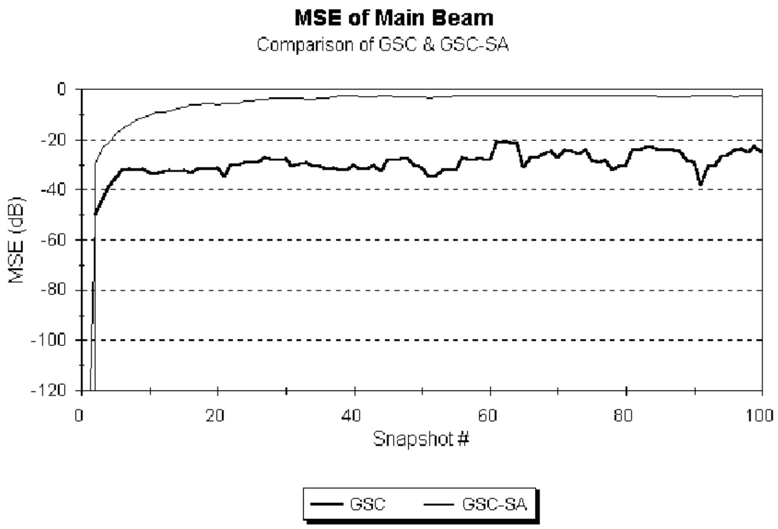

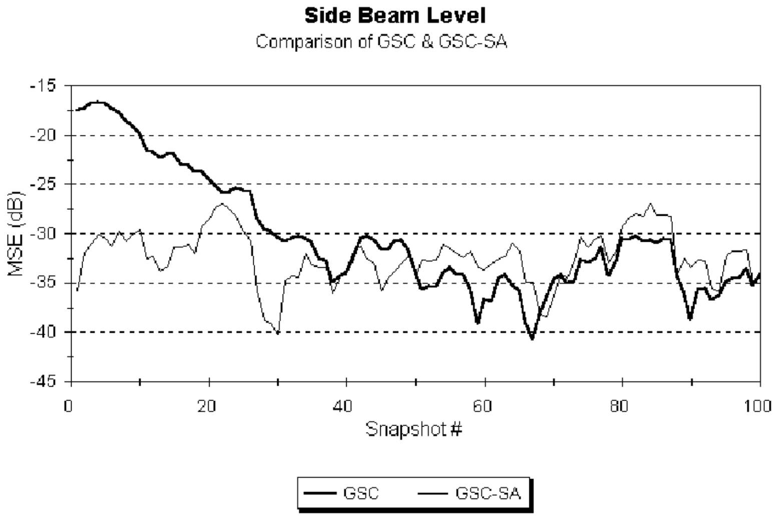

Figure 14: (a) MSE of the main beams of the GSC/NLMS and the GSC-SA/NLMS algorithms. (b) Side-beam levels of the above algorithms.

The graph in the lower part of Figure 14 shows the output level of an immediate side beam, again for the same step size μ. The side beam was selected as the beam right next to the main beam. The GSC-SA algorithm appears superior at minimizing the output of the side beam. It reaches its convergence level almost immediately, while the GSC algorithm requires approximately thirty snapshots to reach the same level. This indicates that the GSC-SA algorithm should be superior at cancelling time varying interferers. By selecting a higher value for μ the time required for convergence will be reduced but the MSE of the main beam will be higher.

5.1.2 Convergence Characteristics of STMV and STMV-SA Beamformers

As with the GSC/NLMS and GSC-SA/NLMS beamformers, the STMV and the STMV sub-aperture (STMV-SA) beamformers were compared against each other to determine if there was any improvement in the time required for convergence when using the sub-aperture configuration. The graph in the upper part of Figure 15 shows the comparison of the MSE of the main beams of both algorithms. The graph shows that the STMV-SA algorithm reaches a steady state value of MSE within the first few snapshots.

The STMV algorithm is incapable of producing any output for at least eight snapshots as tested. Before this time the matrices that are used to compute the adaptive steering vectors are not invertible. After this initial period the algorithm has already reached a steady state value of MSE. Unlike the case of the GSC algorithm the misadjustment from sub-aperture processing is smaller. The lower part of Figure 15 shows the output level of the side beam for both the STMV and the STMV-SA beamformers. Again the side beam was selected as the beam right next to the main beam. As before there is an initial period during which the STMV algorithm is computing an estimate of the STCM and is incapable of producing any output, after that period the algorithm has reached steady state, and produces lower side beams than the sub-aperture algorithm.

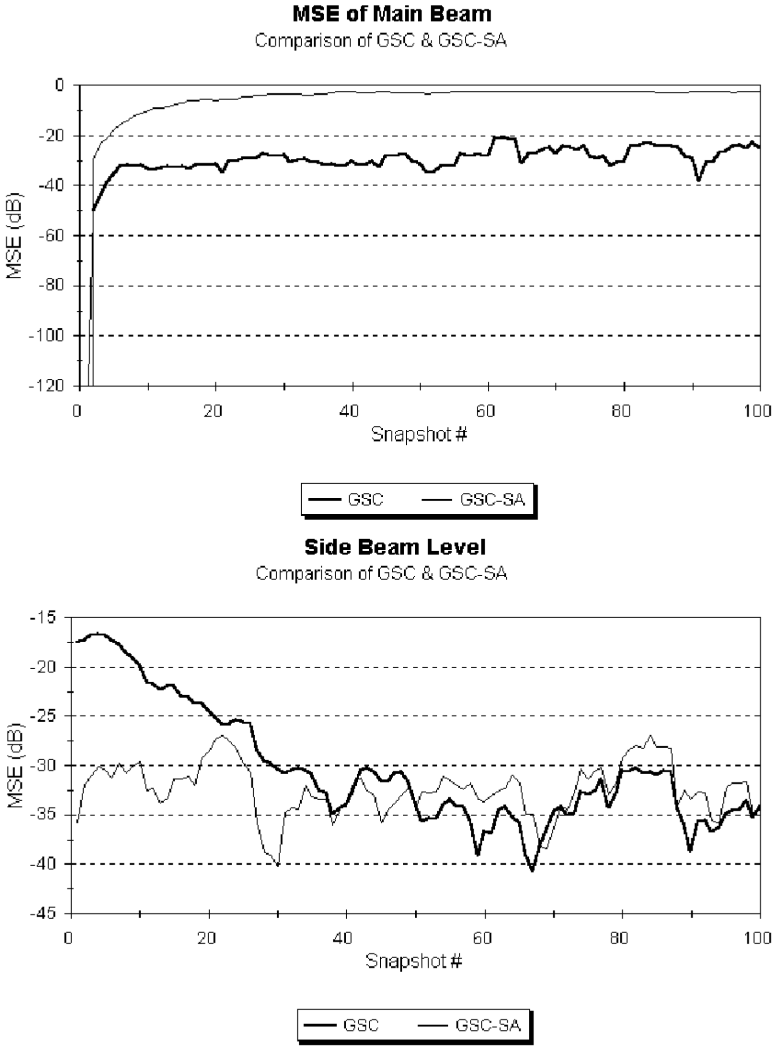

Figure 15: (a) MSE of the main beams of the STMV and the STMV-SA algorithms. (b) Side-beam levels of the above algorithms.

5.1.3 Signal Cancellation Effects of the Adaptive Algorithms

Testing of the adaptive algorithms of this study for signal cancellation effects was carried out with simulations that included two signals arriving from 64 degrees and 69 degrees [37]. All of the parameters of the signals were set to the same values for all the beamformers, conventional, GSC/NLMS, GSC-SA/NLMS, STMV and STMV-SA. Details about the above simulated signal cancellation effects can be found in Reference [37]. In the narrowband outputs of the conventional beamformer the signals appear at the frequency and beam at which they were expected. As anticipated, however, the sidelobes are visible in a number of other beams. The gram outputs of the GSC/STMV algorithm indicated that there is signal cancellation. In each case the algorithm failed to detect either of the two CWs. This suggests that there is a shortcoming in the GSC/NLMS algorithm, when there is strong correlation between two signal arrivals received by the line array. The narrowband outputs of the GSC-SA/NLMS algorithm showed that in this case the signal cancellation effects have been minimized and the two signals were detected only at the expected two beams with complete cancellation of the side-lobe structure. For the STMV beamformer, the grams indicated a strong side-lobe structure in many other beams. However, the STMV-SA beamformer successfully suppresses the side-lobe structure that was present in the case of the STMV beamformer. From all these simulations [37], it was obvious that the STMV-SA beamformer, as a broadband beamformer, is not as robust for narrowband applications as the GSC-SA/NLMS.

5.2 Generic Multi-Dimensional Sub-Aperture Structure for Adaptive Schemes

The decomposition of the 2-D and 3-D beamformer into sets of line and/or circular array beamformers, which has been discussed in Section 3.2, provides a first-stage reduction of the numbers of degrees of freedom for an adaptation process. Furthermore, the sub-aperture configuration is considered in this study as a second stage reduction of the number of degrees of freedom for an adaptive beamformer. Then, the implementation effort for adaptive schemes in multi-dimensional arrays is reduced to implementing adaptive processes in line and circular arrays. Thus, a multi-dimensional adaptive beamformer can now be divided into two coherent modular steps which lead to efficient system oriented implementations.

5.2.1 Sub-Aperture Configuration for Line Arrays

For a line array, a sub-aperture configuration includes a large percentage overlap between contiguous sub-apertures. More specifically, a line array is divided into a number of sub-arrays that overlap, as shown in Figure 16. These sub-arrays are beamformed using the conventional approach; and this is the first stage of beamforming. Then, we form a number of sets of beams with each set consisting of beams that are steered at the same direction but each one of them generated by a different sub-array. A set of beams of this kind is equivalent to a line array that consists of directional sensors steered at the same direction, with sensor spacing equal to the space separation between two contiguous sub-arrays and with the number of sensors equal to the number of sub-arrays. The second stage of beamforming implements an adaptive scheme on the above kind of set of beams, as illustrated in Figure 16.

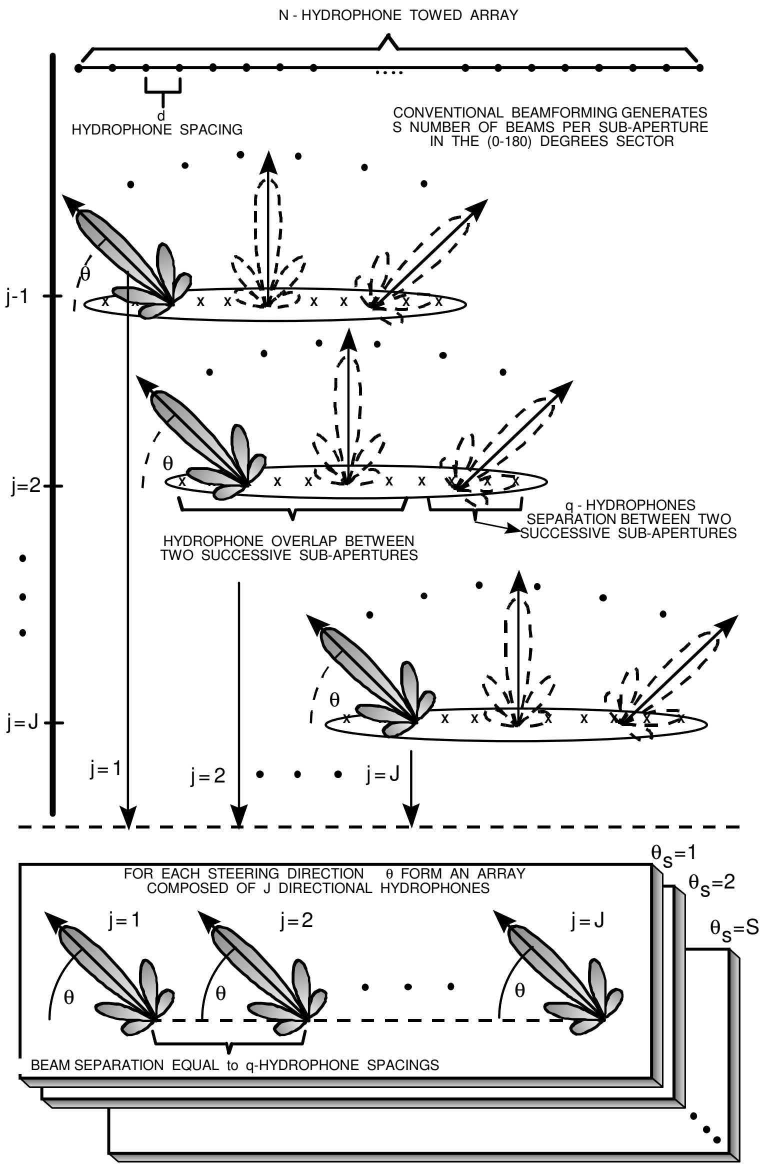

Figure 16: Concept of adaptive sub-aperture structure for line arrays. Schematic diagram shows the basic steps that include: (1) formation of J sub-apertures, (2) for each sub-aperture formation of S conventional beams, and (3) for a given beam direction, formation of line sensor arrays that consist of J number of directional sensors (beams). The number of line arrays with directional sensors (beams) are equal to the number S of steered conventional beams in each sub-aperture. For each line array, the directional sensor time series (beams) are provided at the input of an adaptive beamformer.

5.2.2 Sub-Aperture Configuration for Circular Array

Consider a circular array with M -sensors as shown in Figure 17. The first circular sub-aperture consists of the first M-G+1 sensors with $n=1,2,...,M-G+1$, where n is the sensor index and G is the number of sub-apertures. The second circular sub-aperture array consists of *M-G+1* sensors with *n=2,3,...,M-G+2*. The sub-aperture formation goes on till the last sub-aperture consists of *M-G+1* sensors with *n=G,G+1,...,M*. In the first stage, each circular sub-aperture is beamformed as discussed in Section 3.1.2 and this first stage of beamforming generates *G* sets of beams.

As in the previous section, we form a number of sets of beams with each set consisting of beams that are steered at the same direction but each one of them generated by a different sub-array. For *G<5*, a set of beams of this kind can be treated approximately as a line array that consists of directional sensors steered at the same direction, with sensor spacing equal to the space separation between two contiguous sub-arrays and with the number of sensors equal to the number of sub-arrays. The second stage of beamforming implements an adaptive scheme on the above kind of set of beams, as illustrated in Figure 17, for *G=3*.

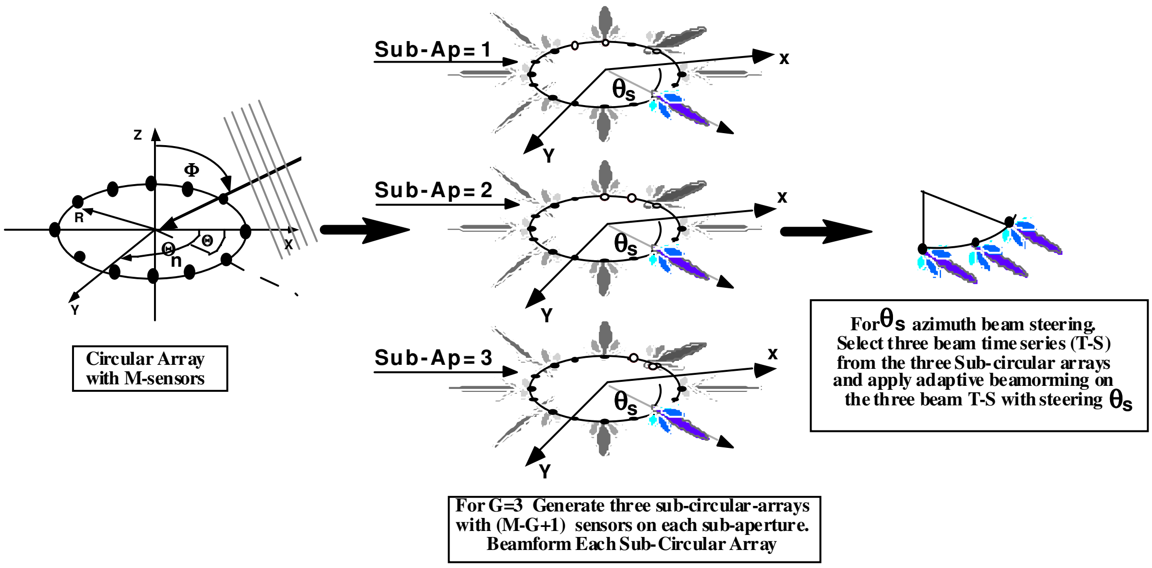

Figure 17: Concept of adaptive sub-aperture structure for circular arrays, which is similar to that for line arrays shown in Figure 16

5.2.3 Sub-Aperture Configuration for Cylindrical Array

Consider the cylindrical array shown in Figures 5 and 18 with the number of sensors $\aleph = NM$, where N is the number of circular rings and M is the number of sensors on each ring. Let n be the ring index, m be the sensor index for each ring and G be the number of sub-apertures. The formation of sub-apertures is as follows:

- The first sub-aperture consists of the first $(N-G+1)$ rings, where *n = 1,2,...,N-G+1*. In each ring we select the first set of $(M-G+1)$ sensors, where *m=1,2,...M-G+1*. However, each ring has *M* sensors, but only *(M-G+1)* sensors are used to form the sub-aperture. These sensors form a cylindrical array cell, as shown in the upper right hand side corner of Figure 18.

In other words, the sub-aperture includes the sensors of the full cylindrical array except for *G-1* sensors from *G-1* rings, which are denoted by small circles in Figure 18, that have been excluded in order to form the sub-aperture. Next, the generic decomposition concept of the conventional cylindrical array beamformer, presented in Section 3.2.1, is applied to the above sub-aperture cylindrical array cell. For a given pair of azimuth and elevation steering angles {θ_s, ϕ_s}, the output of the generic conventional multi-dimensional sub-aperture beamformer provides beam time series, $b_{g=1}(t_i, \theta_s, \phi_s)$, where the subscript *g=1* is the sub-aperture index.

- The <u>second sub-aperture</u> consists of the next set of $(N-G+1)$ rings, where *n = 2,...,N-G+2*. In each ring we select the next set of $(M-G+1)$ sensors, where *m=2,...M-G+2*. However, each ring has *M* sensors, but only *(M-G+1)* sensors are used to form the sub-aperture. These sensors form the second sub-aperture cylindrical array cell.

Again, the generic decomposition concept of the conventional cylindrical array beamformer, presented in Section 3.2.1, is applied to the above sub-aperture cylindrical array cell. For a given pair of azimuth and elevation steering angles {θ_s, ϕ_s}, the output of the generic conventional multi-dimensional sub-aperture beamformer provides beam time series, $b_{g=2}(t_i, \theta_s, \phi_s)$ with sub-aperture index *g=2* .

- This kind of sub-aperture formation continues till the <u>last sub-aperture</u> which consists of a set of $(N-G+1)$ rings, where *n =G, G+1,...,N*. In each ring we select the last set of $(M-G+1)$ sensors, where *m=G,G+1,...M*. Please note also that each ring has *M* sensors, but only *(M-G+1)* sensors are used to form the sub-aperture.

As before, the generic decomposition concept of the conventional cylindrical array beamformer is applied to the last sub-aperture cylindrical array cell. For a given pair of azimuth and elevation steering angles {θ_s, ϕ_s}, the output of the generic conventional multi-dimensional sub-aperture beamformer would provide beam time series, $b_{g=G}(t_i, \theta_s, \phi_s)$ with sub-aperture index *g=G*.

As in the previous section 4.2.2, we form a number of sets of beams with each set consisting of beams that are steered at the same direction but each one of them generated by a different sub-aperture cylindrical array cell. For *G<5*, a set of beams of this kind can be treated approximately as a line array that consists of directional sensors steered at the same direction, with sensor spacing equal to the space separation between two contiguous sub-aperture cylindrical array cells and with the number of sensors equal to the number of sub-arrays. Then, <u>the second stage of beamforming</u> implements an adaptive scheme on the above kind of set of beams, as illustrated in Figure 18.

For the particular case, shown in Figure 18, <u>the second stage of beamforming</u> implements an adaptive beamformer on a line array that consists of the *G=3* beam time series $b_g(t_i, \theta_s, \phi_s)$, *g=1,2,...,G*. Thus, for a given pair of azimuth and elevation steering angles {θ_s, ϕ_s}, the cylindrical adaptive beamforming process is reduced to an adaptive line array beamformer that includes as input only three beam time series $b_g(t_i, \theta_s, \phi_s)$, *g=1,2,3* with spacing

$\delta = \left[(R2\pi / M)^2 + \delta_z^2\right]^{1/2}$, which is the spacing between two contiguous sub-aperture cylindrical cells, where $(R2\pi / M)$ is the sensor spacing in each ring and δ_z is the distance between each ring along z-axis of the cylindrical array. The output of the adaptive beamformer provides one or more adaptive beam time series with steering centered on the pair of azimuth and elevation steering angles { θ_s, ϕ_s }.

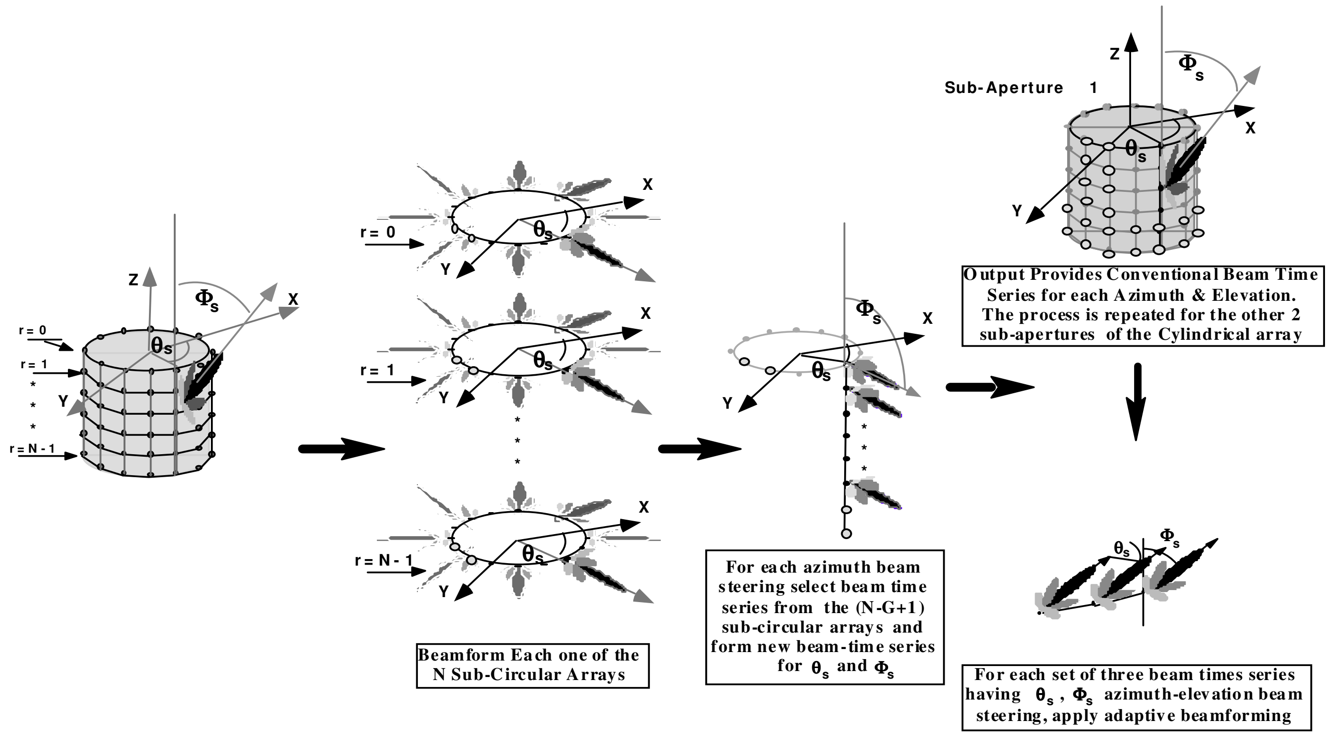

Figure 18: Coordinate system and geometric representation of the concept of adaptive sub-aperture structure for cylindrical arrays. In this particular example the number of sub-apertures was G=3. The $\aleph = NM$ sensor cylindrical array beamformer consists of N circular arrays with M being the number of sensors in each circular array. Then, the sub-aperture adaptive structure for cylindrical arrays is reduced to the basic steps of adaptive sub-aperture structures for circular and line arrays as defined in the schematic diagrams of Figure 17 and 16, respectively. Thus , for a given azimuth θs and elevation ϕs beam steering and G=3, these steps include: (1) formation of a sub-aperture per circular array with M-G+1 sensors, (2) for each sub-aperture formation of S conventional beams, and (3) formation of N-G+1 vertical line sensor arrays that consist of directional sensors (beams). This arrangement defines a circular sub-aperture. The process is repeated to generate two additional sub-aperture circular arrays. The beam output response of the G=3 sub-aperture circular arrays is provided at the input of a line array adaptive beamformer with G=3 number of directional sensors.

As expected, the adaptation process in this case will have near-instantaneous convergence because of the very small number of degrees of freedom. Furthermore, because of the generic characteristics, the proposed 3-D sub-aperture adaptive beamforming concept may include a wide variety of adaptive techniques such as MVDR, GSC and STMV that have been discussed in References [1,37].

5.2.4 Sub-Aperture Configuration for Planar and Spherical Arrays

The sub-aperture adaptive beamforming concepts for planar and spherical arrays are very similar to that of the cylindrical array. In particular, for planar arrays, the formation of sub-apertures is based on the sub-aperture concept of line arrays that has been discussed in Section 5.2.1. The different steps of sub-aperture formation for planar arrays as well as the implementation of adaptive schemes on the G beam time series $b_g(t_i, \theta_s, \phi_s)$, $g=1,2,...,G$, that are provided by the G sub-apertures of the planar array, are similar with those in Figure 18 by considering the composition process for planar arrays shown in Figure 6. Similarly, the sub-aperture adaptive concept for spherical arrays is based on the sub-aperture concept of circular arrays, that has been discussed in Section 5.2.2.

5.3 Signal Processing Flow of a 3-D Generic Sub-Aperture Structure

As it was stated before, the discussion in this report has been devoted in designing a generic sub-aperture beamforming structure that will decompose the computationally intensive multi-dimensional beamforming process into coherent sub-sets of line and/or circular sub-aperture array beamformers for ultrasound, radar and integrated active-passive sonar systems. In a sense the proposed generic processing structure is an extension of a previous effort discussed in Reference [1].

The previous study [1] included the design of a generic beamforming structure that allows the implementation of adaptive, synthetic aperture and high-resolution temporal and spatial spectral analysis techniques in integrated active-passive line-array sonars. Figure 19, which is identical with Figure 4 in [62], shows the configuration of the signal processing flow of the previous generic structure that allows the implementation of Finite Impulse Response (FIR) filters, conventional, adaptive and synthetic aperture beamformers [1,40,41,42]. A detailed discussion about the content of Figure 19 is provided later in [62].

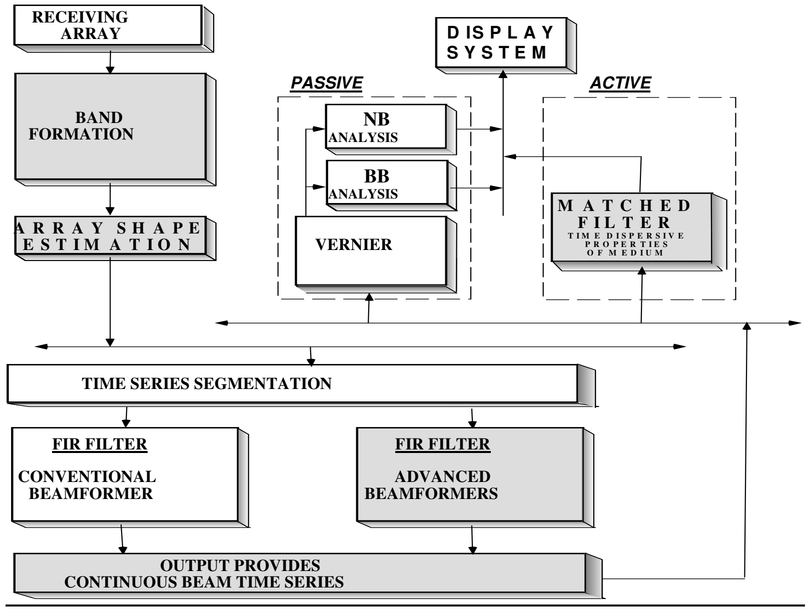

Figure 19: Schematic diagram of a generic signal processing flow that allows the implementation of conventional, adaptive and synthetic aperture beamformers in line-array sonar and ultrasound systems.

Shown in Figure 20 is the proposed configuration of the signal processing flow that includes the implementation of line and circular array beamformers as Finite Impulse Response (FIR) filters [40,41,42]. The processing flow is for 3-D cylindrical arrays. The reconfiguration of the different processing blocks in Figures 19 and 20 allows the application of the proposed configuration to a variety of ultrasound, radar and integrated active-passive sonar systems with planar, cylindrical or spherical arrays of sensors. [62] and [63] present a set of real data results that were derived from the implementation of the signal processing flow of Figure 20 in integrated active-passive towed array sonars and 3D/4D ultrasound imaging systems, respectively.

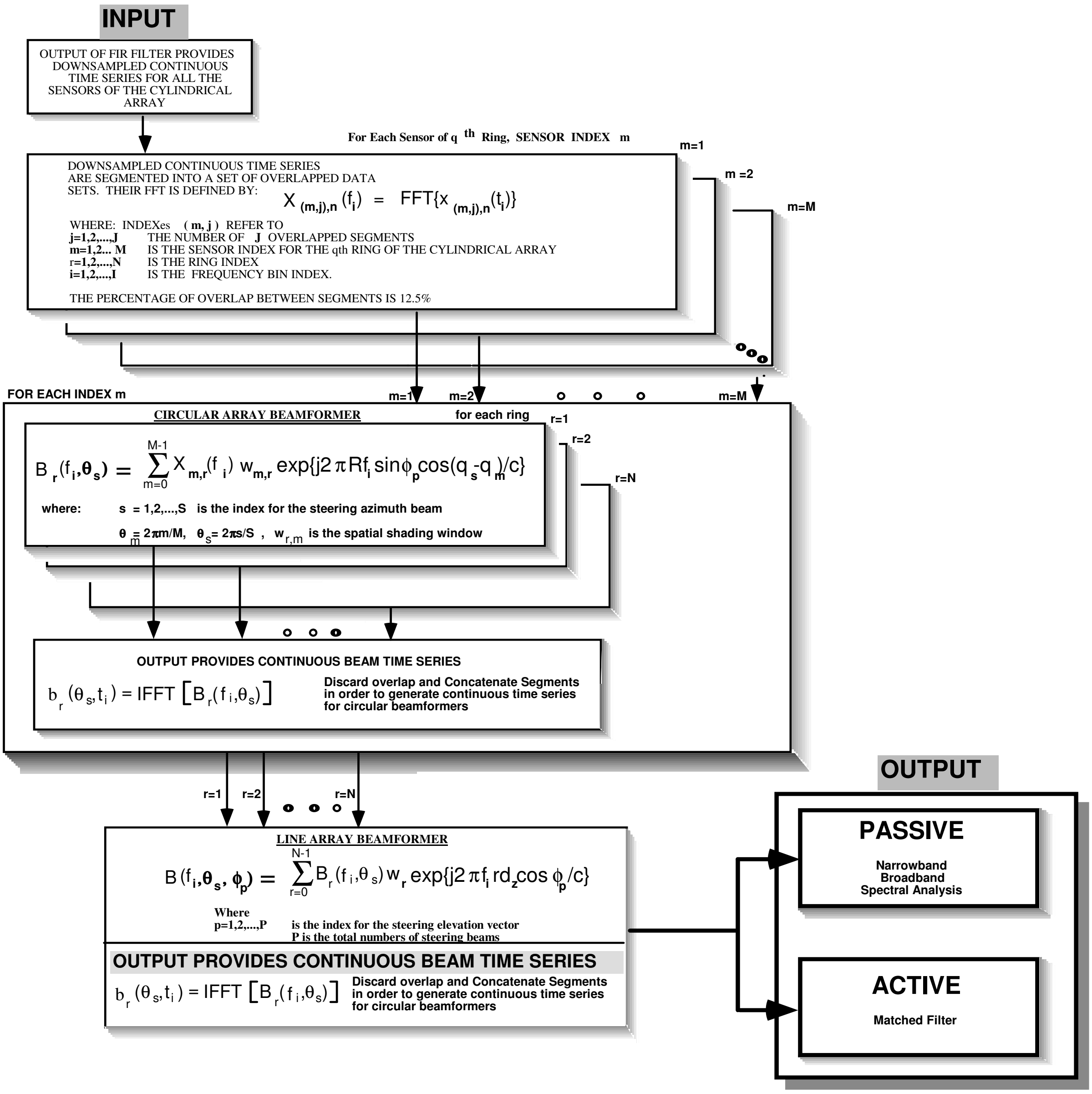

Figure 20: Signal processing flow of generic structure decomposing the 3-D beamformer for cylindrical arrays of sensors into coherent sub-sets of line and circular array beamformers.

As discussed at the beginning of this section, the output of the beamforming processing block in Figure 20 provides continuous beam time series. Then the beam time series are provided at the input of a vernier for passive narrowband / broadband analysis or a matched filter for active applications. This modular structure in the signal processing flow is a very essential processing arrangement in order to allow for the integration of a great variety of processing schemes such as the ones considered in this report. The details of the proposed generic processing flow, as shown in Figure 20, are very briefly the following:

- The first block in Figure 20 includes the partitioning of the time series from the receiving sensor array, the computation of their initial spectral FFT, the selection of the signal's frequency band of interest via band-pass FIR filters and downsampling. The output of this block provides continuous time series at reduced sampling rate [41,42].
- The second and third blocks titled *Circular Array Beamformer* and *Line Array Beamformer* provide continuous directional beam time series by using the FIR implementation scheme of the spatial filtering via circular convolution [40]. The segmentation and overlap of the time series at the input of each one of the above beamformers takes care of the wraparound errors that arise in fast-convolution signal processing operations. The overlap size is equal to the effective FIR filter's length [41,42].
- The block named *Active, Matched-Filter* is for the processing of echos for active sonar and radar applications.
- The block *Passive, Narrowband and Broadband Spectral Analysis* includes the final processing steps of a temporal spectral analysis.

Finally, data normalization processing schemes are being used in order to map the output results into the dynamic range of the display devices in a manner which provides a constant false alarm rate, CFAR capability [34].

In the passive unit, the use of verniers and the temporal spectral analysis (incorporating segment overlap, windowing and FFT coherent processing) provide the narrowband results for all the beam time series. Normalization and OR-ing are the final processing steps before displaying the output results. Since a beam time sequence can be treated as a signal from a directional sensor having the same array gain and directivity pattern as that of the beamformer, the display of the narrowband spectral estimates for all the beams follows the so-called GRAM presentation arrangements, as shown in subsequent Figures (25-28) in Section 6. This includes the display of the beam-power outputs as a function of time, steering beam (or bearing) and frequency [34].

Broadband outputs in the passive unit are derived from the narrowband spectral estimates of each beam by means of incoherent summation of all the frequency bins in a wideband of interest [34]. This kind of energy content of the broadband information is displayed as a function of bearing and time [1,34,43].

In the active unit, the application of a matched-filter (or replica correlator) on the beam time series provides coherent broadband processing. This allows detection of echoes as a function of range and bearing for reference waveforms transmitted by the active transducers of ultrasound, sonar or radar systems. The displaying arrangements of the correlator's output data are similar to the GRAM displays and include as parameters: range as a function of time and bearing [1].

Next, presented in Figure 21, is the signal processing flow of the generic adaptive sub-aperture structure for multi-dimensional arrays. The first processing block includes the formation of sub-apertures as discussed in Section 5.2. Then , the sensor time series from each sub-aperture are beamformed by the generic multi-dimensional beamforming structure that has been introduced in Section 3.3 and presented in Figure 20. Thus, for a given pair of azimuth and elevation steering angles $\{\theta_s, \phi_s\}$, the output of the generic conventional multi-dimensional beamformer would provide G beam time series, $b_g(t_i, \theta_s, \phi_s)$, $g=1,2,...,G$. The second stage of beamforming includes the implementation of an adaptive beamformer as discussed in Section 3.4.2.

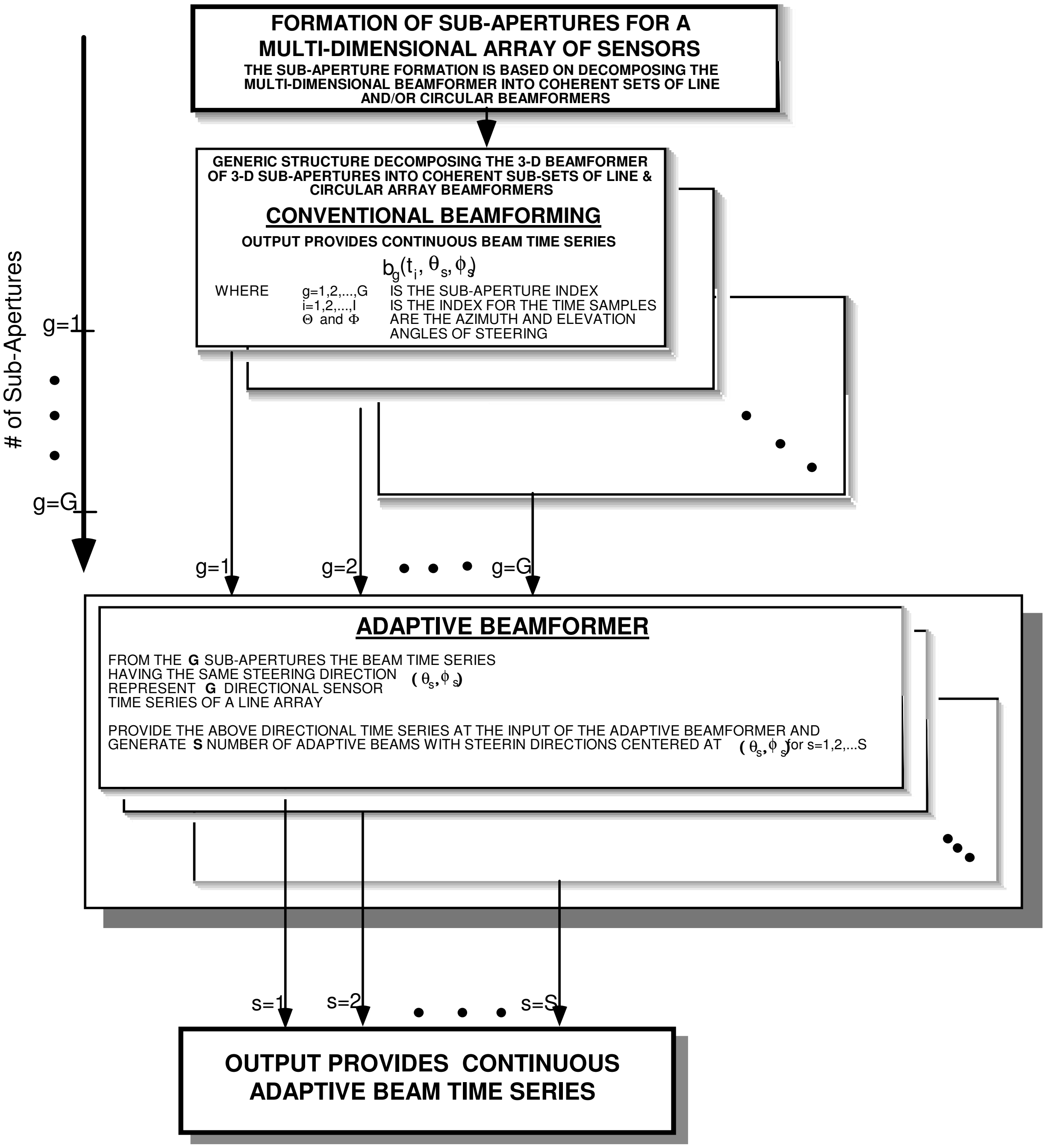

Figure 21: Signal processing flow of a generic adaptive sub-aperture structure for multi-dimensional arrays of sensors.

For the synthetic aperture processing scheme, however, there is an important detail regarding the segmentation and overlap of the sensor time series into sets of discontinuous segments. It is assumed here that the received sensor signals are stored as continuous time series. Therefore, the segmentation process of the sensor time series is associated with the tow speed and the size of the synthetic aperture as this was discussed in Section 4.1.4. So, in order to achieve continuous data flow at the output of the overlap correlator, the *N*-continuous time series are segmented into discontinuous data sets as shown in Figure 22. Our implementation scheme in Figure 22 considers 5 discontinuous segments in each data set. This arrangement will provide at the output of the overlap correlator *3N*-continuous sensor time series, which are provided at the input of the conventional beamformer as if they were the sensor time series of an equivalent physical array. Thus the basic processing steps include: time series segmentation, overlap and grouping of 5 discontinuous segments, which are provided at the input of the overlap correlator, as shown by the group of blocks at the top part of Figure 22. $T = M/f_S$, is the length in seconds of the discontinuous segmented time series and M defines the size of FFT. The rest of the blocks provide the indexing details for the formation of the synthetic aperture. These indexes provide also details for the implementation of the segmentation process of the synthetic aperture flow in a generic computing architecture.

The processing arrangements and the indexes in Figure 23 provide the details needed for the mapping of this synthetic aperture processing scheme in sonar or ultrasound computing architectures. The basic processing steps include:

1. time series segmentation, overlap and grouping of 5 discontinuous segments, which are provided at the input of the overlap correlator, shown by the block at the top part of schematic diagram. Details of this segmentation process are shown also in Figure 22.

2. The main block called **ETAM: Overlap Correlator** provides processing details for the estimation of the phase correction factor to form the synthetic aperture and finally

3. formation of the continuous sensor time series of the synthetic aperture are obtained through IFFT, discardation of overlap and concatenation of segments to form continuous time series, which is shown by the left hand side block.

It is important to note here that the choice of 5 discontinuous segments was based on experimental observations [10,30] regarding the temporal and spatial coherence properties of the underwater medium. These issues of coherence are very critical for synthetic aperture processing and they have been addressed in Section 3.3.

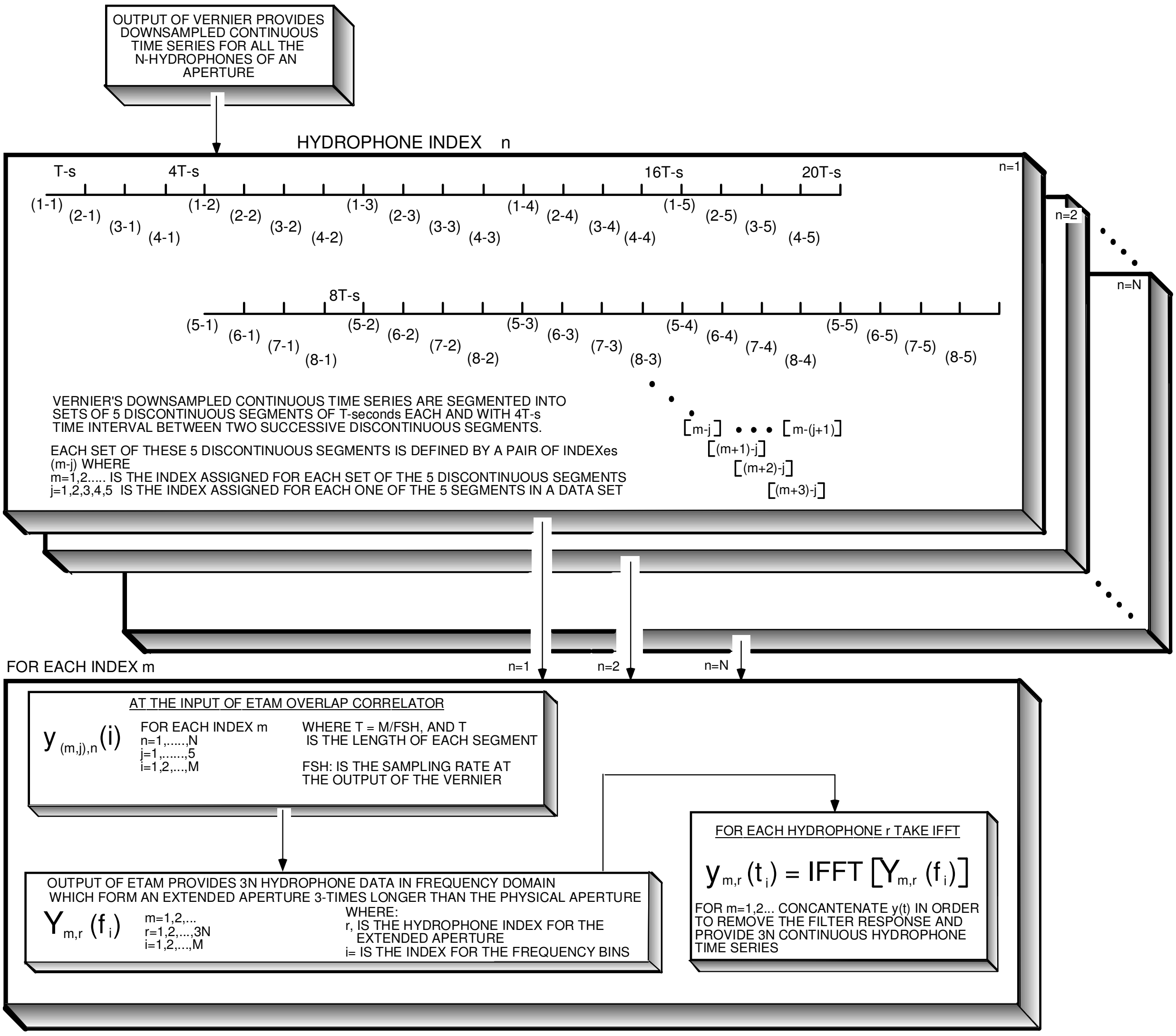

Figure 22: Schematic diagram of the data flow for the ETAM algorithm and the sensor time series segmentation into a set of 5 discontinuous segments for the overlap correlator. The basic processing steps include: time series segmentation, overlap and grouping of 5 discontinuous segments, which are provided at the input of the overlap correlator, (shown by group of blocks at the top part of schematic diagram). T = M/fs, is the length in seconds of the discontinuous segmented time series and M defines the size of FFT. The rest of the blocks provide the indexing details for the formation of the synthetic aperture. These indexes provide details for the implementation of the segmentation process of the synthetic aperture flow in a generic computing architecture. The processing flow is shown in Figure 23.

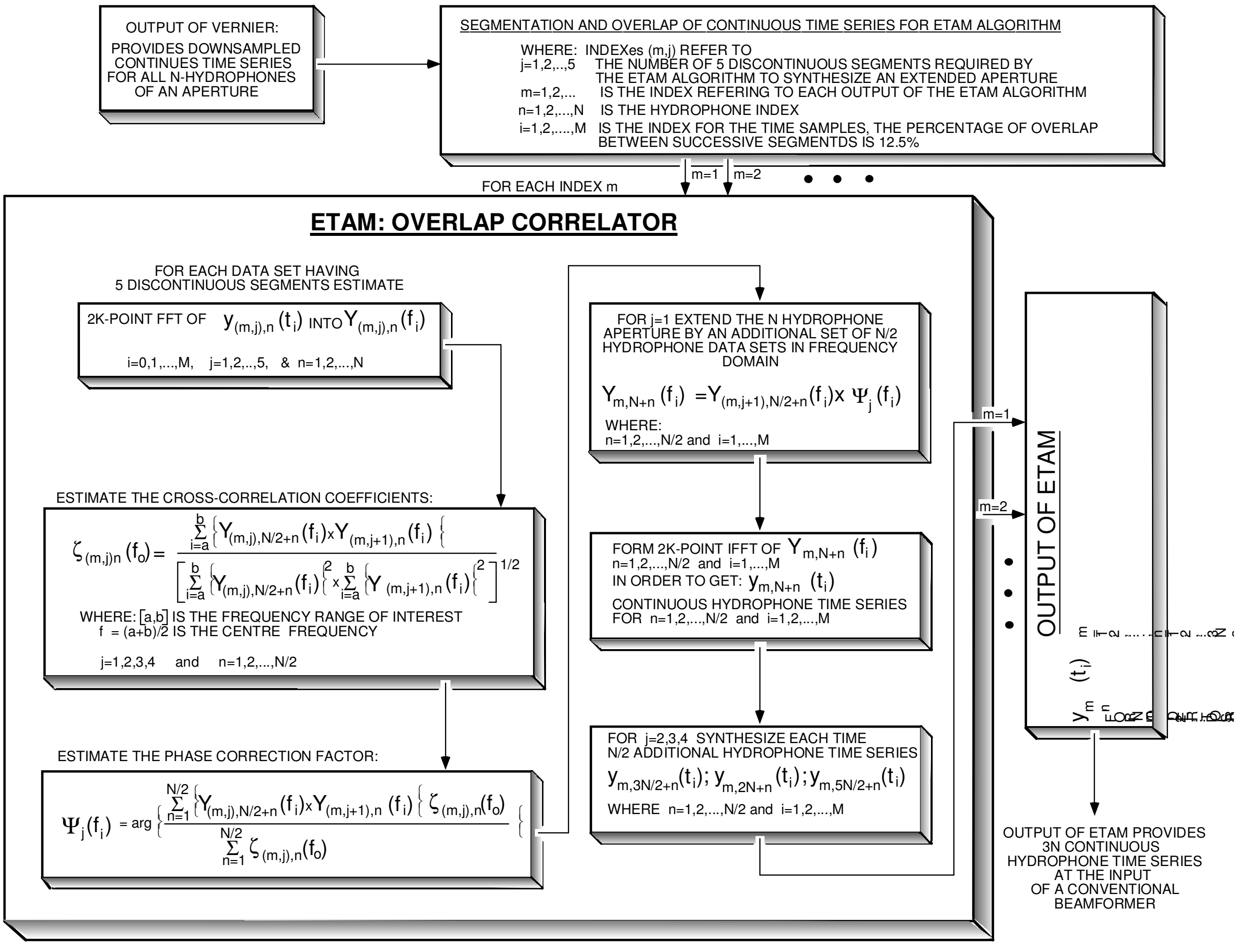

Figure 23: Schematic diagram for the processing arrangements of ETAM algorithm. The basic processing steps include: (1) <u>time series segmentation, overlap and grouping of 5 discontinuous segments, which are provided at the input of the overlap correlator</u>, shown by the block at the top part of schematic diagram. Details of the segmentation process are shown also by Figure 3.22. (2) <u>The main block called ETAM: Overlap Correlator provides processing details for the estimation of the phase correction factor to form the synthetic aperture</u>, and finally (3) <u>generation of the continuous sensor time series of the synthetic aperture are obtained through IFFT, discardation of overlap and concatenation of segments to form continuous time series</u> (left hand side block). The various indexes provide details for the implementation of the synthetic processing flow in a generic computing architecture.

6 Concept Demonstration: *Simulations*

Performance assessment and testing of the generic sub-aperture multi-dimensional adaptive beamforming structure has been carried out with synthetic and real data sets. [62] and [63] present a set of real data results that were derived from the implementation of the generic signal processing structure of this report in integrated active-passive towed array sonar and 3D/4D ultrasound imaging systems, respectively.

The synthetic data sets include narrowband and hyperbolic frequency modulated (HFM) signals for passive and active applications, respectively. For sonar applications, the frequencies of the passive narrowband signals are taken to be 330 Hz and the active signal consists of HFM pulses with pulse-width of 8 seconds long, 100-Hz bandwidth centered at 330 Hz, with 120 seconds pulse repetition period, or pulses with pulse-width of 500 μs long, 10-KHz bandwidth centered at 200 KHz, with arbitrary pulse repetition period. For ultrasound applications, the synthetic signals consist of FM pulses with 4MHz bandwidth centered at 3MHz. The scope here is to demonstrate that the implementation of adaptive schemes (i.e. GSC and STMV) in real time systems is feasible. Moreover, it is shown that the proposed generic configuration of adaptive schemes provides array gain improvements when compared with the performance characteristics of the multi-dimensional conventional beamformer. As for active applications, it is shown that the adaptive schemes of the proposed generic sub-aperture structure achieve near instantaneous convergence, which is essential for active ultrasound, sonar and radar applications.

The generic adaptive sub-aperture processing structure and the associated signal processing algorithms were implemented in a computer workstation. The memory of the workstation was sufficient to allow processing of long continuous sensor time series. However, the available memory restricts the number of sensors and the number of steered beams.

Nevertheless, the simulations of this report are sufficient to demonstrate that system oriented applications of the proposed generic sub-aperture adaptive structure for multi-dimensional arrays of sensors can be more effective than the relevant mainstream signal processing concepts. In fact, the conclusions derived from the present simulations are substantiated by the real data results reported in [62] and [63] for integrated active passive towed array sonar and 3D/4D ultrasound imaging applications.

6.1 SONAR Simulations: Cylindrical Array Beamformer

6.1.1 Synthetic Sonar Data: *Passive*

A cylindrical array with 160 sensors (16 rings with 10 sensors on each ring) was considered where the distance between rings along z-axis is taken to be equal to the angular spacing between sensors of the rings (i.e., $\delta_z = 2\pi R / M = \delta = 2.09m$). Continuous sensor time series were provided at the inputs of the generic conventional and adaptive beamformers with the processing flows as shown in Figures 20 and 21, respectively. The total number of steering beams for both the adaptive and conventional beamformers, was 144. For the decomposition process of the generic beamformer, expressed by Eq. (33), there were 16 beams steered in the angular sector of (0 -- 360^o) for azimuth bearing and 9 beams formed in the angular sector of (0 -- 180^o) for elevation bearing. Thus, the generic beamformer provided 16 azimuth beams for each of the 9 elevation steering angles, giving a total of 144 beams.

In the upper part of Figure 24, the left hand side diagram shows the output power of the azimuth beams at the expected elevation bearing of the signal source for the generic 3-D cylindrical array conventional beamformer; the right hand side of Figure 24 shows the output power of the elevation beams at the expected azimuth angle of the signal source. In both cases, no spatial window has been applied. The results at the left hand side of the lower part of Figure 24 correspond to the azimuth beams for the conventional beamformer with Hamming as a spatial window (dotted line) and the adaptive (solid line) sub-aperture beamformer. In this case, the number of sub-apertures was $G=3$ with Hamming as a spatial window applied on the sub-aperture conventional circular beamformer.

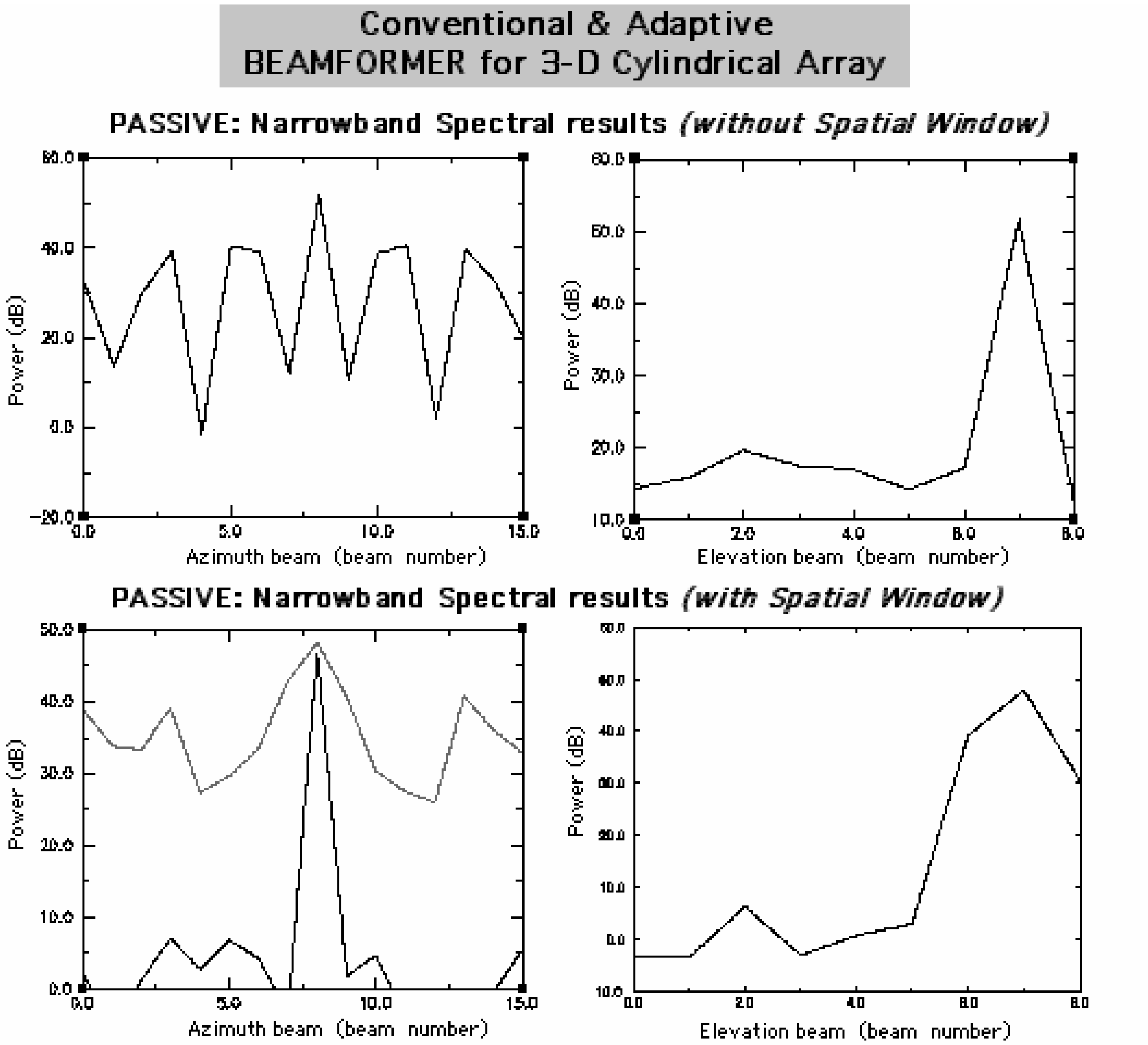

Figure 24: Passive beamforming results for a cylindrical array. Upper part shows azimuth and elevation bearing response for the proposed generic multi-dimensional beamformer. Lower left hand side part shows beamforming results of the conventional with spatial window (dotted line) and adaptive (solid line) beamformers. Lower right hand side part shows elevation bearing response for the conventional cylindrical beamformer with spatial window.

It is apparent by these results that the spatial shading has significantly suppressed the side-lobe structure of the conventional beamformer and has widen the beamwidth, as expected.

Moreover, the adaptive beamforming results demonstrate a significant improvement in suppressing the side-lobe structure as compared with the conventional results. The right hand side of the lower part of Figure 24 includes elevation bearing response for the conventional beamformer with spatial shading. At this point it is important to note that the application of spatial shading on the fully coherent 3-D cylindrical beamformer would have been a much more elaborate process than the one that has been used for the generic multi- dimensional beamformer.

This is because the decomposition process for the latter allows two much simpler and separate applications of spatial shading (i.e. one for circular arrays and the other for line arrays) discussed analytically in Section 3.3.2 and in References [7,25-28].

Figure 25 shows the narrowband spectral estimates of the generic 3-D cylindrical array conventional beamformer with Hamming spatial shading for all the azimuth beams according to the so-called GRAM presentation arrangement, discussed in Section 3.4 and in Reference [34]. The GRAMs in this figure represent the spectrograms of the output of the azimuth beams steered at the signal's expected elevation bearing. The GRAMs in Figure 26 show the corresponding results when the azimuth beams are steered at an elevation angle which is 55 degrees off the expected elevation bearing of the signal. It is obvious from the results of Figure 26 that the array gain of the conventional beamformer with spatial shading is not very high.

For the same sensor time series, when the adaptive sub-aperture schemes are implemented in the generic multi-dimensional beamformer the corresponding results are shown in Figure 27. When the results of Figure 27 are compared with the corresponding conventional results of Figure 25, the directional array gain improvements of the generic multi-dimensional beamformer become apparent. In this case the adaptive technique was the sub-aperture GSC-SA. As expected and because of the array gain improvements provided by the adaptive beamformer, the signal of interest is not present in the GRAMs of Figure 28, which provides the azimuth beams steered at an elevation angle which is by 55 degrees off the expected elevation bearing of the signal. The results of Figure 28 are in sharp contrast with those of Figure 26 for the conventional beamformer.

An explanation for the poor angular resolution performance of the conventional beamformer requires interpretation of the results of Figures 24 and 26. In particular, for the simulated cylindrical array, Figure 24 shows that that conventional beamformer with spatial shading has 13 dBs side-lobe suppression in azimuth beam steering and approximately 60 degrees beam-width in elevation. Furthermore, to improve detection the power beam outputs shown in the GRAMs of Figures 25 and 27 have been normalized [34], since this is a typical processing arrangement for operational sonar displays. However, the detection improvements of the normalization process would enhance the detection of the side-lobe structure shown in Figure 24. Thus, the results of Figures 24 and 26 provide typical angular resolution performance characteristics for sonars deploying cylindrical array beamformers.

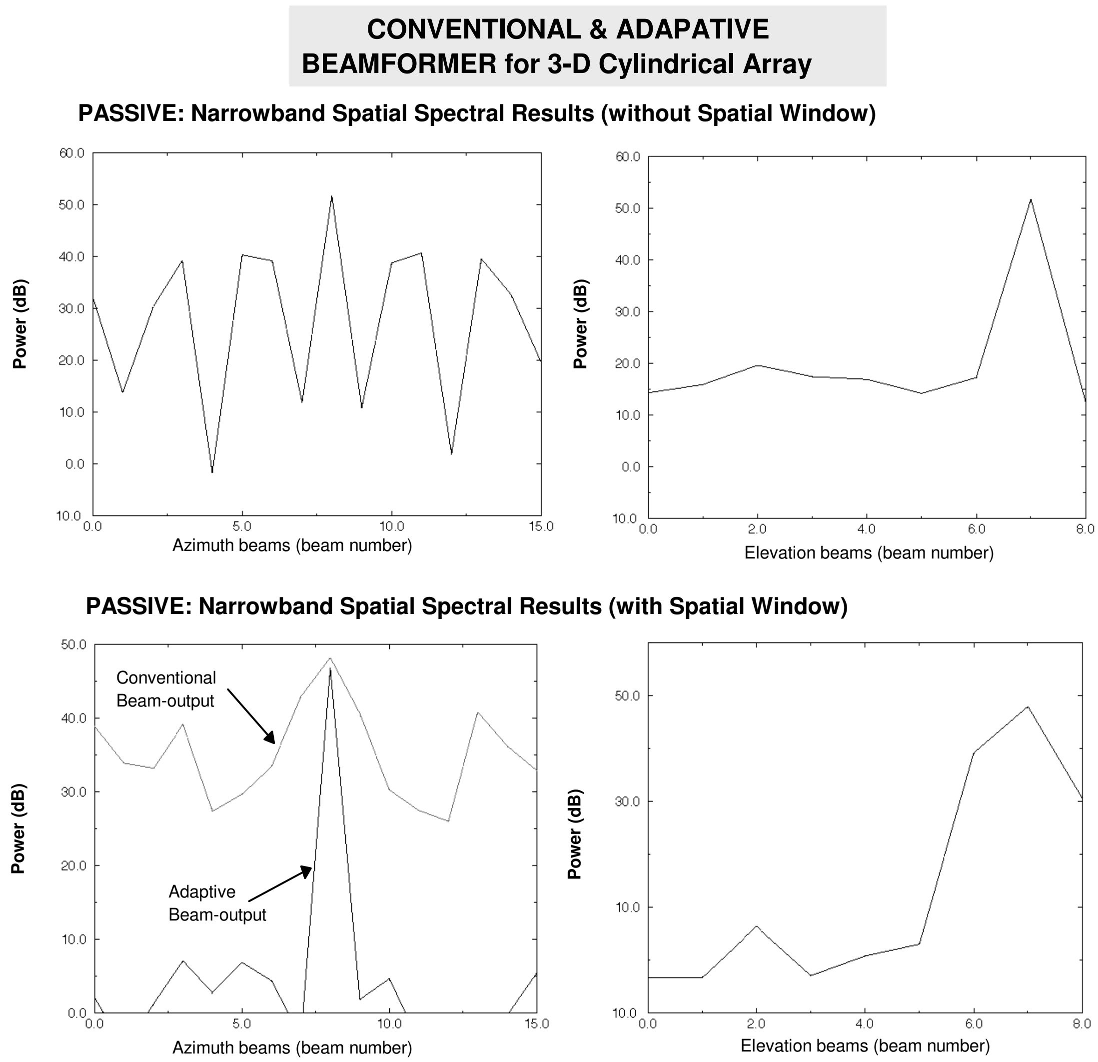

Figure 25: Narrowband spectral estimates of the generic 3-D cylindrical array conventional beamformer for all the azimuth beams steered at the signal's expected elevation angle. The 25 windows of this display correspond to the 25 steered beams equally spaced in [1, -1] cosine space. The acoustic field included two narrowband signals that the very poor angular resolution performance of the conventional beamformer has failed to resolve.

In summary, the results of Figures 24-28, with an appropriate scaling on the actual array dimensions and the frequency ranges of the signals that have been considered in the simulations, may project the performance characteristics for a variety of sonars deploying cylindrical arrays with conventional or adaptive beamformers.

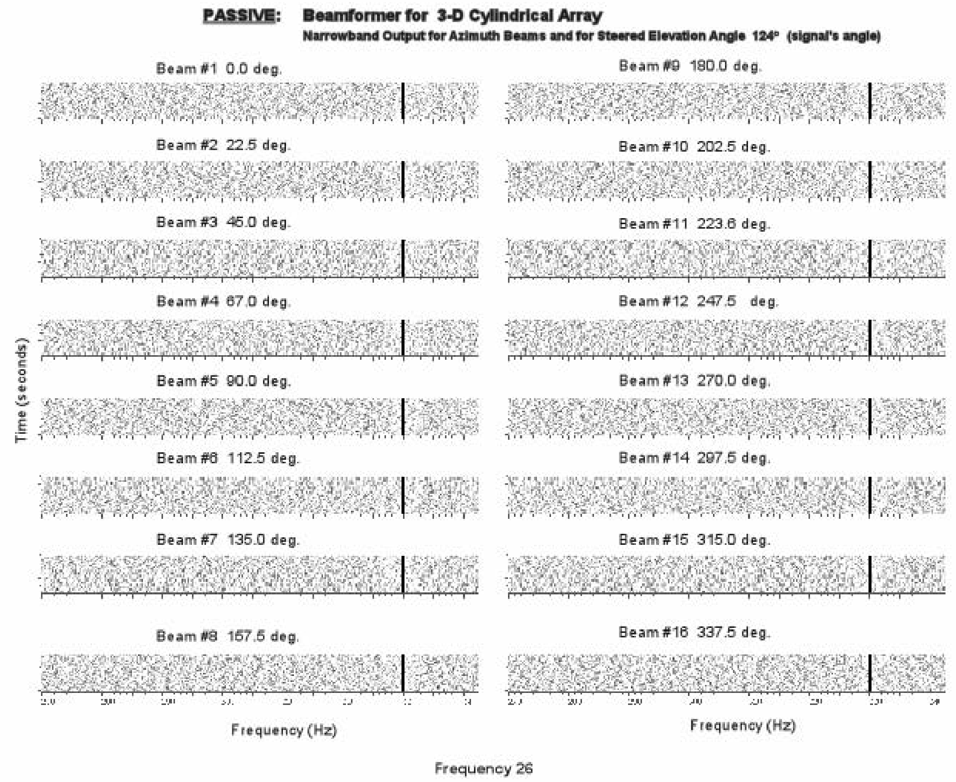

Figure 26 Narrowband spectral estimates of the generic 3-D cylindrical array conventional beamformer for all the azimuth beams steered at an elevation bearing, which is 55 degrees off the expected signal's elevation angle. The 25 windows of this display correspond to the 25 steered beams equally spaced in [1, -1] cosine space. The acoustic field at this steering does not include signals. However, the very poor side-lobe suppression of the conventional beamformer reveals signals that do not exist at this steering.

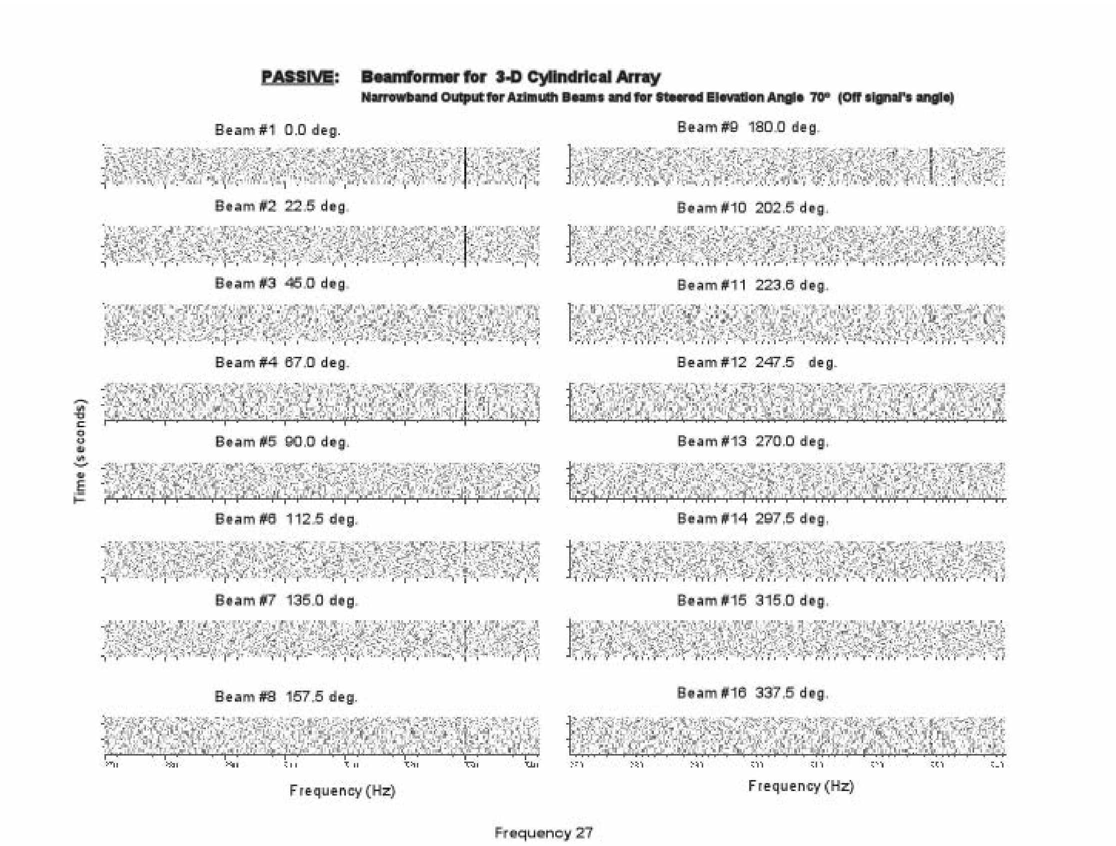

Figure 27: Narrowband spectral estimates of the generic 3-D cylindrical array adaptive (GSC) beamformer for all the azimuth beams steered at the signal's expected elevation angle. Input data sets are the same as in Figure 24. The 25 windows of this display correspond to the 25 steered beams equally spaced in [1, -1] cosine space. The acoustic field included two narrowband signals that the very good angular resolution performance of the sub-aperture adaptive beamformer resolves the bearings of the two signals.

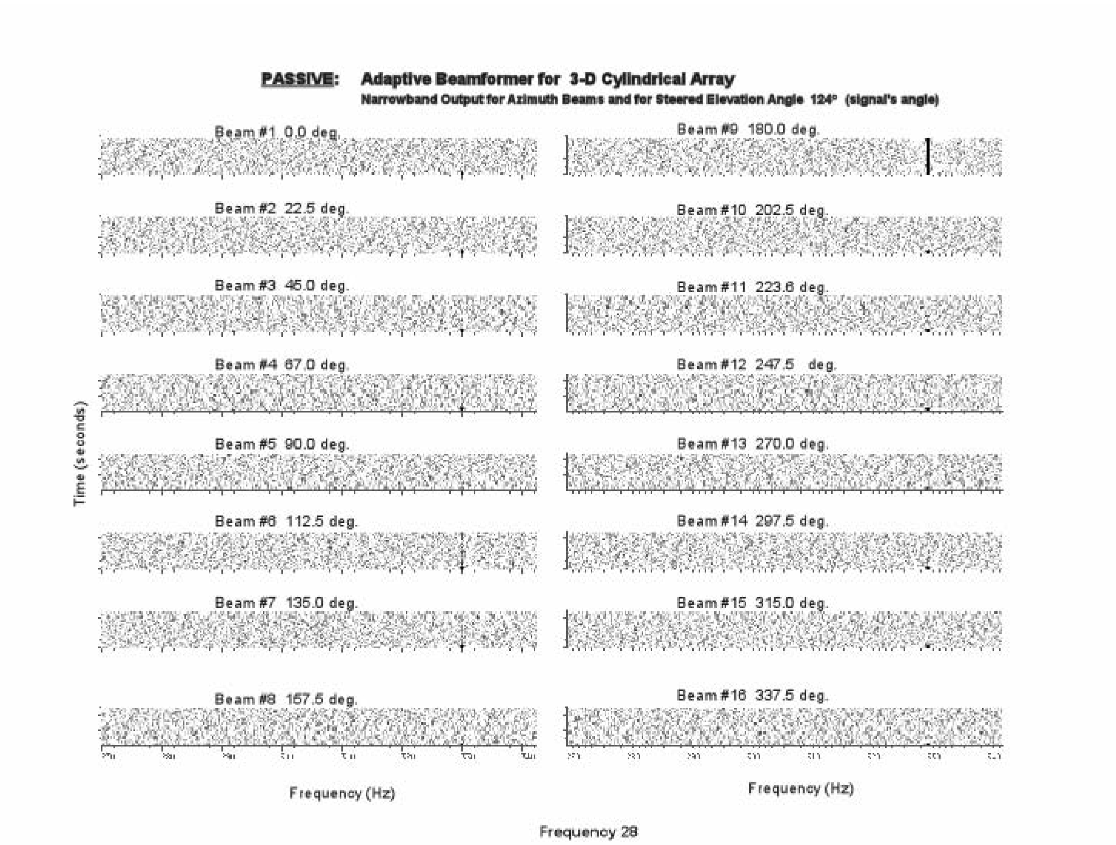

Figure 28: Narrowband spectral estimates of the generic 3-D cylindrical array adaptive (GSC) beamformer for all the azimuth beams steered at an elevation bearing, which is 55 degrees off the expected signal's elevation angle. Input data sets are the same as in Figure 25. The 25 windows of this display correspond to the 25 steered beams equally spaced in [1, -1] cosine space. The acoustic field at this steering does not include signals. Thus, the very good side-lobe suppression of the sub-aperture adaptive beamformer shows that there are no signals present at this steering.

6.1.2 Synthetic Sonar Data: *Active*

It was discussed before that the configuration of the generic beamforming structure providing continuous beam time series to the input of a matched filter or a temporal spectral analysis unit, forms the basis for integrated active or passive sonar applications. However, before the adaptive aperture processing schemes are integrated with a matched filter, it is essential to demonstrate that the beam time series from the outputs of the non-conventional beamformers have sufficient temporal coherence and correlate with the reference signal. For example, if the signal received by a sonar array consists of frequency-modulated (FM) pulses with a pulse repetition period of a few minutes, then questions may be raised about the efficiency of an adaptive beamformer to achieve near-instantaneous convergence in order to provide beam time series with coherent content for the FM pulses. This is because partially adaptive processing schemes require at least a few iterations to converge to a sub-optimum solution.

To address this question, the matched filter and the conventional and adaptive beamformers, shown in Figures 20 and 21, were tested with simulated data sets including HFM pulses 8-s long with 100-Hz bandwidth. The pulse repetition period was 120 seconds. Although this may be considered as a configuration for bistatic active sonar applications, the findings from this experiment can be applied to monostatic active sonar systems as well.

In the next figure we will present some results from the output of the active unit of the generic signal processing structure. Figure 29 shows the output of the replica correlator for the conventional and adaptive beam time series of the sub-aperture GSC and STMV adaptive techniques [1,37]. In this case, the steering angles are the same with those of the data sets shown in Figures 25-28. The horizontal axis in this figure represents range or time delay ranging from 0 to 120-s, which is the pulse repetition period. While the three beamforming schemes provide artifact-free outputs, it is apparent from the values of the replica correlator-output that the conventional beam time series exhibit better temporal coherence properties than the beam time series of the sub-aperture GSC adaptive beamformer. The significance and a quantitative estimate of this difference can be assessed by comparing the amplitudes of the correlation outputs in Figure 29. The replica correlator amplitudes are 12.06, 11.81, 12.08 for the conventional, and the adaptive schemes: GSC-SA (Sub-Aperture), STMV-SA (Sub-Aperture) respectively. These results also show that the beam time series of the STMV sub-aperture scheme have temporal coherence properties equivalent to those of the conventional beamformer, which is the optimum case.

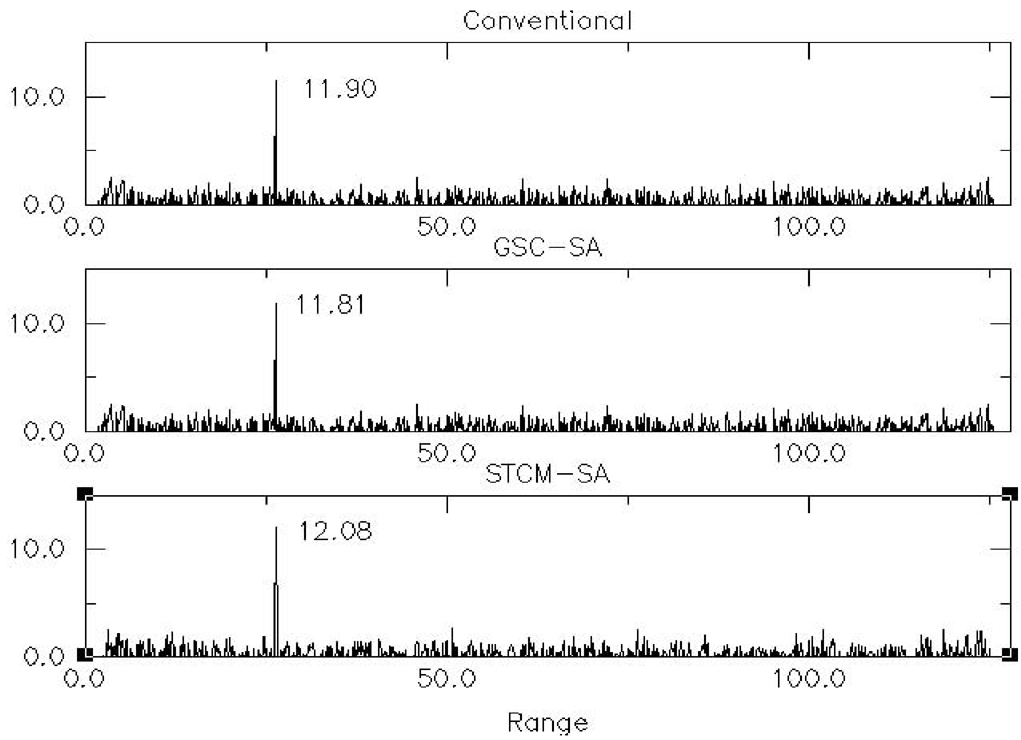

Figure 29: Output of replica correlator for the conventional and sub-aperture adaptive (GSC, STMV) beam time series of the generic cylindrical array beamformer. The azimuth and elevation beams are steered at the signal's expected bearings, which are the same with those in Figures 24 - 26.

6.1.3 Real Data: Active Cylindrical Sonar System

The proposed system configuration and the conventional and adaptive signal processing structures of this study was also tested with real data sets from an operational sonar system. Echoes of HFM pulses were received by a cylindrical array having comparable geometric configuration and sensor arrangements as discussed in the simulations. Continuous beam time series were provided at the input of the sub-aperture cylindrical adaptive beamformer with processing flow as defined in Figures 20 and 21. The total number of steering beams for both the adaptive and conventional beamformers was 144. Figure 30 provides the matched filter output results for a single pulse. The upper part of Figure 30 shows the matched filter output of the conventional beamformer and the lower part shows the output of the sub-aperture STMV adaptive algorithm [1,37]. The horizontal axis corresponds to the azimuth angular space ranging from 0 to 360 degrees. The vertical axis corresponds to the time delay or range estimate, which is determined by the location of the pick of the matched filter output and the color shows the magnitude of the matched filter output. In a sense, each vertical color-coded line of Figure 30 represents the matched filter output (e.g., see Figure 29) for a giver azimuth steering angle.

Since these are unclassified results provided by an operational sonar, there were no real targets present during the experiments. In a sense, the results of Figure 30 present the scattering properties of the medium as they were defined by the received echoes. Although the results of Figure 30 are normalized [34], the amplitudes of the output of the matched filter in Figure 30 for the conventional (upper figure) and adaptive (lower figure) beam time series were compared before the use of the normalization processing and they were found to be approximately the same. Again, these results show that the beam time series of the sub-aperture adaptive scheme have temporal coherence properties equivalent to those of the conventional beamformer, as this was also confirmed with simulated data, discussed in Section 6.1.2.

In summary, the basic difference between the conventional and adaptive matched filter output results is that the improved directionality (or array gain) of the adaptive beam time series localizes the detected HFM pulses and the associated echo returns more accurately than the conventional beamformer.

This kind of array gain improvement, provided by the adaptive beamformer, suppresses the reverberation effects during active sonar operations, as this is confirmed by the results of Figure 30. It is anticipated that the adaptive beamformers will enhance the performance of integrated active-passive and mine-hunting sonars by means of precise detection and localization of echoes that are embedded in reverberation noise fields.

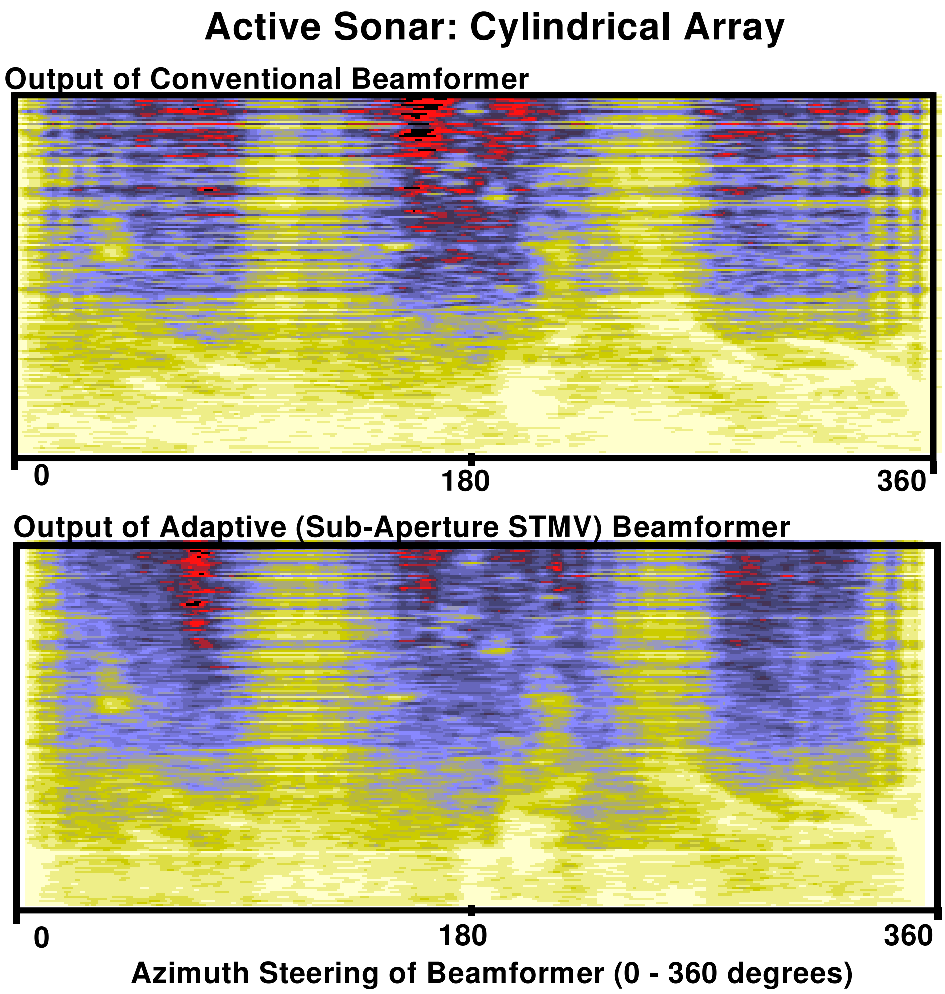

Figure 30: Upper part shows the matched filter output of the conventional and the lower part of the sub-aperture STMV adaptive algorithm for a cylindrical beamformer. The horizontal axis refers to the angular space covering the bearing range of (0, 360 degrees). The vertical axis refers to time delay or range estimates of the matched filter and the color refers to the correlation output. Each vertical color-coded line of Figure 30 represents a correlation output of Figure 27 for a given bearing angle. The basic difference between the conventional and adaptive matched filter output results is that the improved directionality (or array gain) of the adaptive beam time series localizes the detected HFM pulses and the associated echo returns in a smaller number of beams than the conventional beamformer.

6.2 Ultrasound Imaging Systems: Line and Planar Array Beamformers

Performance assessment and testing of the generic sub-aperture adaptive beamformers that have been discussed in this report, have been carried out with simulated ultrasound data. The parameters in these simulations were identical with those of an advanced 3D/4D experimental fully digital ultrasound imaging system that is discussed in [63].

The results presented in this section are divided into two parts. The first part discusses the simulations for linear phased arrays and the second part the results for planar phased array systems, respectively. The scope with these simulation is to evaluate the angular (azimuth) resolution performance of the

- 2D, 3D Adaptive Beamforming for ultrasound imaging,

The impact and merits of this technique will be contrasted with the angular resolution performance obtained using the 2D, 3D conventional phased array beamforming. The requirement for synthetic aperture processing for ultrasound imaging applications is discussed in detail in [63]. Synthetic aperture processing in this case is required for the data acquisition and digitization process of the sensor channels of large size planar array ultrasound probes by A/DC peripherals that have smaller number of A/D channels than those in the probes. For details about the synthetic aperture processing, the reader is asked to see Reference [1]. The synthetic aperture scheme is called ETAM algorithm and has been tested only with line and planar arrays [11,12,14,30].

It was discussed in Section 5.3 that the configuration of the generic beamforming structure to provide continuous beam time series at the input of a matched filter and a temporal spectral analysis unit, forms the basis for ultrasound and integrated passive and active sonar applications. For ultrasound imaging applications, to address this question the matched filter and the sub-aperture adaptive processing scheme, shown in Figures 20 and 21, were tested with synthetic data sets including CW (for Doppler applications) and FM pulses.

Normalization of the output of a matched filter, such as the results of Figure 29, and the display of the beam time series as GRAMS provides a waterfall display of ranges (depth) as a function of beam-steering, which define the reconstructed images of an ultrasound system.

6.2.1 Ultrasound Imaging System with Linear Phased Array Probe

The first simulation considered a 32-elements linear phased array probe, having pitch equal to 0.4mm. The sampling frequency was 33 MHz. The position and frequency characteristics of the received sensor time series relevant with the reference image are defined in Table 1. Figure 31 shows the normalized beam cross-sections obtained with adaptive beamforming and with conventional beamforming apodized in space. The adaptive beamformer beam width is noticeably smaller than the one obtained with the conventional apodized beamforming procedure, defined in Section 5.2.4.

Table 1: Parameters for simulated ultrasound time series for a linear phased array ultrasound probe

	Fc	**BW**	**Bearing**	**Depth**
Point Target #1	4.0 MHz	2.0 MHz	80°	10 mm
Point Target #2	4.0 MHz	2.0 MHz	92°	25 mm
Point Target #3	2.0 MHz	1.0 MHz	84°	40 mm
Point Target #4	2.0 MHz	1.0 MHz	96°	50 mm

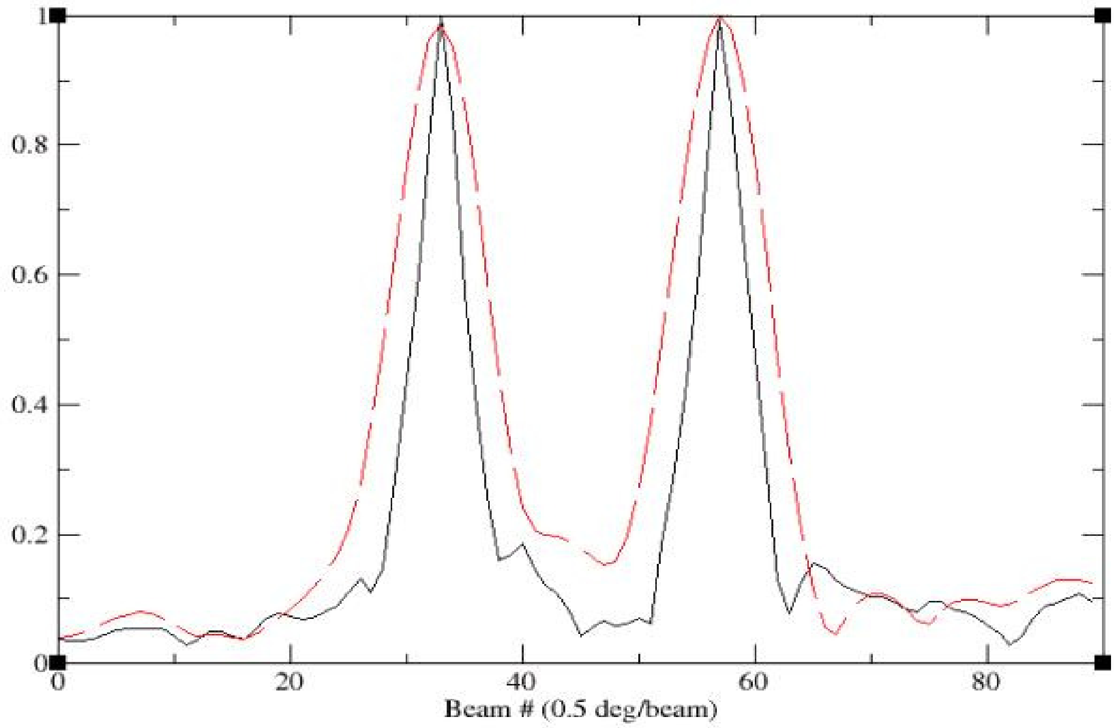

Figure 31: Beam Cross-Section for two sources at 65mm depth: Left source –6° from broadside (@ 2.1MHz, BW 50%), right source +6° from broadside (@) 2.0MHz, BW 50%). Adaptive (solid line) and conventional beamforming (apodized in space, dashed line).

The next figure 32, shows the reconstructed images for the simulated point targets defined in Table 1. The first image at the left hand side of Figure 32 shows the reconstructed image from the output of the beam time series of a conventional phased array beamformer applied on the synthetic 32-sensor probe time series. The middle image in Figure 32 shows the reconstructed image from the beam time series of the sub-aperture adaptive beamformer applied on the same synthetic 32-sensor probe time series, as before. The image at the right of Figure 32 shows the reconstructed image from the time series of a conventional phased array beamformer applied on 96-sensor phased array probe for the same structure of data defined in Table 1. It is apparent from these simulations that the sub-aperture adaptive beamforming provides better angular resolution with respect to conventional beamforming. Moreover, the 32-elements adaptive beamformer achieves almost the same performances as a 96-elements conventional beamformer.

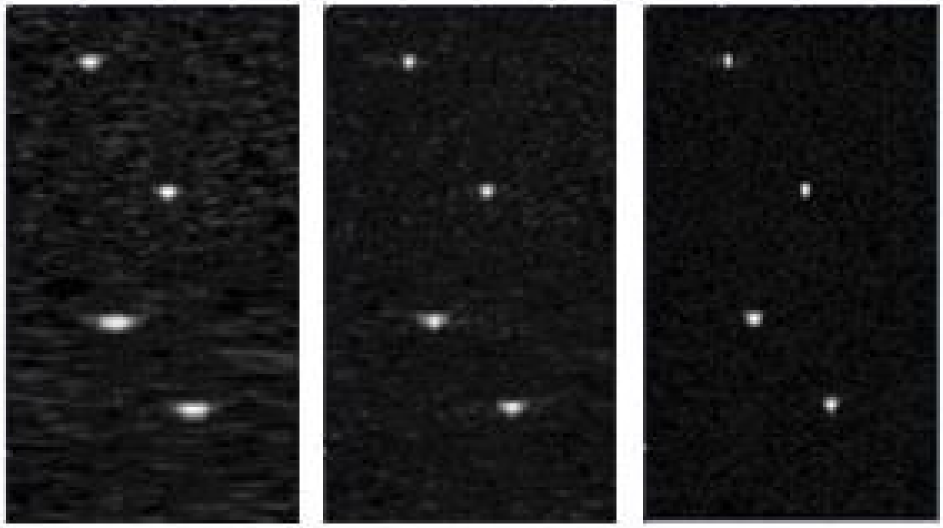

Figure 32: First image from the left shows reconstructed image from beam time series of a conventional phased array beamformer applied on the synthetic data defined in Table 1, for a 32-sensor phased array probe. The central image in this figure, shows the output of the sub-aperture adaptive beamformer applied on the same 32-sensor data; and the right panel shows the reconstructed image from the time series of a conventional phased array beamformer applied on 96-sensor phased array probe for the same structure of data defined in Table 1.

6.2.2 Ultrasound Imaging System with Planar Phased Array Probe

Deployment of planar arrays by ultrasound medical imaging systems gains increasing popularity because of their advantage to provide 3-D images of organs under medical examination. However, if we consider that a state-of-the-art line array ultrasound system consists of 256 sensors, then a planar array ultrasound system should include at least 4096 sensors (16x256) in order to achieve the angular resolution performance of a line array system and the additional 3-D image reconstruction capability provided by the elevation beam steering of a planar array. Thus, increased angular resolution in azimuth and elevation beam steering for ultrasound systems means larger sensor arrays with consequent technical and higher cost implications. As discussed in Section 4, the alternative is to use synthetic aperture and or sub-aperture adaptive beam processing.

In the simulations discussed in this section, a planar array with 121 (11×11) sensors was considered that provided continuous sensor time series at the input of the conventional and sub-aperture adaptive beamformers with processing flow similar to that shown in Figures 20 and 21 for a cylindrical array. As in the case of the cylindrical beamforming results, the power outputs of the beam time series of the conventional and the sub-aperture adaptive techniques implemented in a planar array, demonstrated the same performance characteristics with those of Figures 24-28 for the cylindrical array. Supporting evidence for this claim are the real data results, from an experimental 3D/4D ultrasound imaging system deploying a planar array with 16x16=256 sensors, that are presented in [63].

The synthetic data experiments for the planar array, discussed in this section, were carried out using the Field II ultrasound simulator program obtained from the Technical University of Denmark [60]. The Field II program simulates point sources, and was set up to simulate 5,000 point sources arranged in a spherical shell, conforming to the specifications of an ultrasound imaging system with a planar phased array probe. More specifically, in the simulations the probe was assumed to have a 16x16 channel planar array as receiver and a 6x6 channel planar array as transmitter, with element spacing of 0.4mm and sampling frequency of 33 MHz. The FM pulse was centred at 2.5MHz, with a bandwidth of 4.0 MHz. The simulated illumination pattern was identical with that defined in [63] for an experimental planar array ultrasound system and included six illumination beams along azimuth and six beams along elevation spaced 10° apart covering 60° is each direction (azimuth and elevation). The result was a total of 36 angular sectors for illumination. A conventional beamformer was used to process the data received by the 16x16 planar array. The decomposition process of the 3D planar array beamformer was carried according to the details defined in Section 5.2.4, to obtain 3D azimuth and elevation beams. A complete image reconstruction of the beams into a 4D (i.e., 3D+time) volume was then performed.

Figure 33 shows the C-scans derived from the 3D reconstructed volumes of the simulated spherical shell. In this image, which shows a slice (C-scan) of the spherical shell from the 3D volumetric image, the expected ring that corresponds to the cross section of a shell is visible. The left and right images in Figure 33 correspond to the 3D conventional and adaptive beamformers, respectively. The better performance of the adaptive beamformer is evident in this case as it provides better detection and image definition of the spherical shell than that of the corresponding conventional beamformer. The 3D visualization software, which is discussed in [61], was provided by Prof. Sakas (i.e., Fraunhofer IGD, Germany), as part of our technical exchanges within the framework of the collaborative European-Canadian project ADUMS (EC-IST-2001-34088).

The next Figure 34 shows the 3D volume reconstruction of the spherical shell using the 3D conventional (left image) and the 3D adaptive (right image) ultrasound beamformers defined in this report. As was the case with the C-scans (Figure 33), the results in Figure 34 show that the 3D adaptive beamformer provides better image definition than the corresponding 3D conventional beamforming results.

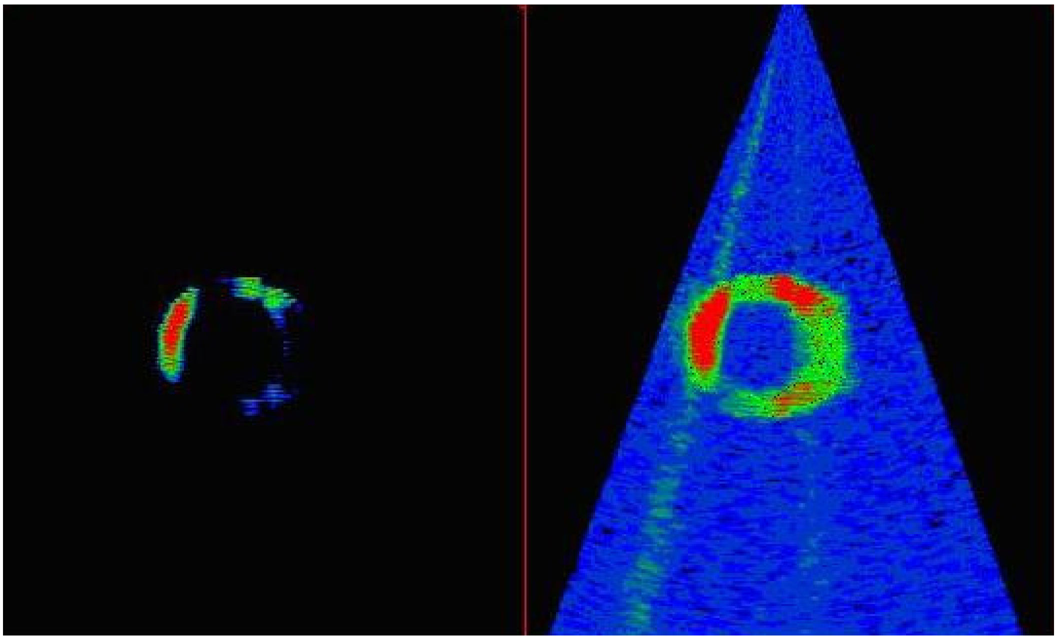

Figure 33: C-scans derived from the 3D reconstructed images of the simulated spherical shell. Left image, shows image reconstruction from the beam time series of the 3D conventional beamformer. Right image, shows reconstructed image from the beam time series of the 3D adaptive beamformer.

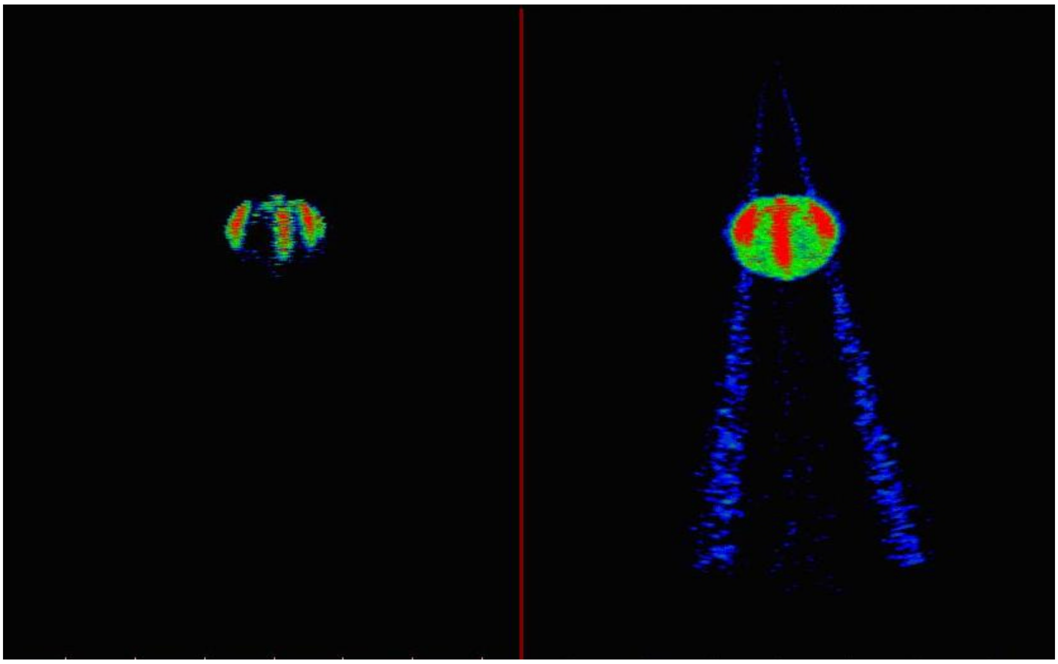

Figure 34: 3D volume reconstruction of the simulated spherical shell. Left image, reconstructed with the 3D conventional beamformer. Right image, reconstructed with the 3D adaptive beamformer.

7 Conclusion

The synthetic data results of this report indicate that the generic multi-dimensional adaptive concept addresses practical concerns of near-instantaneous convergence, shown in Figures 24-33, for ultrasound imaging and integrated active-passive sonar systems. The performance characteristics of the sub-aperture adaptive beamformer compared with that of the conventional beamformer are reflected as improvements in directional estimates of azimuth and elevation angles and suppression of reverberation effects. This kind of improvement in azimuth and elevation bearing estimates is essential for 3-D ultrasound, sonar and radar operations. The conclusions of this report are supported also by the real data results presented in [62] and [63] for integrated active passive towed array sonar and 3D/4D ultrasound imaging systems, respectively.

In summary, a generic beamforming structure has been developed for multi-dimensional sensor arrays that allows the implementation of conventional, synthetic aperture and adaptive signal processing techniques in integrated active-passive real time systems. The proposed implementation is based on decomposing the 2-D and 3-D beamforming process in sub-sets of coherent processes and creating sub-aperture configurations that allow the minimization of the number of degrees of freedom of the adaptive processing schemes. The proposed approach has been applied to line, planar, and cylindrical arrays of sensors where the multi-dimensional beamforming is decomposed into sets of line-array and/or circular array beamformers. Moreover, the application of spatial shading on the generic multi- dimensional beamformer is a much simpler process than that of the fully coherent 3-D beamformer. This is because the decomposition process allows two simple and separate applications of spatial shading (i.e., one for circular and the other for line arrays).

The fact that the sub-aperture adaptive beamformers provided array gain improvements for CW and HFM signals under a real time data flow as compared with the conventional beamformer demonstrates the merits of these advanced processing schemes for practical ultrasound, sonar and radar applications. In addition, the generic implementation scheme of this study suggests that the design approach to provide synergism between the conventional beamformer, the synthetic aperture and the adaptive processing schemes, (e.g., see Figures 20 and 21) is an essential property for system applications.

Although the focus of the implementation effort included only a few adaptive processing schemes, the consideration of other types of spatial filters for real time ultrasound, sonar and radar applications should not be excluded. The objective here was to demonstrate that adaptive processing schemes can address some of the challenges that the next generation ultrasound and active-passive sonar systems will have to deal with in the near future. Once a generic signal processing structure is established, as suggested in the report, the implementation of a wide variety of processing schemes can be achieved with minimum efforts for real time systems deploying multi-dimensional arrays. Finally, the results presented in this report indicate that the sub-aperture STMV adaptive scheme address the practical concerns of near-instantaneous convergence associated with the implementation of adaptive beamformers in integrated active-passive sonar systems. It is the understanding of the investigators of this study that the CSA-SA, (i.e., with near instantaneous convergence requirement for a single active transmission to generate a single image), is the most appropriate adaptive beamformer for cost efficient ultrasound imaging applications. However, the MVDR-SA adaptive beamformer, (i.e., with near instantaneous convergence requirement for 3-successive transmissions to generate a single image), may provide much better image resolution than the CSA-SA algorithm.

References

[1] S. Stergiopoulos, “Implementation of adaptive and synthetic aperture processing schemes in integrated active-passive sonar systems”, *Proc. IEEE* , **86**(2), 358-396, Feb.-98.

[2] W.C. Knight, R.G. Pridham and S.M. Kay, "Digital Signal Processing for Sonar", *Proceedings of the IEEE*, **69**(11), pp. 1451-1506, 1981.

[3] B. Windrow et. al., "Adaptive Antenna Systems", *Proceedings IEEE*, **55**(12), pp. 2143-2159, 1967.

[4] A. A. Winder, "Sonar System Technology, *IEEE Trans. on Sonic Ultrasonics*, **SU-22**(5), pp. 291-332, 1975.

[5] A.B. Baggeroer, "Sonar Signal Processing" (article in Applications of Digital Signal Processing - Editor: A.V. Oppenheim), Prentice-Hall, 1978.

[6] S. Stergiopoulos and A.T. Ashley, "*Guest Editorial* " for a Special Issue on Sonar System Technology, *IEEE, J. Oceanic Eng.,* **18**(4), 361-366, 1993.

[7] Dhanantwari A.C., Stergiopoulos S. and Grodski J., “*Implementation of Adaptive processing in Integrated Active-Passive Sonars deploying cylindrical arrays*”, Proceedings of Underwater Technology ‘98, **UT’98**, Tokyo Japan, April-1998.

[8] W. C. Queen, “The Directivity of sonar receiving arrays”, *J. Acoust. Soc. Am.*, **47**, 711-720, 1970.

[9] V. Anderson and J. Munson, “Directivity of spherical receiving arrays”**,** J. *Acoust. Soc. Am.*, **35** 1162-1168, 1963.

[10] W. M. Carey and W.B. Moseley, "Space-time processing, environmental-acoustic effects", *IEEE J. Oceanic Eng.*, **16**, pp. 285-301, 1991; also in *Progress in Underwater Acoustics*, N.Y.: Plenum, pp. 743-758, 1987.

[11] S. Stergiopoulos and E.J. Sullivan, "Extended towed array processing by overlapped correlator ", *J. Acoust. Soc. Am.*, **86**(1), 158-171, 1989.

[12] S. Stergiopoulos, "Optimum bearing resolution for a moving towed array and extension of its physical aperture ", *J. Acoust. Soc. Am.*, **87**(5), 2128-2140, (1990).

[13] E.J. Sullivan, W.M. Carey and S. Stergiopoulos, "Editorial" special issue on Acoustic Synthetic Aperture processing, *IEEE J. Oceanic Eng.*, **17**(1), 1-7, 1992.

[14] S. Stergiopoulos and H. Urban, "An Experimental Study in Forming a Long Synthetic Aperture at Sea" , *IEEE J. Oceanic Eng.*, **17**(1), 62-72, 1992.

[15] G.S. Edelson and E.J. Sullivan, "Limitations on the overlap-correlator method imposed by noise and signal characteristics", *IEEE J. Oceanic Eng.*, **17**(1), pp. 30-39, 1992.

[16] G.S. Edelson and D.W. Tufts, "On the ability to estimate narrow-band signal parameters using towed arrays", *IEEE J.Oceanic Eng.*, **17**(1), pp. 48-61, 1992.

[17] N.L. Owsley, "Sonar array processing", S. Haykin, Editor, Prentice-Hall Signal Processing Series, A.V. Oppenheim series editor, pp.123, 1985.

[18] B. Van Veen and K. Buckley, "Beamforming: a Versatile Approach to Spatial Filtering", *IEEE ASSP Mag.*, pp. 4-24, 1988.

[19] H. Cox, R.M. Zeskind and M.M. Owen, "RobustAdaptive Beamforming", *IEEE- Trans. Acoustic Speech Signal Proc.,* **ASSP-35**(10), pp. 1365-1376, 1987,

[20] H. Cox, "Resolving power and sensitivity to mismatch of optimum array processors", *J. Acoust. Soc. Am.*, **54**(3), pp. 771-785, 1973.

[21] A.H. Sayed and T. Kailath, "A State-Space Approach to Adaptive RLS Filtering", *IEEE SP Mag.*, pp. 18-60, July-1994.

[22] J. Capon, "High resolution frequency wavenumber spectral analysis", *Proc. IEEE*, **57**, pp. 1408-1418, 1969.

[23] T.L. Marzetta, "A new interpretation for Capon's Maximum Likelihood Method of frequency-Wavenumber Spectra Estimation", *IEEE- Trans. Acoustic Speech Signal Proc.,* **ASSP-31**(2), pp. 445-449, 1983.

[24] S. Haykin, "Adaptive Filter Theory", Prentice-Hall, Englewood Cliffs, NJ, 1986.

[25] A. Tawfik, A.C. Dhanantwari, and S. Stergiopoulos, “A Generic beamforming structure allowing the implementation of adaptive processing schemes into 2-D & 3-D arrays of sensors”, *Proceedings MTS/IEEE OCEANS’97*, Halifax, Nova Scotia, Oct. 1997.

[26] A. Tawfik, A.C. Dhanantwari, and S. Stergiopoulos, “A Generic beamforming structure for adaptive schemes implemented in 2-D & 3-D arrays of sensors”, *J. Acoust. Soc. Am.*, **101**(5) Pt. 2, 3025, 1997.

[27] S. Stergiopoulos, A. Tawfik and A.C. Dhanantwari , “Adaptive Microphone 2-D and 3-D Arrays for Enhancement of Sound Reception in Coherent and Incoherent Noise Environment”, *Proceedings of Inter-Noise’97*, OPAKFI H-1027 Budapest, August 1997.

[28] A. Tawfik A. and S. Stergiopoulos, “A Generic Processing Structure Decomposing the Beamforming process of 2-D & 3-D Arrays of Sensors into Sub-Sets of Coherent Processes”, *Proc. of CCECE’97*, Canadian Conference on Electrical & Computer Engineering, St. John’s, NF, May 1997.

[29] N.L. Owsley, "Systolic array adaptive beamforming" NUWC Report **7981**, Sept. 1987.

[30] S. Stergiopoulos, "Limitations on towed-array gain imposed by a non isotropic ocean", J. *Acoust. Soc. Am.*, **90**(6), pp. 3161-3172, 1991.

[31] A.D. Whalen, "Detection of Signals in Noise", Academic Press, NY, 1971.

[32] D. Middleton, "Introduction to Statistical Communication Theory", New York, McGraw-Hill, 1960.

[33] H.L. Van Trees, "Detection, estimation and modulation theory," New York, Wiley, 1968.

[34] S. Stergiopoulos, "Noise Normalization Technique for Beamformed Towed Array Data ", *J. Acoust. Soc. Am.*, **97**(4), 2334-2345, (1995).

[35] S. Stergiopoulos, "Influence of Underwater Environment's Coherence Properties on Sonar Signal Processing", *Proceedings of 3rd European Conference on Underwater Acoustics, FORTH-IACM*, Heraklion-Crete, **V-I**, 453-458, 1996.

[36] F.J. Harris, "On the use of windows for harmonic analysis with discrete Fourier transfor", *Proc. IEEE*, **66**, 51-83, 1978.

[37] A. C. Dhanantwari, "Adaptive Beamforming with Near-Instantaneous Convergence for Matched Filter Processing", *Master Thesis*, Dept. of Elect. Eng., Technical University of Nova Scotia, Halifax, N.S., Canada, Sept. 1996.

[38] J. Krolik and D.N. Swingler, "Bearing Estimation of Multiple Broadband Sources using Steered Covariance Matrices", *IEEE Trans. Acoust. Speech, Signal Proc.*, **ASSP-37**, pp. 1481-1494, 1989.

[39] H. Wang and M. Kaveh, "Coherent signal-subspace processing for the detection and estimation of angles of arrival of multiple wideband sources", *IEEE Trans. Acoust. Speech, Signal Proc.*, **ASSP-33**, pp. 823-831, 1985.

[40] A. Antoniou, "Digital Filters: Analysis, Design, and Applications", 2nd Ed., McGraw-Hill, NY, 1993.

[41] A. Mohammed, "A high-resolution spectral analysis technique", DREA Memorandum **83/D**, Defence Research Establishment Atlantic, Dartmouth, N.S., Canada, 1983.

[42] A. Mohammed, "Novel methods of digital phase shifting to achieve arbitrary values of time delays", *DREA* **Report 85/106**, Defence Research Establishment Atlantic, Dartmouth, N.S., Canada, 1985.

[43] S. Stergiopoulos & A.T. Ashley, "An Experimental Evaluation of Split-Beam Processing as a Broadband Bearing Estimator for Line Array Sonar Systems", *J. Acoust. Soc. Am.*, **102**(6), 3556-3563, Dec. 1997.

[44] L.J. Griffiths, C.W. Jim, "An Alternative Approach to Linearly Constrained Adaptive Beamforming", *IEEE Trans. on Antennas and Propagation.*, **AP-30**, pp. 27-34, 1982.

[45] D.T.M. Slock, “On the Convergence Behavior of the LMS and the Normalized LMS Algorithms”, *IEEE Trans. Acoust. Speech, Signal Proc.*, **ASSP-31**, pp. 2811-1825, 1993.

[46] D. Middleton and R. Esposito, "Simultaneous Otpimum Detection and Estimation of Signals in Noise", *IEEE Trans. of Information Theory*, **IT-14**, pp. 434-444, 1968.

[47] P. Wille and R. Thiele, "Transverse horizontal coherence of explosive signals in shallow water", *J. Acoust. Soc. Am.*, **50**, pp. 348-353, 1971.

[48] P.A. Bello, "Characterization of randomly time-variant linear channels", *IEEE Trans. Commun. Syst.*, **10**, pp. 360-393, 1963.

[49] D.A. Gray, B.D.O. Anderson and R.R. Bitmead, "Towed Array Shape Estimation Using Kalman Filters - Theoretical Models", *IEEE J. Oceanic Eng.*, **18**(4), October 1993.

[50] B.G. Ferguson," Remedying the Effects of Array Shape Distortion on the Spatial Filtering of Acoustic Data from a Line Array of Sensors", *IEEE J. Oceanic Eng.*, **18**(4), Oct. 1993.

[51] J.L. Riley and D.A. Gray, "Towed Array Shape Estimation Using Kalman Filters - Experimental Investigation", *IEEE J. Oceanic Eng.*, **18**(4), October 1993.

[52] B.G. Ferguson, "Sharpness applied to the adaptive beamforming of acoustic data from a towed array of unknown shape", *J. Acoust. Soc. Am.*, **88**(6), pp. 2695-2701, 1990.

[53] Lu Feng, Milios E., Stergiopoulos S., and Dhanantwari A., "*A New Towed Array Shape Estimation Scheme for Real Time Sonar Systems* ", IEEE J. Oceanic Eng., **28**(3), 552-563, Sept, 2003..

[54] N.C. Yen and W. Carey, "Application of synthetic-aperture processing to towed-array data", *J. Acoust. Soc. Am.*, **86**, pp. 754-765, 1989.

[55] S. Stergiopoulos and H. Urban, " A New Passive Synthetic Aperture Technique for Towed Arrays" , *IEEE J. Oceanic Eng.*, **17**(1), pp. 16-25, 1992.

[56] V.H. MacDonald and P.M. Schulteiss, "Optimum passive bearing estimation in a spatially incoherent noise environment", *J. Acoust. Soc. Am.*, **46**(1), pp. 37-43, 1969.

[57] G.C. Carter, "Coherence and time delay estimation", *Proc. IEEE*, **75**(2), pp. 236-255, 1987.

[58] C.H. Knapp and G.C. Carter, "The generalized correlation method for estimation of time delay", *IEEE Trans. Acoust. Speech Signal Processing*, **ASSP-24**, pp. 320-327, 1976.

[59] D.C. Rife and R.R. Boorstyn, "Single-tone parameter estimation from discrete-time observations", *IEEE Trans. Infor. Theory*, **20**, pp. 591-598, 1974.

[60] http://www.it.dtu.dk/~jaj/field

[61] G. Sakas, G. Karangelis and A. Pommert, "Advanced Applications of Volume Visualization Methods in Medicine", Handbook on Advanced Signal Processing for Sonar, Radar and Medical Imaging Systems, Editor: Stergiopoulos, CRC Press LLC, Boca Raton, FL, 2000.

[62] B. Balaji, M. McDonald and A. Damini, "Detection Paradigms for Radar", Handbook on Advanced Signal Processing for Sonar, Radar and Medical Imaging Systems, 2nd Edition, Editor: Stergiopoulos, CRC Press LLC, Boca Raton, FL, 2008.

[63] S. Stergiopoulos and G. Edelson , "Theory and Implementation of Advanced Signal Processing for Active and Passive Sonar Systems" Handbook on Advanced Signal Processing for Sonar, Radar and Medical Imaging Systems, Editor: Stergiopoulos, CRC Press LLC, Boca Raton, FL, 2000.

List of symbols/abbreviations/acronyms/initialisms

DND	Department of National Defence
DRDC	Defence Research & Development Canada
DRDKIM	Director Research and Development Knowledge and Information Management
R&D	Research & Development

Distribution list

Document No.: DRDC Toronto TR 2008-101

LIST PART 1: Internal Distribution by Centre

0 TOTAL LIST PART 1

LIST PART 2: External Distribution by DRDKIM

1 Library and Archives Canada

1 TOTAL LIST PART 2

1 TOTAL COPIES REQUIRED

DOCUMENT CONTROL DATA
(Security classification of the title, body of abstract and indexing annotation must be entered when the overall document is classified)

1. ORIGINATOR (The name and address of the organization preparing the document, Organizations for whom the document was prepared, e.g. Centre sponsoring a contractor's document, or tasking agency, are entered in section 8.) Publishing: DRDC Toronto Performing: DRDC Toronto Monitoring: Contracting:	2. SECURITY CLASSIFICATION (Overall security classification of the document including special warning terms if applicable.) UNCLASSIFIED

3. TITLE (The complete document title as indicated on the title page. Its classification is indicated by the appropriate abbreviation (S, C, R, or U) in parenthesis at the end of the title)

Advanced Beamformers (U)
(U)

4. AUTHORS (First name, middle initial and last name. If military, show rank, e.g. Maj. John E. Doe.)

Stergios Stergiopoulos

5. DATE OF PUBLICATION (Month and year of publication of document.) July 2008	6a NO. OF PAGES (Total containing information, including Annexes, Appendices, etc.) 106	6b. NO. OF REFS (Total cited in document.) 63

7. DESCRIPTIVE NOTES (The category of the document, e.g. technical report, technical note or memorandum. If appropriate, enter the type of document, e.g. interim, progress, summary, annual or final. Give the inclusive dates when a specific reporting period is covered.)

Technical Report

8. SPONSORING ACTIVITY (The names of the department project office or laboratory sponsoring the research and development − include address.)

Sponsoring:
Tasking:

9a. PROJECT OR GRANT NO. (If appropriate, the applicable research and development project or grant under which the document was written. Please specify whether project or grant.) 16CL−01 &16CL−03	9b. CONTRACT NO. (If appropriate, the applicable number under which the document was written.)
10a. ORIGINATOR'S DOCUMENT NUMBER (The official document number by which the document is identified by the originating activity. This number must be unique to this document) DRDC Toronto TR 2008−101	10b. OTHER DOCUMENT NO(s). (Any other numbers under which may be assigned this document either by the originator or by the sponsor.)

11. DOCUMENT AVAILABILITY (Any limitations on the dissemination of the document, other than those imposed by security classification.)

Unlimited distribution

12. DOCUMENT ANNOUNCEMENT (Any limitation to the bibliographic announcement of this document. This will normally correspond to the Document Availability (11), However, when further distribution (beyond the audience specified in (11) is possible, a wider announcement audience may be selected.))

Unlimited announcement

DOCUMENT CONTROL DATA
(Security classification of the title, body of abstract and indexing annotation must be entered when the overall document is classified)

13. ABSTRACT (A brief and factual summary of the document. It may also appear elsewhere in the body of the document itself. It is highly desirable that the abstract of classified documents be unclassified. Each paragraph of the abstract shall begin with an indication of the security classification of the information in the paragraph (unless the document itself is unclassified) represented as (S), (C), (R), or (U). It is not necessary to include here abstracts in both official languages unless the text is bilingual.)

(U) The aim with this report is to bring together some of the recent theoretical developments on beamformers; and provide suggestions of how modern technology can be applied to the development of current and next generation ultrasound systems and integrated active and passive sonars. It will focus on the development of an advanced beamforming structure that allows the implementation of adaptive and synthetic aperture signal processing techniques in ultrasound systems and integrated active−passive sonars deploying multi−dimensional arrays of sensors.

(U) Le but du présent rapport est de faire le point sur les avancées théoriques récentes en matière de conformateurs de faisceaux et de formuler des propositions sur la façon dont la technologie moderne peut être appliquée au perfectionnement des systèmes à ultrasons en place et de prochaine génération et des sonars actifs et passifs intégrés. Le présent rapport porte principalement sur la mise au point d'une structure évoluée de mise en forme de faisceaux qui permet la mise en place de techniques de traitement de signaux de radar à ouverture synthétique et de radar adaptatif dans des systèmes à ultrasons et des sonars actifs−passifs intégrés déployant des réseaux de capteurs à plusieurs dimensions.

14. KEYWORDS, DESCRIPTORS or IDENTIFIERS (Technically meaningful terms or short phrases that characterize a document and could be helpful in cataloguing the document. They should be selected so that no security classification is required. Identifiers, such as equipment model designation, trade name, military project code name, geographic location may also be included. If possible keywords should be selected from a published thesaurus, e.g. Thesaurus of Engineering and Scientific Terms (TEST) and that thesaurus identified. If it is not possible to select indexing terms which are Unclassified, the classification of each should be indicated as with the title.)

(U) Acoustic scattering,, Beam steering, Bi−static active sonar, Circular array, Covariance matrices, Cylindrical array, Delay estimation, Doppler frequency shift, FIR digital filters, Fourier transforms, Frequency domain analysis, Line array, Maximum likelihood estimation, Mine warfare sonar, Multi−dimensional arrays, Multi−static active sonar, Near−instantaneous convergence, Planar array, Plane wave beamformer, Signal detection, Signal tracking, Side−scan sonar, Sonar tracking, Spectral analysis, Spherical arrays, Synthetic aperture sonar, Target motion analysis, Ultrasound Systems

Defence R&D Canada

Canada's Leader in Defence
and National Security
Science and Technology

R & D pour la défense Canada

Chef de file au Canada en matière
de science et de technologie pour
la défense et la sécurité nationale

DEFENCE DÉFENSE

www.drdc-rddc.gc.ca